

RAPPORT

Jürgen König, Lars Walleij

**Timber frame assemblies
exposed to standard
and parametric fires
Part 2: A design model for
standard fire exposure**

Träteknik

Contents

Preface	3
Summary	4
Sammanfattning	5
1 Introduction	6
2 General presentation of the design model	7
2.1 Charring model for timber frame members	7
2.1.1 Charring phases	7
2.1.2 Initially unprotected surfaces - charring phase 1	8
2.1.3 Members protected by wood or wood-based panels	9
2.1.4 Members protected by non-combustible panels	10
2.2 Residual cross section	11
2.2.1 General	11
2.2.2 Rectangular shape	11
2.2.3 Real shape	12
2.2.4 Strength and stiffness parameters	12
2.3 Structural model for wall studs	13
3 Thermal model of heat transfer and charring	15
3.1 General	15
3.2 Thermal properties	17
3.2.1 Wood	17
3.2.2 Mineral wool	19
3.2.3 Linings	20
3.2.3.1 Joint configurations in linings	20
3.2.3.2 Gypsum plasterboard	21
3.2.3.3 The effect of joints in gypsum plasterboard sheets	25
3.2.3.4 Plywood	26
3.2.3.5 Effect of a void cavity between the lining and the timber member	27
3.3 Determination of charring depths and charring rates	27
3.3.1 Unprotected member — Charring phase 1	27
3.3.2 Protection phase — Charring phase 2	29
3.3.2.1 Protection by lining against charring	29
3.3.2.2 Charring rate	30
3.3.3 Post-protection phase — Charring phase 3	32
3.4 Residual cross section	34
3.4.1 Bending about stiff axis	34
3.4.2 Bending about weak axis	38
4 Mechanical model of timber cross section	40
4.1 General	40
4.2 Computer program for cross section of timber member	41
4.3 Determination of apparent bending strength	42
4.3.1 Expressions	42
4.3.2 Mechanical properties of timber	42
4.3.2.1 Normal temperature	42
4.3.2.2 Mechanical properties of timber at elevated temperature	45
4.3.2.2.1 General	45
4.3.2.2.2 Modulus of elasticity	45
4.3.2.2.3 Strength	51

4.3.2.3 Effect of timber quality	60
4.4 Determination of apparent modulus of elasticity in bending.....	61
4.5 Mechanical properties for bending about weak axis	64
5 Performance of linings.....	65
5.1 General	65
5.2 Failure of lining	65
6 Structural model for wall studs.....	69
7 References	70
Appendix A – Effect of grid configuration	73
Appendix B – Modification factors for fire.....	75

Preface

The investigations reported here were part of the Nordic research project "Fire safe wooden buildings – Phase 2" within the Nordic Wood Programme of the Nordic Industrial Fund. The work was funded by the Swedish timber and building materials industry, Träforsk, NUTEK, Brandforsk and the Nordic Industrial Fund.

The investigations were carried out by Träteknik - Swedish Institute of Wood Technology Research, in continuation of the work carried out during phase I of the Nordic research project.

Summary

A design model for solid timber frame members in floor and wall assemblies exposed to ISO 834 standard fire exposure is developed. The assemblies considered consist of solid timber members – joists or studs – linings of gypsum plasterboard or gypsum plasterboard backed with wood-based panels, and cavity insulation made of rock or glass fibre. Ceiling linings may be fixed to resilient channels perpendicular to the direction of the joists.

The design model is based on two sub-models: a charring model for the determination of the residual cross section of the timber member, and a mechanical model giving modification factors for the reduction of mechanical properties of the residual cross section. The charring model takes into account different stages of protection provided by the lining. The performance of linings is characterised by the ability of the lining to delay the start of charring and to remain attached to the timber frame in order to protect it against direct fire exposure as long as possible. Where linings remain in place although the timber member is charring behind the lining, a reduced charring rate is accounted for due to the insulating effect of the lining. After failure of the lining, an increased charring rate is accounted for during the post-protection phase. The failure of the lining is dependent on thermal degradation of the lining material and effective fixing.

The charring model is based on a thermal model of two-dimensional heat transfer. Calculations were performed using the computer program TEMPCALC, and thermal material properties that were calibrated to test results. The char-line is defined as the position of the 300-degree isotherm; its propagation along the symmetry line of the cross section serves as the charring depth characterising the magnitude of charring during different charring phases. For simplicity, in the design model, the non-linear relationships between charring depth and time are replaced by linear relationships, and the irregularly shaped residual cross section is replaced by a rectangular residual cross section by using notional charring rates and charring depths.

The strength and stiffness parameters of the residual timber cross section were determined using a mechanical model of the timber cross section. The model uses temperature values obtained as output from heat transfer calculations, and reduced material properties of strength and modulus of elasticity for tension and compression. Starting with properties found in other sources, these properties were further calibrated to test results, comparing deflections and failure loads. The obtained reductions of properties include the effect of moisture, time and mechano-sorptive creep, all of them being important especially in a temperature range around 100°C. Using spreadsheet programming, modification factors for fire were calculated, giving the reduction of strength and stiffness properties of the residual cross section.

The failure time of the gypsum plasterboard lining is dependent on two parameters: the temperature of mechanical degradation of the material, and the length of fasteners where charring occurs behind the lining.

Sammanfattning

I denna rapport presenteras en beräkningsmodell för dimensionering av träregelstommen i väggar och bjälklag som exponeras för en brandbelastning enligt standardbrandkurvan enligt ISO 834. De här behandlade träregelkonstruktionerna är sammansatta av regler av konstruktionsvirke, skivbeklädnader och isolering i konstruktionens hålrum. Som beklädnad används en eller två lager gipsskivor eller ett lager gipsskivor i kombination med bakomliggande träskivor. Hålrumsisoleringen består av sten- eller glasullsisolering. Beklädnadsskivor i tak kan även vara monterade på akustikprofiler av tunnplåt som monterats tvärs bjälkarna.

Beräkningsmodellen avsedd för konstruktören baseras dels på en inbränningsmodell som beaktar olika skyddsfaser med avseende på beklädnadens verkan, dels på en mekanisk modell som ger omräkningsfaktorer som anger reduktionen av resttvärsnittets hållfasthets- och styvhetsparametrar på grund av temperaturpåverkan. Beklädnadens förmåga att skydda regelstommen karakteriseras dels av dess förmåga att fördröja starttiden för inbränningen i träregeln, dels – när den förmår att förbli i sitt läge efter att inbränningen börjat – att genom sin isolerande verkan ge skydd mot direkt brandpåverkan och reducera inbränningshastigheten i regeln. När beklädnaden fallit ned beaktas den kraftigt ökade inbränningshastigheten i efter-skyddsfasen. Beklädnadens nedfallstid är beroende av dess termiska nedbrytning och dess infästningssätt.

Inbränningsmodellen baseras på en termisk modell som tillämpar tvådimensionell värmetransport. Beräkningarna utfördes med hjälp av datorprogrammet TEMPCALC och termiska materialdata som kalibrerats med avseende på försöksresultat. Inbränningsdjupet är definierat som 300-gradersisotermin; dess förändring med tiden längs tvärsnittets symmetrilinje karakteriserar inbränningen under de olika inbränningsfaserna. Som förenkling ersätts i beräkningsmodellen de olinjära sambanden mellan inbränning och tid med linjära samband, och resttvärsnittets oregelbundna form av ett rektangulärt genom tillämpning av fiktiva inbränningshastigheter och -djup.

Resttvärsnittets mekaniska egenskaper, d v s omräkningsfaktorer för brandpåverkan som anger reduktionen av resttvärsnittets hållfasthets- och styvhetsparametrar framtoogs med hjälp av en mekanisk modell som använder sig av temperaturfält bestämda med hjälp av den termiska modellen samt träets reducerade hållfasthet och elasticitetsmodul vid dragning och tryck på grund av förhöjd temperatur. Utgående från materialdata från andra källor kalibrerades dessa med avseende på försöksresultat genom att jämföra deformationer och brottlaster. De erhållna reduktionerna av materialegenskaperna inkluderar inverkan av fukt, tid och mekano-sorptiv krypning som alla är viktiga inom ett temperaturområde omkring 100°C. Beräkningarna genomfördes med hjälp av kalkylbladsprogrammering.

Gipsskivornas nedfallstider är beroende av två parametrar: dels temperaturen vid vilken den mekaniska nedbrytningen sker, dels längden hos fästelementen när inbränning förekommer bakom beklädnaden.

1 Introduction

Unlike heavy timber structures where the char-layer of fire exposed members performs as an effective protection of the remaining unburned residual cross section, the fire performance of light timber framed members is crucial to the protection provided by the linings and the cavity insulation. This is also valid for strength and stiffness parameters that are considerably more dependent on the effect of fire exposure than in heavy timber cross sections, since greater portions of the residual cross section are affected by elevated temperatures. Due to the importance of materials or components providing complete or partial protection against the fire, it is therefore desirable to model these effects in an adequate way in order to reflect the performance, and to prevent costly fire testing as far as possible.

In present design codes for structural fire design of timber structures, e.g. the Fire Part of Eurocode 5 (ENV 1995-1-2, 1994), the performance of fire exposed wall and floor assemblies is dealt with in a crude way, leading to results that are either unduly conservative or unsafe. This is partly due to the wish to make design rules simple; one should keep in mind, however, that simplicity should never lead to unsafe results. On the other hand, too conservative design rules will make designers feel reluctant to apply them.

During the recent decade, comprehensive experimental research has been conducted on light timber frame assemblies, both on wall assemblies in full and medium scale, and on assemblies in bending in small-scale fire tests (König, J. 1995 and König et al. 1997) with standard fire exposure according to ISO 834 as well as natural fire exposure applying parametric fire curves. Following these investigations, as a first step, a design model has been developed for standard fire exposure, with the main purpose to provide the designer with a tool that is easy to use, but sufficiently precise to describe the performance adequately, and to take into account different failure modes. The model deals only with timber framed wall and floor assemblies with linings of gypsum plasterboard or gypsum plasterboard backed with wood-based boards, and cavities completely filled with rock or glass fibre insulation.

In the following Section 2, a short general description of the design model is given. The parameters used in the design model, and their background, are given in the subsequent sections. In Section 3 the thermal model is described. The material properties were calibrated to previous test results and used in the thermal analysis for the calculation of charring depths in the timber frame members, the temperature in the timber member needed for the mechanical model, and critical temperatures of the lining. The residual cross-sectional properties of the timber member, i.e. the area, section modulus and second moment of area are derived. In Section 4, the mechanical model of the residual cross section of the timber member is presented. Using temperature dependent reduction of material strength and modulus of elasticity of wood, modification factors are derived for the reduction of strength and stiffness parameters of the residual cross section. The performance of linings is analysed in Section 5, considering different failure modes, i.e. thermal degradation and failure of fixing of the lining. In Appendix B, model parameters are given, previously published in a Nordic design manual by Östman et al. (1999).

2 General presentation of the design model

2.1 Charring model for timber frame members

2.1.1 Charring phases

In König et al. (1997), the following protection and charring phases were identified, see Figure 2.1-2.3:

- Charring phase 1 of initially unprotected wood
- Protection phase before failure of boards
 - Pre-charring phase (complete protection against charring)
 - Charring phase 2 (incomplete protection against charring)
- Post-protection phase after failure of boards: charring phase 3

The protection phase is defined as the time period, during which the protection¹ is attached to the timber member, i.e. the member is not directly exposed to the fire. The protection phase ends at time t_{bf} (board failure). Using wood-based panels as protection, the start of charring t_{pr} coincides with the failure time t_{bf} . In the general case, e.g. when non-combustible panels are used, the protection phase consists of the pre-charring phase with complete protection against charring terminated at time t_{pr} , and charring phase 2 where charring of the timber member takes place behind the lining. Finally, after failure of the protection, during the post-protection phase the member is directly exposed to the fire. With respect to charring, this stage is called charring phase 3.

In the following, reference is made to these protection and charring phases. For simplicity, linear relationships are assumed between charring depth and time in order to obtain simple expression to be used by the designer.

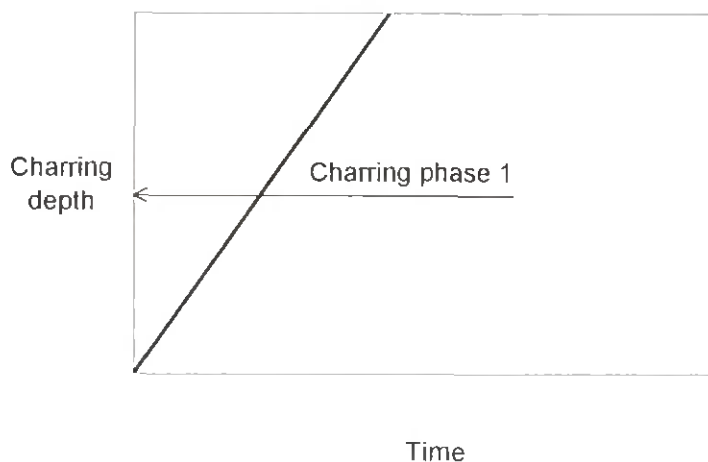


Figure 2.1: Charring phase 1 - initially unprotected wood

¹ In this report, more specific, also the term lining is used for the protection. For the materials forming the lining the terms panels and boards are used.

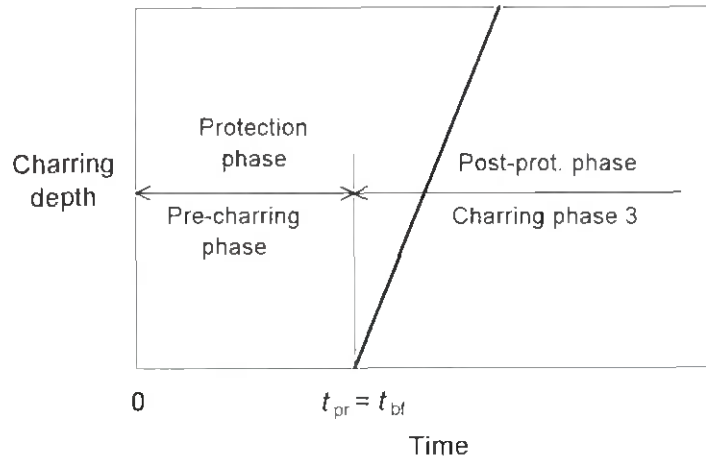


Figure 2.2: Charring phases of wood protected by wood-based boards

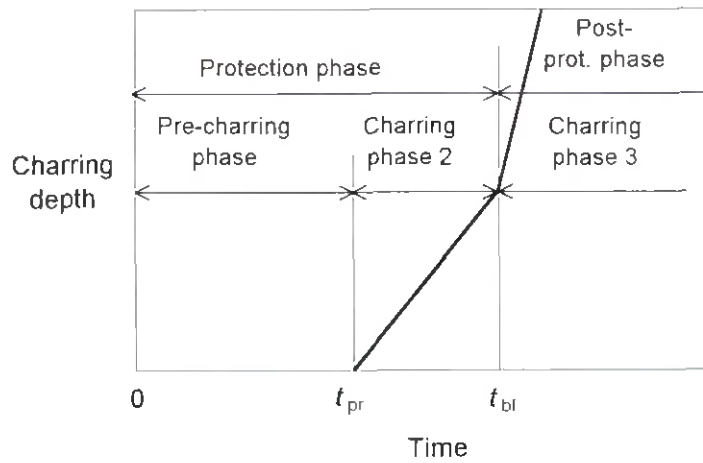


Figure 2.3: Charring phases of protected wood in general

2.1.2 Initially unprotected surfaces - charring phase 1

For wide timber members, the heat transfer is mainly one-dimensional and the charring depth is therefore not affected by the roundings at arrises. For standard fire exposure, the charring depth is

$$d_{\text{char}} = \beta_0 t \quad (2.1)$$

where

β_0 is the charring rate for one-dimensional charring of initially unprotected wood exposed to standard fire (for softwoods 0,67 mm/min.)

t is the time of fire exposure

For timber frame members in wall and floor assemblies with cavities filled with insulating material, the residual cross section typically has a shape as shown in Figure 2.4.

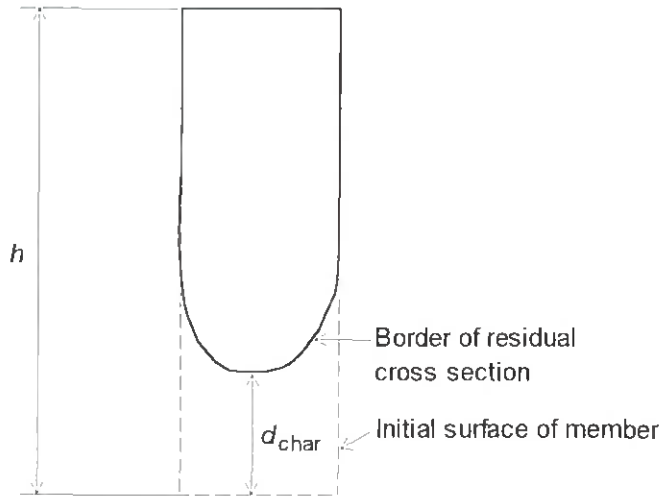


Figure 2.4: Residual cross section of timber frame member with cavity insulation in contact with the wide sides of the member

Charring occurs mainly on the fire-exposed narrow side of the member, while the wide sides are more or less protected by the insulation. Due to the degradation of the insulation material close to the fire-exposed arrises of the member, the influence of the rounding of the char line can be considerable. Thus the charring depth is greater than in wide members where the heat flux is mainly one-dimensional except near the arrises.

Introducing the cross-section factor κ_s taking into account this effect, the charring depth in the middle of the narrow side (see Figure 2.4) can be determined as

$$d_{char} = \kappa_s \beta_0 t \quad (2.2)$$

with

$$\kappa_s = \frac{\beta_1}{\beta_0} \quad (2.3)$$

where β is the charring rate for two-dimensional charring in the middle of the narrow side. Values of κ_s are derived in 3.3.1.

2.1.3 Members protected by wood or wood-based panels

Where the member is protected by wood or wood-based panels, the onset of charring is delayed until time t_{br} (which is equal to t_{pr}). Now, in the post-protection phase, the charring rate is different from the charring rate during charring phase 1. In the case of standard fire exposure, during that stage the temperature is considerably higher than at the beginning ($t = 0$) where the temperature rise starts at ambient values, leading to the charring rate being greater than in the case of initially unprotected surfaces.

Provided that the cavity is filled with rock fibre bats being capable of protecting the wide sides of the timber member, the charring rate during charring phase 3 is given by (see Figure 2.5)

$$\beta_3 = \kappa_s \kappa_3 \beta_0 \quad (2.4)$$

where

κ_s is the cross section factor according to 2.1.2

κ_3 is the post protection factor

β_0 is the charring rate for one-dimensional charring of initially unprotected wood exposed to standard fire

The charring depth is

$$d_{\text{char},3} = \kappa_s \kappa_3 \beta_0 (t - t_{\text{pr}}) \quad (2.5)$$

Values of κ_3 are derived in 3.3.3.

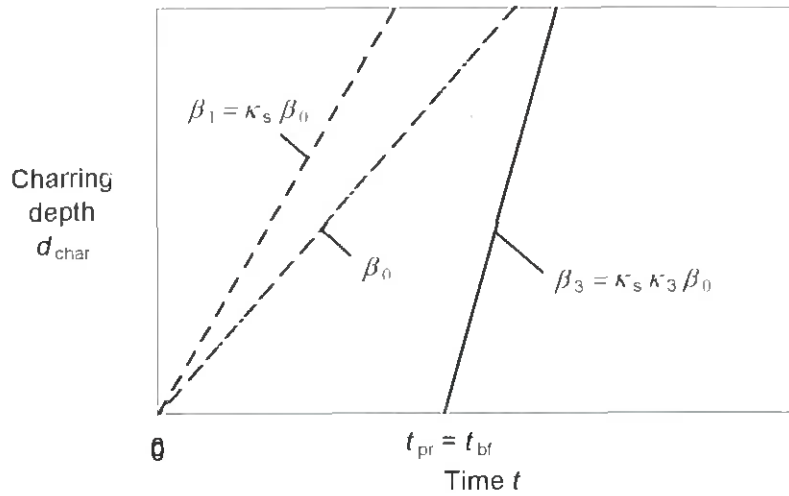


Figure 2.5: Charring during charring phase 3 (post-protection phase)

For assemblies with cavity insulation made of glass fibre, charring phase 3 should not be taken into account in the design, since the insulation, now being directly exposed to the fire, would melt within a very short time after failure of the lining, and the timber member be subject to extensive charring leading to collapse.

2.1.4 Members protected by non-combustible panels

The lining provides protection against fire for the timber member, such that the onset of charring of the member is delayed until the time t_{pr} . As long as the lining is attached to the timber frame, due to its thermal insulation, the timber will char, but at a rate that is smaller than in the case of initially unprotected surfaces. The charring rate of phase 2 is

$$\beta_2 = \kappa_s \kappa_2 \beta_0 \quad (2.6)$$

where

κ_s is the cross section factor according to 2.1.2

κ_2 is the insulation factor of the protection

β_0 is the charring rate for one-dimensional charring of initially unprotected wood exposed to standard fire

During charring phase 2, the charring depth is, corresponding to expression (2.5),

$$d_{\text{char},2} = \kappa_s \kappa_2 \beta_0 (t - t_{\text{pr}}) \quad (2.7)$$

For $t > t_{\text{bf}}$, i.e. during the post-protection phase, the charring depth is (see Figure 2.6)

$$d_{\text{char},3} = \kappa_s \beta_0 [\kappa_2 (t_{\text{bf}} - t_{\text{pr}}) + \kappa_3 (t - t_{\text{bf}})] \quad (2.8)$$

For linings consisting of gypsum plasterboard, values of t_{pr} , t_{bf} and κ_2 are derived in 3.3.3.

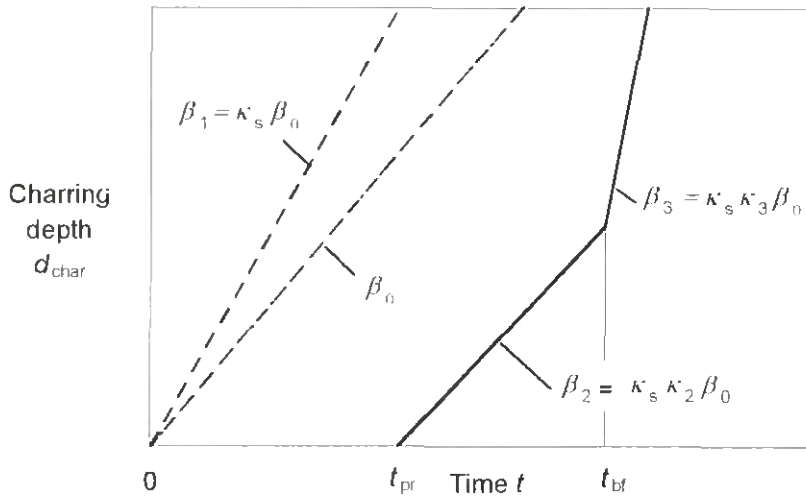


Figure 2.6: Charring during charring phases 2 and 3 (protection and post-protection phases)

2.2 Residual cross section

2.2.1 General

In general, the shape of the residual cross section is more or less irregular, especially due to *corner roundings* and the degree of heat attack to partially protected cross sections. Most fire design codes give rules to determine rectangular cross sections with or without corner roundings. From the designers viewpoint it is desirable to simplify the irregular cross section into a rectangular shape of the residual cross section such that the effect of corner roundings is included, by defining a notional charring depth that is larger than the real one in order to compensate for this approximation.

2.2.2 Rectangular shape

The model adopted here is illustrated in Figure 2.7. Charring is assumed to occur only on the fire-exposed narrow side of the member, while the wide sides are protected by the insulation. The notional charring depth is denoted as $d_{\text{char},n}$.

Three alternative criteria determine the notional charring depth: The equivalent rectangular cross section can be determined such that it has either the same area, section modulus or second moment of area as the real residual cross section. The charring depth is calculated as

$$d_{\text{char},n} = \kappa_n d_{\text{char}} \quad (2.9)$$

where κ_n is a factor for transforming the real cross section into the notional rectangular cross section.

This implies that the magnitude of the cross section is not unambiguous since κ_n is different with respect to area, section modulus and second moment of area as criteria for the transformation, however, for simplicity these three values can be replaced conservatively by a single value $\kappa_n = 1,5$, see 3.4.

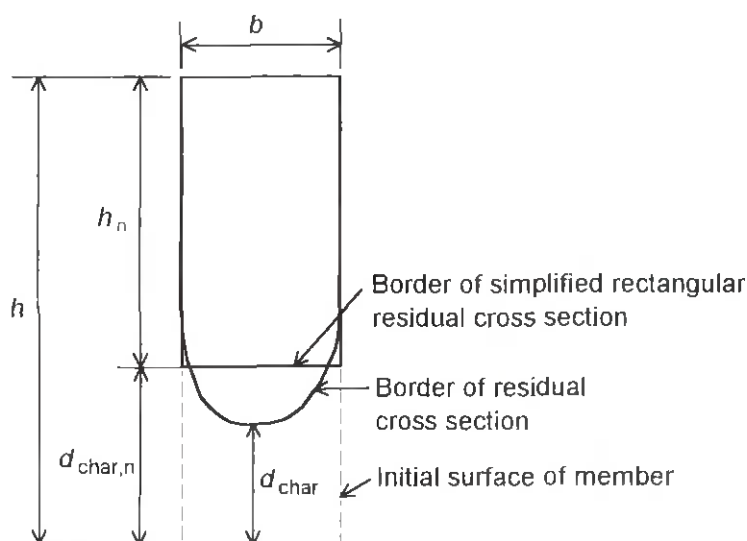


Figure 2.7: Alternative definitions of residual cross section

2.2.3 Real shape

As an alternative to the simplified rectangular cross section, it is possible to use the real shape of the residual cross section. The advantage is that the magnitude of the cross section is unambiguous, however, since the shape is too irregular for simple calculation of the cross sectional parameters, design expressions would be needed as design aids.

2.2.4 Strength and stiffness parameters

The strength of the residual cross section at fire is

$$f_{m,k,fi} = k_{\text{mod},fi,fi} f_k \quad (2.10)$$

where

- $f_{m,k,fi}$ is the characteristic bending strength at fire
- $k_{\text{mod},fi,fi}$ is the modification factor for fire for strength
- $f_{m,k}$ is the characteristic bending strength at normal temperature (modulus of rupture).

The modification factor is a measure of the degradation of the strength of the material. It should not be used for the determination of the local strength, e.g. in a finite element analysis.

For cross sections in bending according to Figure 2.4, the modification factor can be taken as

$$k_{\text{mod,fi,fm}} = \alpha_0 - \alpha_1 \frac{d_{\text{char}}}{h} \quad (2.11)$$

where

α_0, α_1 are dependent on the width b of the beam and the state of stress of the fire-exposed side
 h is the depth of the beam.

The modulus of elasticity of the residual cross section is reduced correspondingly to expression (3.2):

$$E_{k,fi} = k_{\text{mod,fi}} E_k \quad (2.12)$$

with

$$k_{\text{mod,fi,E}} = b_0 - b_1 \frac{d_{\text{char}}}{h} \quad (2.13)$$

where

E_k is the characteristic modulus of elasticity at normal temperature

$k_{\text{mod,fi,E}}$ is the modification factor for fire for stiffness

b_0, b_1 are dependent on the width b of the beam and the state of stress of the fire-exposed side
 h is the depth of the beam.

Derived values of modification factors are given in Appendix B.

2.3 Structural model for wall studs

For axially loaded wall studs, three failure modes are possible:

- Failure mode 1: Out-of-plane column buckling about the stiff axis of the stud
- Failure mode 2: In-plane column buckling about the weak axis of the stud
- Failure mode 3: Torsional buckling.

Above, the terms “stiff” and “weak” refer to the original cross section. The term “plane” refers to wall plane.

The calculation of load bearing capacity can be performed applying buckling formulae given in timber design codes, e.g. ENV 1995-1-1 (1993), and cross-sectional and material properties due to elevated temperature.

For failure mode 1, for wall studs in platform timber frame construction, using the benefit of stabilising reaction moments, a reduced buckling length can be applied of

$$l_{cr} = 0,7 l \quad (2.13)$$

where l is the length of the stud including sole and head plate, see Section 6.

Normally the unexposed side of the studs is clad with board material, bracing the studs effectively with respect to in-plane buckling. In the case of party walls, however, when consisting of two separate stud systems, the studs need to be braced horizontally, normally by noggins, reducing the buckling length with respect to in-plane buckling.

Torsional buckling is normally not observed during fire testing of walls, however this failure mode could be decisive when the depth of the stud is very large (or the aspect ratio h/b is large), in combination with a large load ratio. Cross-section properties with respect to torsional buckling are not included in the design model.

3 Thermal model of heat transfer and charring

3.1 General

In order to determine the progress of the char-line and the temperature field in the assembly, the computer program TEMPCALC – included in the computer program package TCD 3.0 (1990) – was used, developed for the calculation of heat transfer using the Finite Element Method. The computer program solves the two-dimensional, transient, heat transfer differential equation incorporating thermal properties that vary with temperature. Mass transfer is not taken into account. Assemblies comprising several materials and void cavities can be analysed.

The structure is modelled by rectangular finite elements using a grid consisting of boundary, horizontal and vertical lines. The thermal properties of the materials are defined by polynomials of conductivity and heat capacity versus temperature. Time dependent input values for convection and emissivity are included. In the calculations reported here, the convection coefficient γ was taken as $25 \text{ Wm}^{-2}\text{K}^{-1}$ and the emissivity coefficient ϵ was taken as 0,56, following the recommendations of ENV 1991-2-2 (1994).

The temperature at the boundaries of the structure is given by a time-temperature curve. The heat transferred by convection and radiation at the boundaries are modelled as functions of time.

A general problem when using analytical models to calculate the heat transfer through structures is that, due to simplifications and deficiencies of the model, the thermal properties of the materials used as input parameters must be calibrated such that the results are fitted to those obtained by tests. Deviations from the real test conditions may be caused since the model does not take into account the

- mass transfer within the structure
- reaction energy released inside the wood due to pyrolysis
- degradation of material, e.g. the cracking of charcoal which increases the heat transfer of the char layer
- abrupt change of structure, e.g. when the lining falls off.

The influence of mass transfer is most pronounced at temperatures around $100 \text{ }^\circ\text{C}$ when water is evaporated and transported further into the wood where the vapour condenses into water again. The magnitude of heat of reaction has been discussed by several authors (ASCE, 1992, Roberts, 1971, Mehaffey et al. 1994), however its effect is usually ignored.

The objective of the work described in this chapter was to determine the thermal properties of different materials that are included in the wall and floor assemblies, and to model irregularities such as joints in the lining. Starting from material properties given by other sources, they were modified, where necessary, in order to give results in agreement with test results. Due to the “thermal hierarchy” of the different components of the assembly, the process of calibration was performed in single steps. To start with, first the thermal properties of wood were determined, considering the situation of a piece of wood subjected to one-dimensional heat transfer and charring (see 3.2.1). In each of the further steps, one material was added and calibrated to test results, keeping the properties obtained during the previous steps constant. First the cavity insulation was added to the timber member (3.2.2), then also the lining, consisting of one or two layers of gypsum plasterboard (3.2.3.2), and finally the lining consisting of layer of

gypsum plasterboard and a layer of plywood (3.2.3.4). The effect of joints in the lining was modelled by decreasing the thickness of the lining locally (3.2.3.3).

Unfortunately, in version 3.0 of TCD (1990) the number of grid elements was limited to approximately 600, leading to compromises regarding numeric stability and precision. The grid used in this investigation is shown in Figure 3.1. Especially in the main part of the cavity insulation the grid used was coarse. After finalising the main part of this investigation, version 5.0 of TCD (1999) including SUPER TEMPCALC became available, allowing more precise computation. Some comparisons were made between the results of the two versions of the program and the consequences for derived values, see Appendix A.

The lining on the ambient side of the assembly was not taken into account in the calculation, since it's influence could be neglected. In the floor assemblies studied here, due to resilient channels, a 25 mm deep void cavity was between the lining and the timber joists and insulation. Since no effect of this void could be observed, neither in the tests nor in trial calculations, it was not taken into account in the model.

The effect of joints was taken into account by reducing the thickness of the lining, see Figure 3.2 and 3.2.3.2.

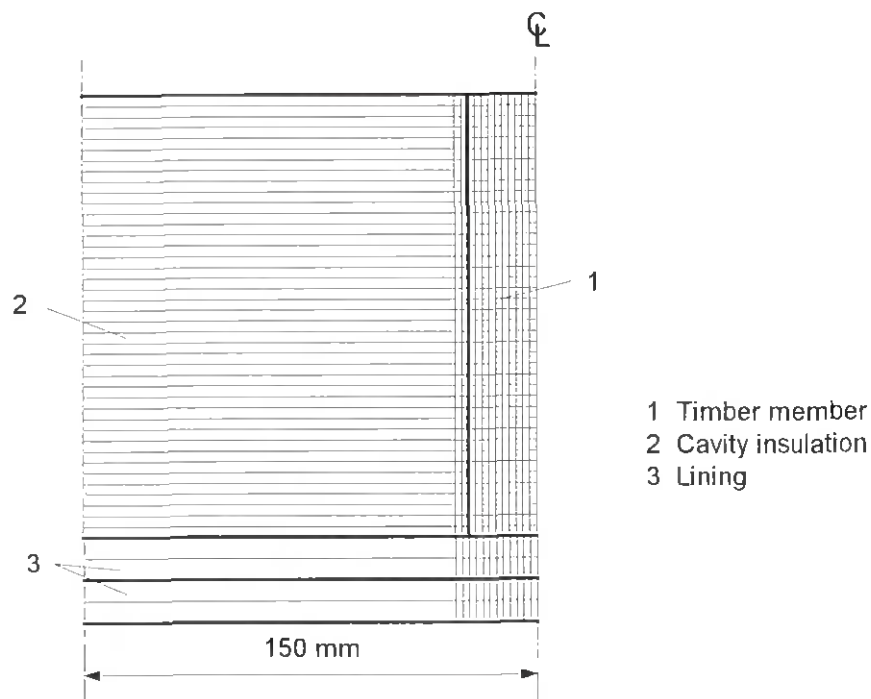


Figure 3.1: Grid modelling the timber member, cavity insulation and lining consisting of two board layers

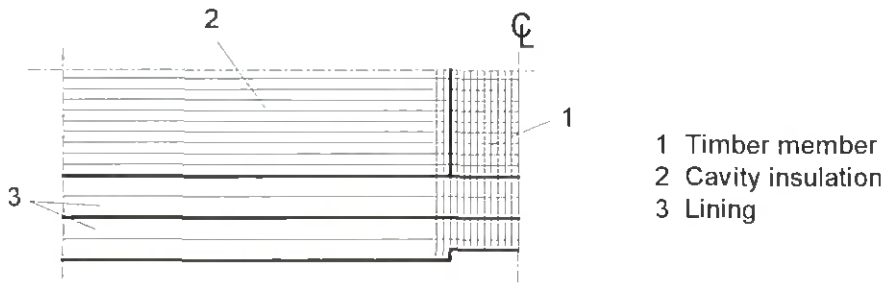


Figure 3.2: Grid model for effect of joint in outer layer of type F gypsum plasterboard

3.2 Thermal properties

3.2.1 Wood

In a previous investigation by König et al. (1994) tests were conducted in order to determine the charring of timber where the heat transfer was predominantly one-dimensional. The thermal properties of timber were calibrated to the test results without any influence of other materials such as gypsum plasterboards and insulation materials. The results of this study are shown in Figure 3.3 and 3.4, and the values of the relationships are given in Table 3.1 and 3.3. For discussion of the results and the comparison with results from other sources shown in the graphs see König et al. (1999). Compared to the data presented in König et al. (1999), however, for temperatures above 200°C, here the values of specific heat were related to density loss as given by Janssens (1999), see Figure 3.5, i.e. the product of specific heat and density was the same. Increasing shrinkage of charcoal and subsequent increased heat transfer through the char layer is taken into account above 800°C. The consumption of charcoal at approximately 1000°C is taken into account by assuming linear decrease to zero of density between 800 and 1200°C. For temperatures up to 100°C, a moisture content of 12 % is assumed

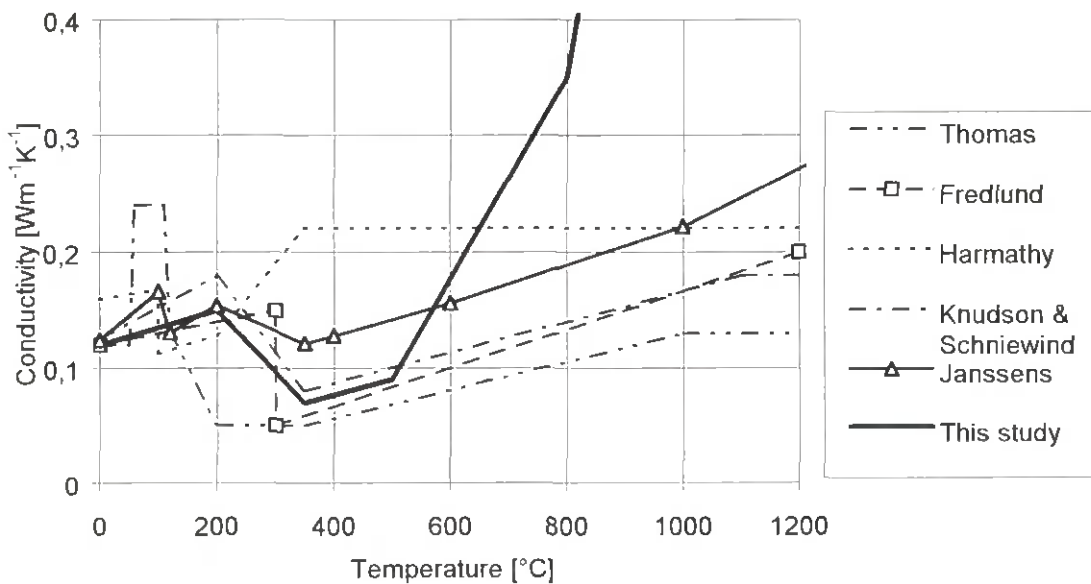


Figure 3.3: Thermal conductivity of wood/char-layer

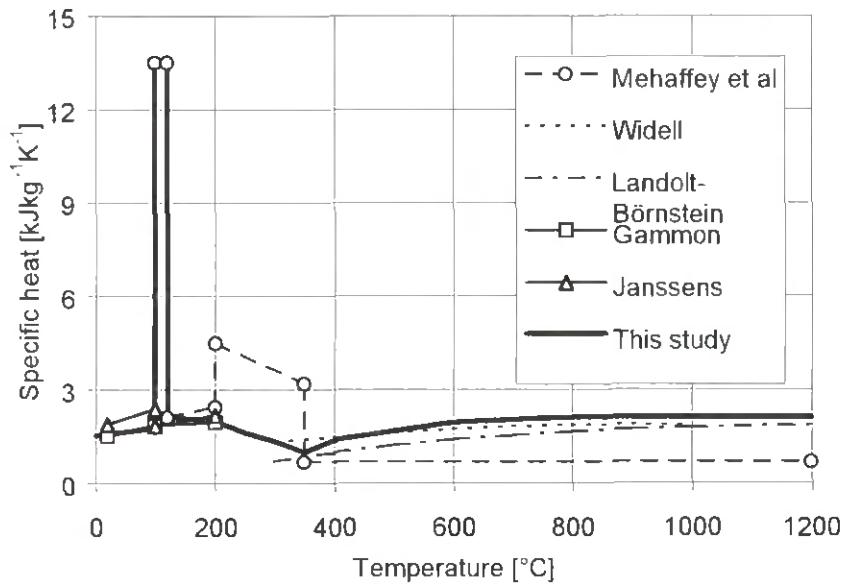


Figure 3.4: Specific heat of wood/char-layer

Table 3.1: Temperature-conductivity relationship for wood as used

Temperature °C	Conductivity Wm ⁻¹ K ⁻¹
0	0,12
200	0,15
350	0,07
500	0,09
800	0,35
1200	1,50

Table 3.2: Specific heat and densities as used in this study

Temperature °C	Specific heat kJ kg ⁻¹ K ⁻¹	Density kg/m ³
20	1,52	476
100	1,76	476
100	13,5	476
120	13,5	425
120	2,12	425
200	2,00	425
250	1,62	393
300	1,36	310
350	0,99	208
400	1,39	149
600	1,95	106
800	2,12	96
1200	2,12	0

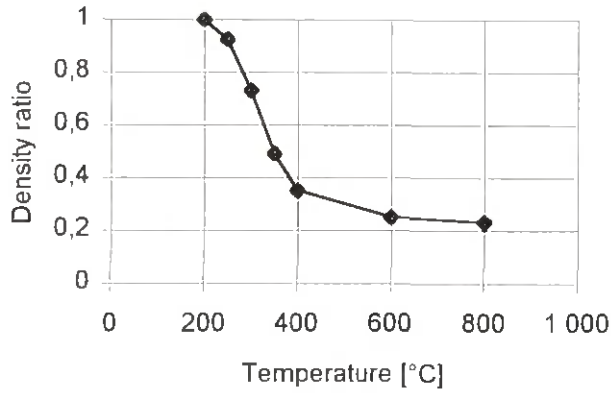


Figure 3.5: Ratio of mass to oven dry mass of softwood versus temperature (Janssens, 1994)

3.2.2 Mineral wool

Thermal conductivity and heat capacity values for rock fibre bats with a density of 50 kg/m^3 are given by Sterner et al. (1990), see Figure 3.6 and 3.7. The values of specific heat shown in Figure 3.4 are calculated from enthalpy values given in the source. Using the test results by König (1995), Thomas (1997) calibrated the thermal conductivity values of rock fibre insulation, while the specific heat values were used according to Sterner et al. (1990). The test assemblies by König (1995) consisted of timber members and rock fibre bats as cavity insulation, however without a lining on the fire-exposed side (test series S1 and S3-S7), see Figure 3.8. The conductivity values obtained by Thomas deviate considerably from those given by Sterner et al. (1990), in order to simulate the effect of degradation of the insulation close to the timber member as observed during the tests. The sets of specific heat and thermal conductivity values used by Thomas are, however not consistent, since the degradation of the insulation material at higher temperatures is not reflected in correspondingly decreasing specific heat values.

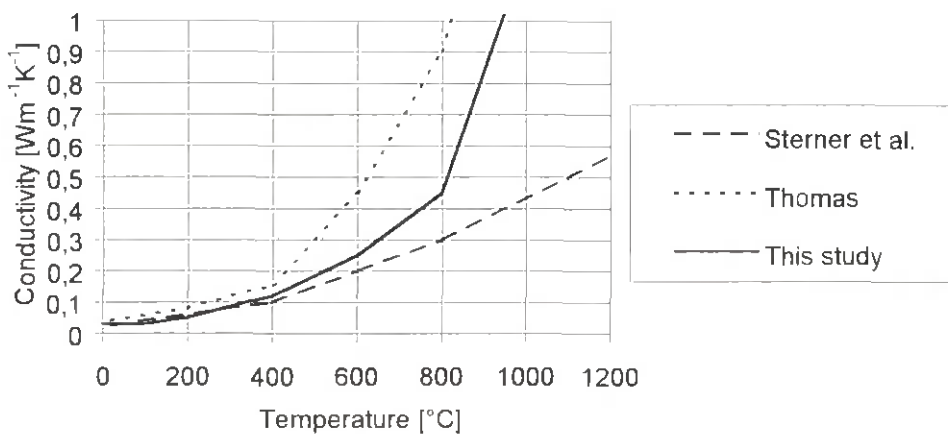


Figure 3.6: Thermal conductivity values for mineral wool

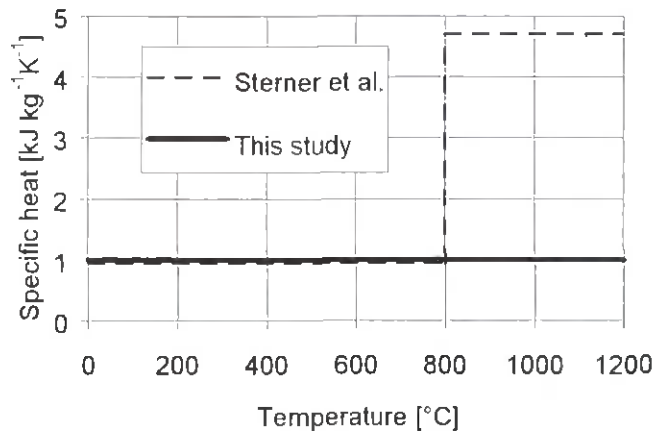


Figure 3.7: Specific heat values for mineral wool

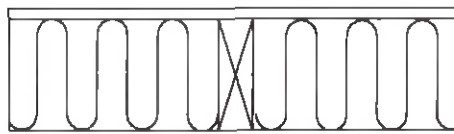


Figure 3.8: Example of section through assembly without protection on the fire-exposed side used in the calibration

The procedure of calibration of thermal properties of rock fibre insulation was carried out with the properties of wood given in 3.2.1. The resultant thermal properties are shown in Figure 3.6 and 3.7. The density of mineral wool was taken as 30 kg/m^2 until 800°C , then it decreased linearly to zero at 1200°C . The density and conductivity values above 800°C were chosen such that increased thermal degradation of the mineral wool could be taken into account. Figure 3.9 shows the calculated charring depth in the timber member shown in Figure 3.8 in comparison with the test results for three member sizes in millimetres as specified in the box. Examples of shapes of the residual cross section at specified times between 10 to 60 minutes are shown in Figure 3.10. See also Appendix A.

3.2.3 Linings

3.2.3.1 Joint configurations in linings

In wall assemblies with studs spaced 600 mm on centres where the sheets, normally of size $1200 \text{ mm} \times 2400 \text{ mm}$ or similar, are fixed to the timber frame in vertical position, board joints are normally situated at timber studs. Depending on the number of board layers, different joint configurations exist, see Figure 3.11. In single layered linings the sheets are jointed at every second stud (joint configuration 1). Joint configuration “0” denotes locations remote from board joints.

In double-layered linings the sheets are normally staggered such that a joint is either situated in the outer layer (joint configuration 2) or in the inner layer (joint configuration 3).

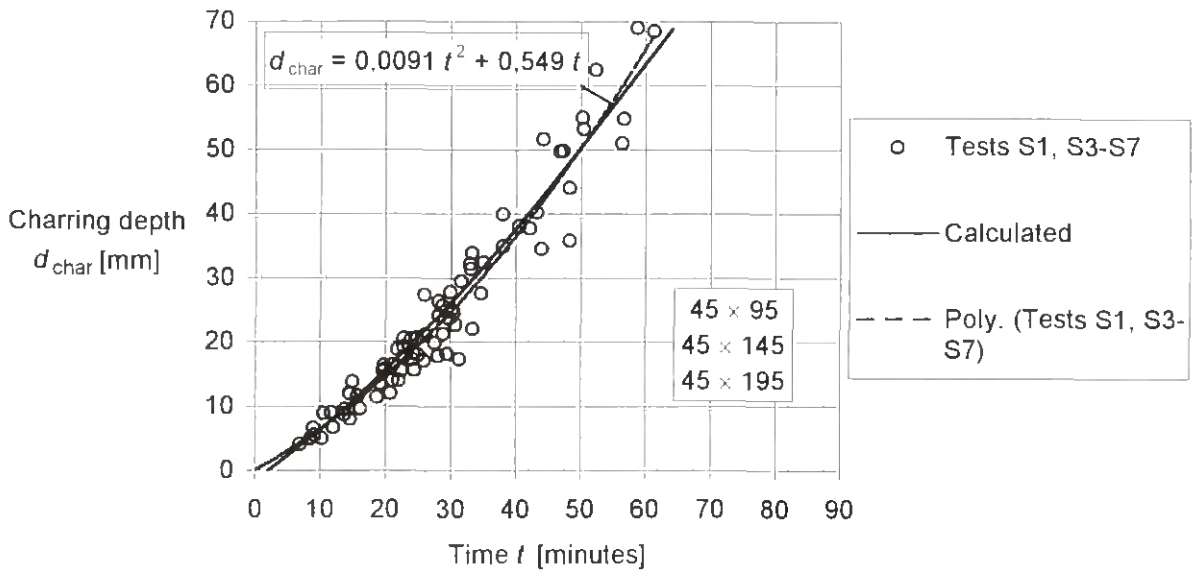


Figure 3.9: Charring depth versus time – Comparison of calculated values with test results according to König (1995) with member sizes in millimetres as shown in the box

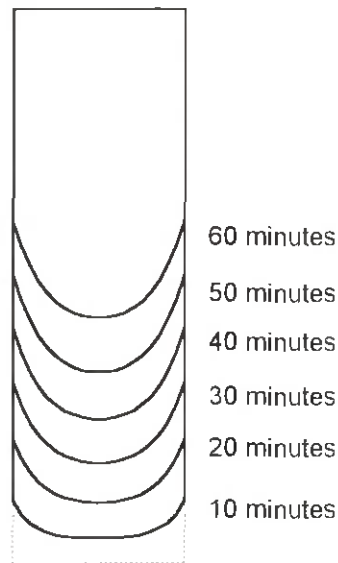


Figure 3.10: Residual cross sections calculated as 300-degree isotherms of original cross section 45 mm × 145 mm with rock fibre

3.2.3.2 Gypsum plasterboard

Examples of measured thermal conductivity values of gypsum plasterboards from different sources (Mehaffey et al., 1994, Harmathy, 1995 and Andersson et al., 1986) are shown in Figure 3.12 for temperatures up to 900 °C. Thomas (1997) and Mehaffey et al. (1994) calibrated conductivity values to test results giving an extended temperature range for input data in calculations. A similar curve was obtained when the data were calibrated to the tests of this investigation. No distinction was made between the two qualities of gypsum plasterboard

used in the tests. This is justified by recent test results by Tsantaridis et al. (1999) regarding the thermal properties of gypsum plasterboard of different origin with respect to the onset of charring and the charring rate of wood behind the gypsum plasterboard. The tests showed that the onset of charring is mainly dependent on the board thickness, while the charring rate is slightly better predicted by the area weight of the boards, irrespective of origin and composition of the boards.

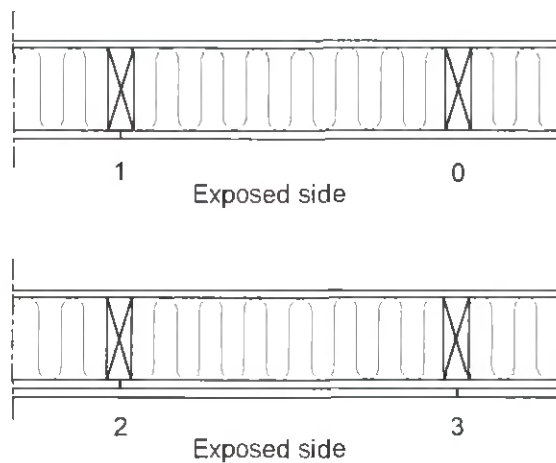


Figure 3.11: Joint configurations of linings.

- 0: No joint**
- 1: Joint in single layer**
- 2: Joint in outer board layer**
- 3: Joint in inner board layer**

Specific heat values for gypsum plasterboards used in this study are shown in Figure 3.13 and Table 3.3. They do not differ much from measured values by Mehaffey et al. (1994) and Andersson et al. (1986). The second peak reported by Andersson et al. (1986) was not taken into account in this study. The heat capacity values were used together with a density of 825 kg/m^3 throughout the whole temperature spectrum considered here. This density is typical for Nordic gypsum plasterboard of type F, however in the calculations it was also used for regular gypsum plasterboard GN with a density of about 700 kg/m^3 .

For the comparison of calculated charring depths with test results, see Figure 3.14-3.16. The results of tests F1-F3, W3 and N1 were taken from König (1995). In the last of these graphs, the comparison is relevant only in the beginning of charring, since the lining consisting of one layer of gypsum plasterboard GN fell off at about 28 minutes, while it is assumed to remain in place in the calculations. In Figure 3.14 one of the experimental curves has a reverse slope. This effect is due to the spacing of thermocouples and the lengthwise variation of charring depth in the tests.

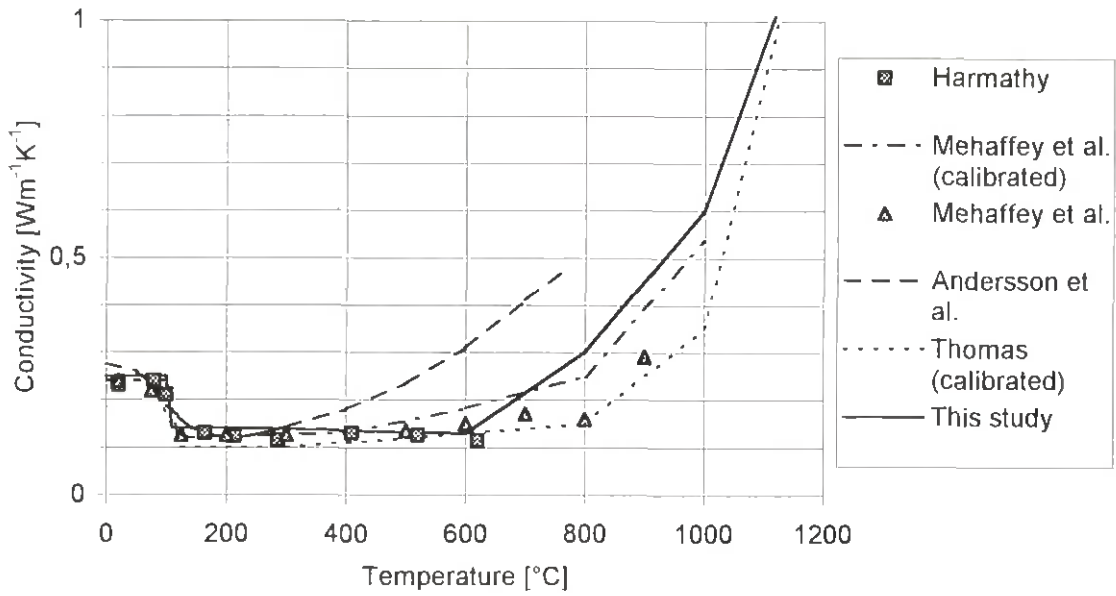


Figure 3.12: Thermal conductivity values for gypsum plasterboard

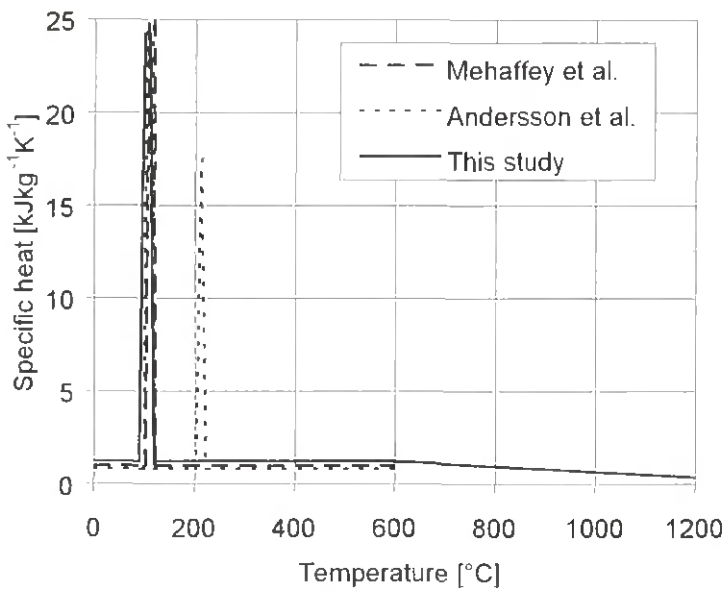


Figure 3.13: Specific heat values for gypsum plasterboard

Table 3.3: Specific heat values used in this study

Temperature °C	Specific heat kJ kg ⁻¹ K ⁻¹
0	1,21
95	1,21
105	48,5
115	1,21
600	1,21
1200	0,36

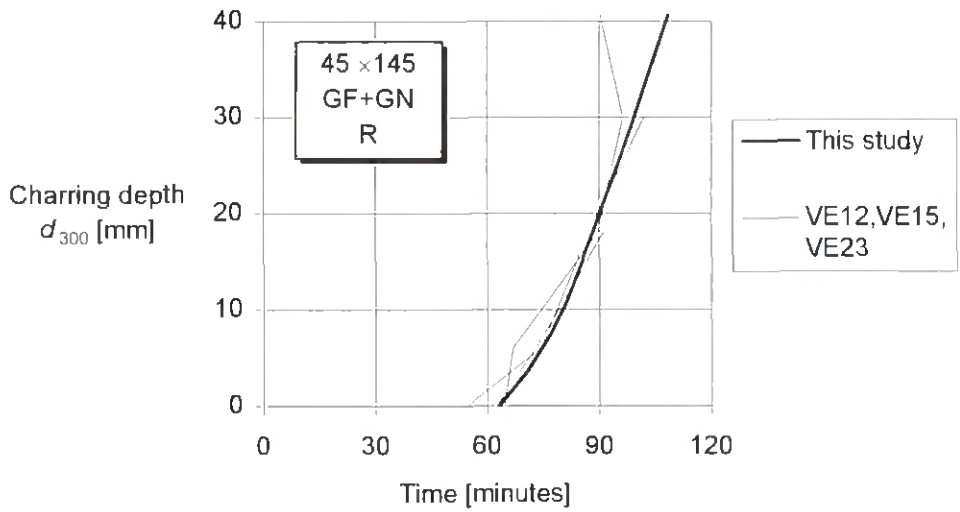


Figure 3.14: Charring depth versus time – Comparison of calculated values with test results for two layers of gypsum plasterboard GF + GN

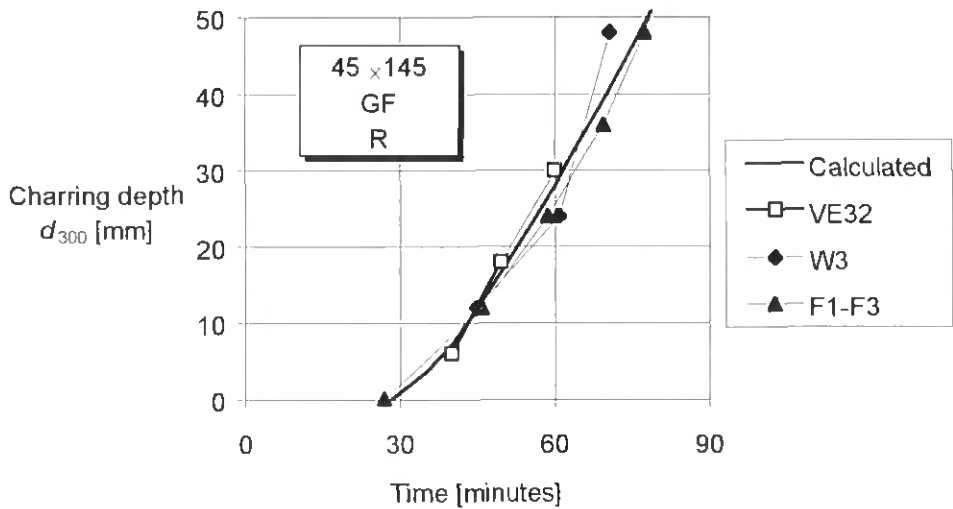


Figure 3.15: Charring depth versus time – Comparison of calculated values with test results for one layer of gypsum plasterboard GF

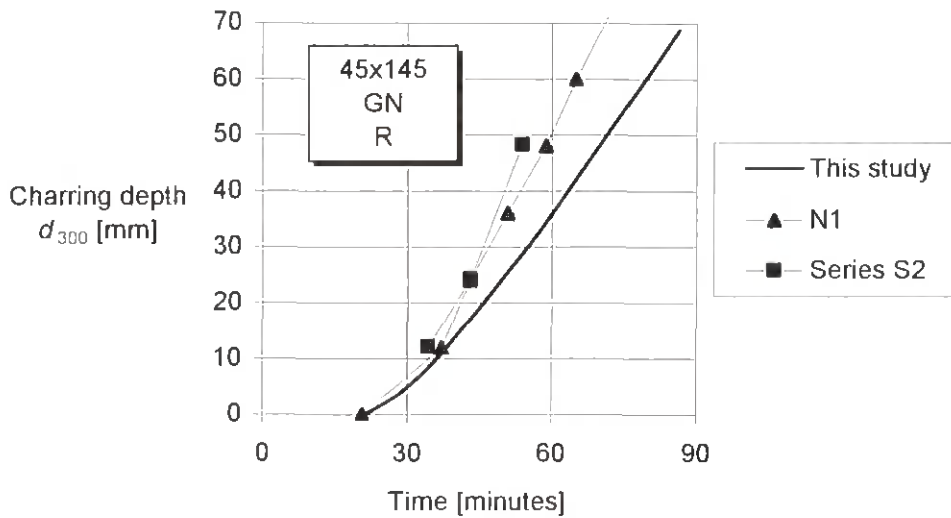


Figure 3.16: Charring depth versus time – Comparison of calculated values with test results for one layer of gypsum plasterboard GN

3.2.3.3 The effect of joints in gypsum plasterboard sheets

Where sheets are jointed the heat transfer through the lining is increased. Two effects contribute to the local weakening of the lining. Normally the thickness of the sheets is reduced along the longitudinal edges for stopping of the joints, see Figure 3.17. Since most gypsum plasterboards exhibit shrinkage when exposed to elevated temperature, dependent on the composition of the boards of different producers, the joint gaps are opening, causing increased convective heat transfer.

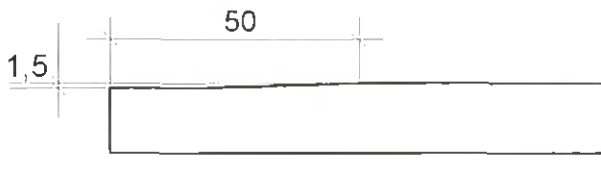


Figure 3.17: Example of reduced thickness along longitudinal edges of gypsum plasterboard sheets

In the model, for joint configurations 1 and 3 (see Figure 3.11) the effect of joints was taken into account by reducing the thickness of the jointed layer by 4 mm locally over a length corresponding to the width of the timber member, see Figure 3.2. Joints in the inner layer of the lining, i.e. joint configuration 2, were not taken into account.

For joint configurations 1 and 3 respectively, in Figure 3.18 and 3.19 calculated charring depths are compared with results from wall test W3 reported by König (1995) and tests VE12, VE15 and VE23 reported by König et al. (1997). For joint configuration 2 with a joint in the inner layer of the lining, a comparison is shown in Figure 3.14.

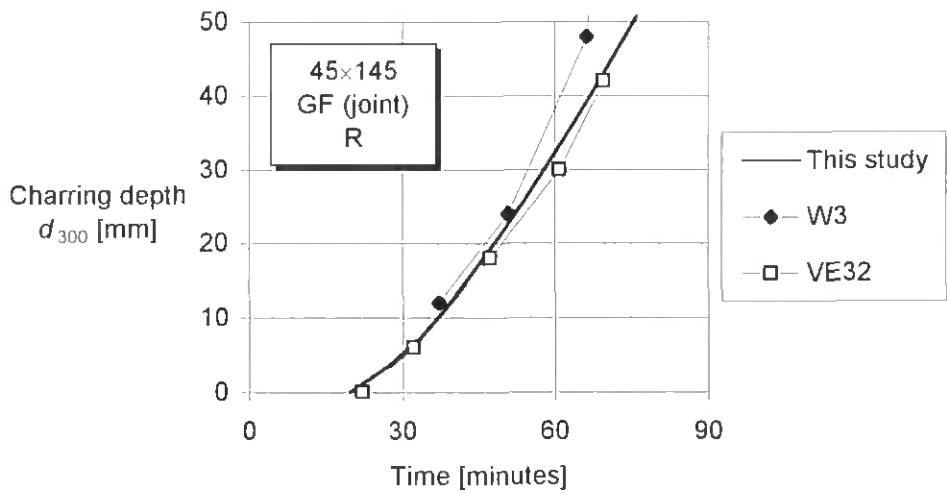


Figure 3.18: Charring depth versus time — Comparison of calculated values with test results for one layer of gypsum plasterboard GF

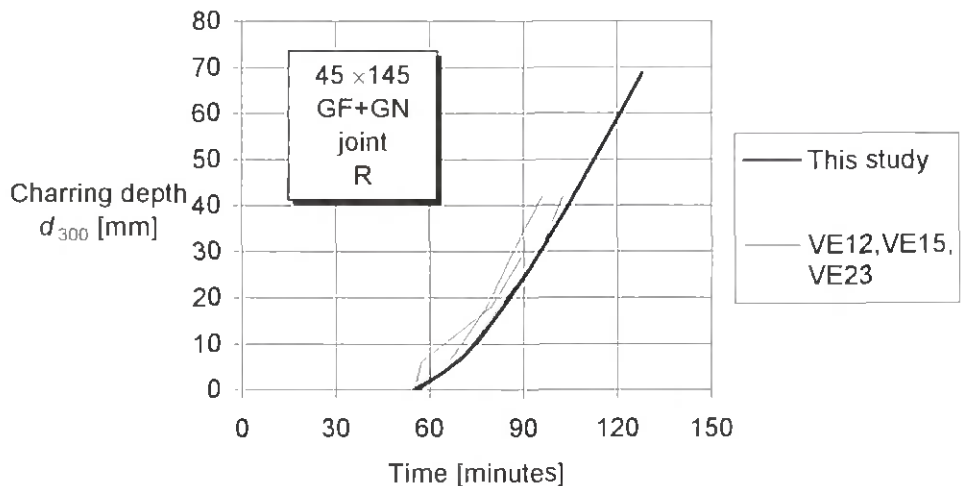


Figure 3.19: Charring depth versus time — Comparison of calculated values with test results for two layers of gypsum plasterboard GF + GN

3.2.3.4 Plywood

König et al. (1997) performed wall tests with linings consisting of an inner layer of 12 mm plywood and an outer layer of 15,4 mm gypsum plasterboard type F. During the calibration of thermal properties of the plywood, the same specific heat values and density ratios were taken as for wood as given in 3.2.1 combined with density values corresponding to a dry density of 510 kg/m^3 . The resultant thermal conductivity values for plywood leading to a good agreement with the test results shown in Figure 3.20 were twice as large as the values for wood.

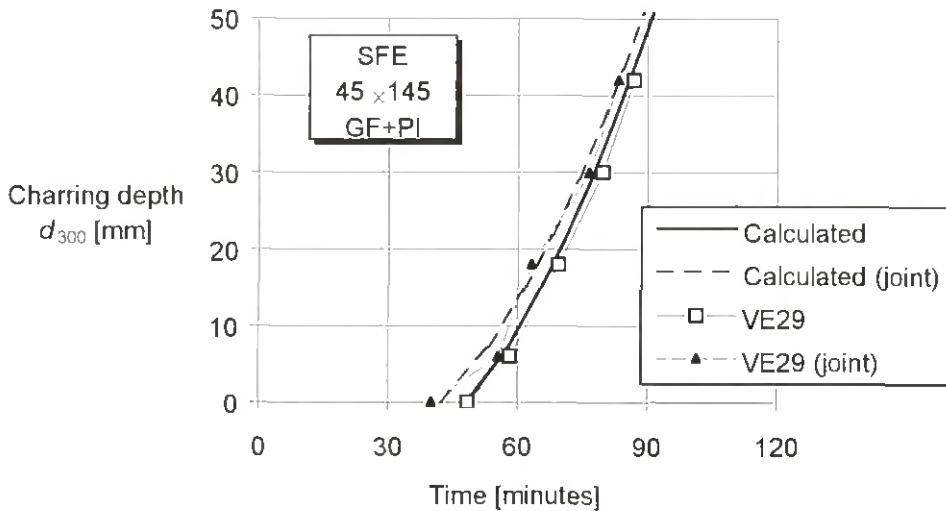


Figure 3.20: Comparison of calculated charring depth in timber member with test results (König et al., 1997) for one outer layer of gypsum plasterboard GF and an inner layer of plywood

3.2.3.5 Effect of a void cavity between the lining and the timber member

In floor assemblies, resilient channels are widely used in order to improve the performance as a noise barrier. The channels are placed between the lining and the floor joists in perpendicular direction, normally at a distance of 400 mm on centres, forming a void cavity between the lining and the joists and cavity insulation between the joists. For channel depths of 25 mm, no influence was observed on the delay of start of charring and the charring rate during charring phase 2, both by testing and calculating.

3.3 Determination of charring depths and charring rates

3.3.1 Unprotected member — Charring phase 1

As shown above, the relationships between the charring depth and time are clearly non-linear. For simplification, as shown in the schematic graphs of clause 2.1, the relationships are fitted by linear curves as follows. For charring phase 1, a linear relationship was chosen with a constant charring rate of 0,86 mm/ minute that was reached in the calculations and in the tests for a charring depth of approximately 25 mm. This linear model is a reasonable approximation of charring depths up to 40 mm, see Figure 3.21.

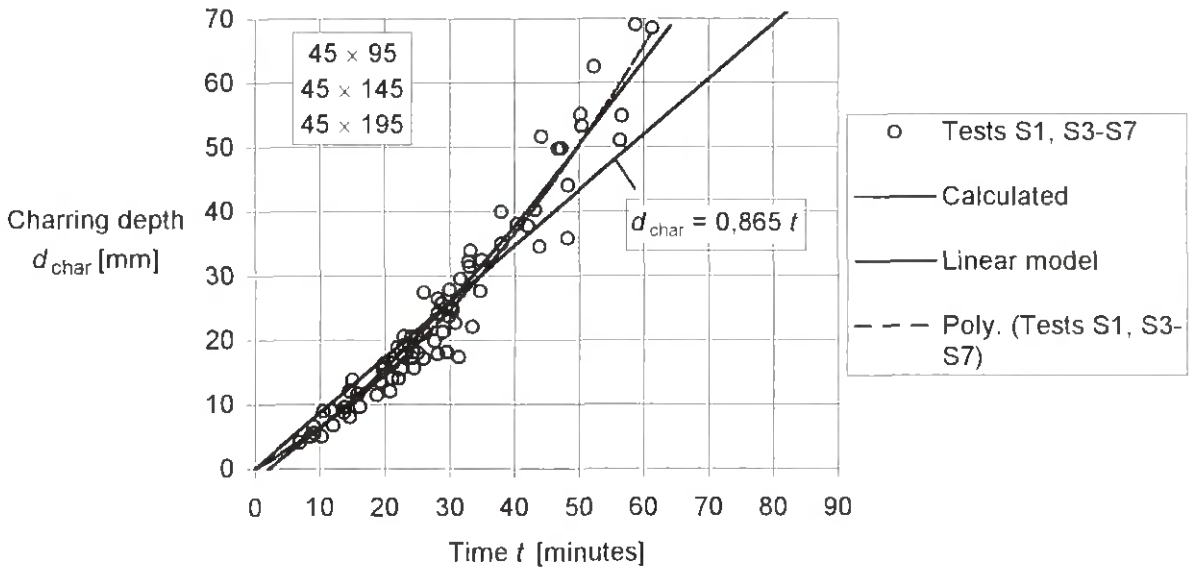


Figure 3.21: Charring depth versus time — Linear model for member width 45 mm

With the basic charring rate $\beta_0 = 0,67$ mm/minute (König et al., 1999) and $\beta = 0,86$ mm/minute inserted in equation (2.3), the cross-section factor is calculated as 1,29. For other member widths similar results were obtained, see Figure 3.22. The data points for member widths between 38 and 90 mm were fitted by a polynomial given as

$$\kappa_s = 0,000167 b^2 - 0,029 b + 2,27 \quad (3.1)$$

For frequently used member sizes values should be used according to Table 3.4.

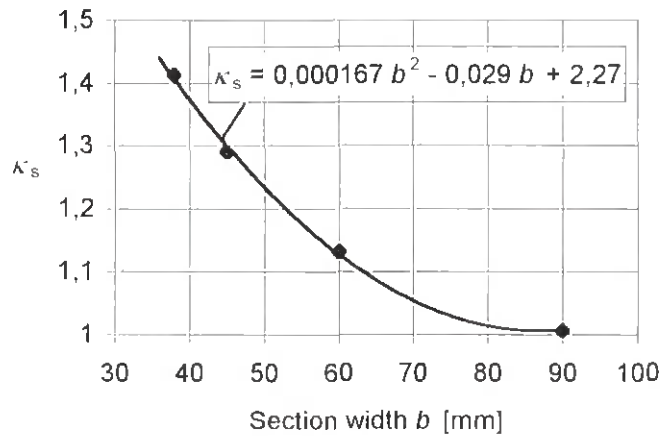


Figure 3.22: Cross-section factor versus width of member

Table 3.4: Cross-section factors for different member widths

b	κ_{σ}
mm	–
38	1,4
45-48	1,3
60	1,1
90	1,0

3.3.2 Protection phase — Charring phase 2

3.3.2.1 Protection by lining against charring

In Figure 3.23 and Figure 3.24, for linings of gypsum plasterboard, calculated times of protection against charring t_{pr} are compared with test results by König (1995) and König et al. (1997). In double layered linings, the outer layer was of type F according to prEN 520 (1999). The calculated data were fitted using a linear model for joint configurations 0 and 1 (see Figure 3.11), i.e. linings without joints in the fire-exposed (outer) layer as

$$t_{pr} = 2,8 h_b - 14,2 \quad (3.2)$$

and

$$t_{pr} = 2,8 h_b - 22,8 \quad (3.3)$$

for joint configurations 1 and 3, i.e. linings with a joint in the fire-exposed (outer) layer. In these expressions, h_b is the thickness of the board in millimetres. For double layered linings, these expressions are only valid if both layers remain in place during the relevant protection times. Both curves have the same slope, however due to joints in a single-layered lining or in the outer sheet of a double-layered lining, the protection time against charring is decreased by about 8 minutes.

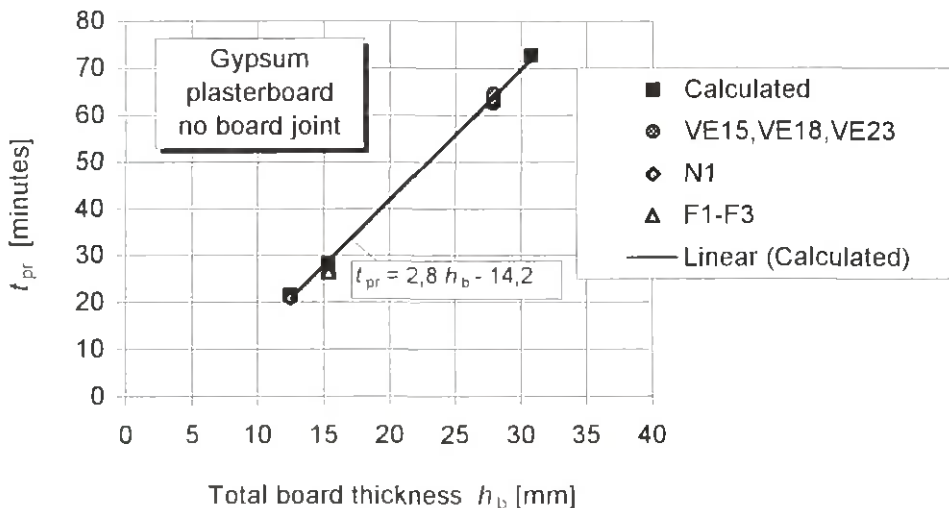


Figure 3.23: Effect of total thickness of lining on delay of charring — gypsum plasterboard without joints

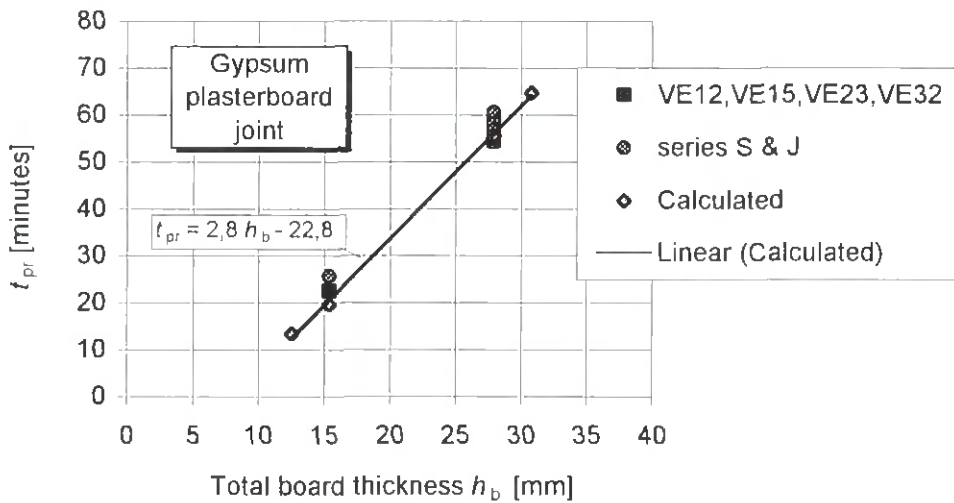


Figure 3.24: Effect of total thickness of lining on delay of charring — gypsum plasterboard with joints (joint configuration 1 or 3)

3.3.2.2 Charring rate

The relationships between charring depth and time as shown in 3.2.3 were simplified by a linear model, chosen such that the constant charring rate was equal to the secant value reached at a charring depth of 20 mm, giving reasonable agreement for charring depths up to 30 mm. The duration of charring phase 2 is – apart from the possibility of failure due to thermal degradation of the board material – limited by failure of the fixing of the lining to the timber members. For normally used fasteners, charring depths exceeding about 30 mm are unlikely to occur. For linings with one and two layers of plasterboard, the linear model is shown in Figure 3.25 and 3.26.

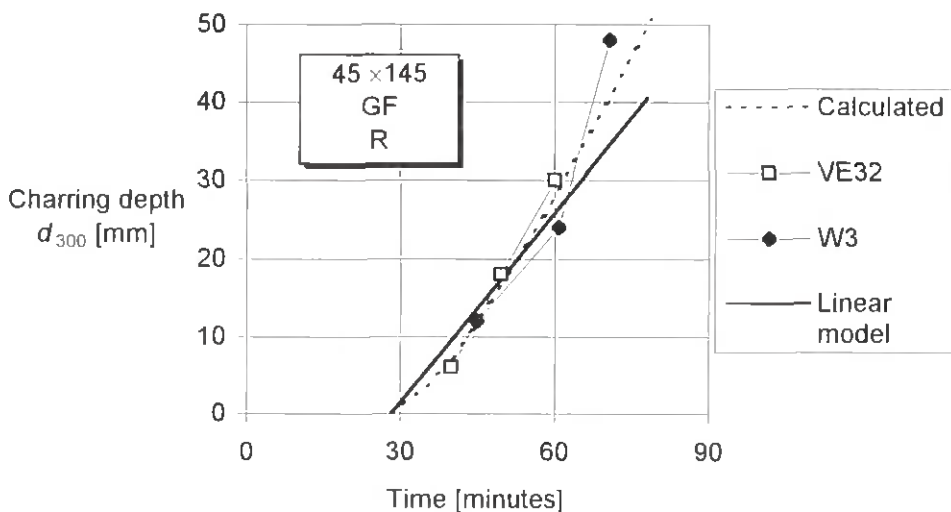


Figure 3.25: Linear model for charring depth for charring phase 2 — lining with one layer of gypsum plasterboard

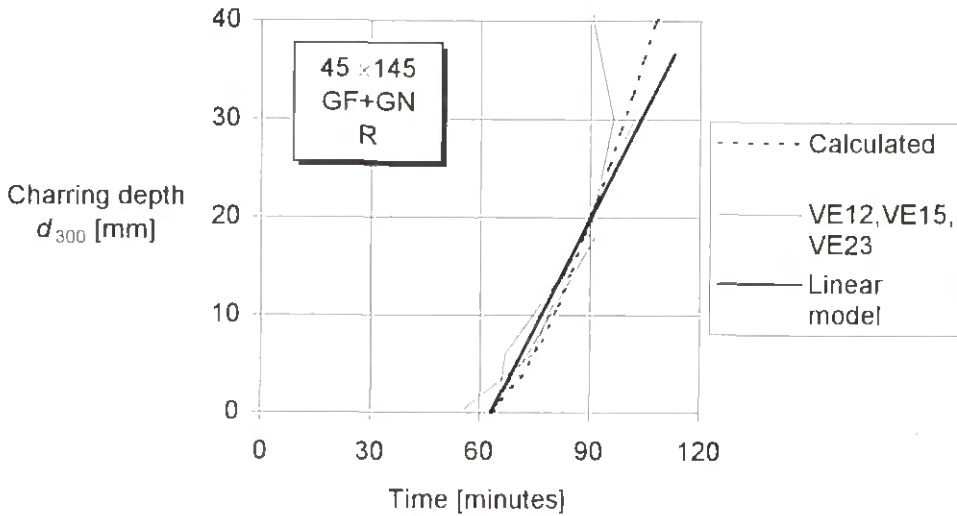


Figure 3.26: Linear model for charring depth for charring phase 2 — lining with two layers of gypsum plasterboard

Using the simplified linear relationship between charring depth and time and the corresponding charring rate $\beta_{2,linear}$, the insulation factor κ_2 was calculated from

$$\kappa_2 = \frac{\beta_{2,linear}}{\kappa_s \beta_0} \quad (3.4)$$

with $\beta_0 = 0,67$ mm/minute and κ_s according to equation (2.1). For members with a width of 45 mm the following results were obtained, see Figure 3.27:

- For boards without joint and joint configuration 2

$$\kappa_2 = -0,0073 h_b + 1,05 \quad (3.5)$$

- For joint configurations 1 and 3

$$\kappa_2 = -0,0037 h_b + 0,86 \quad (3.6)$$

For linings with joints in the outer layer, the charring rate is smaller, since charring starts earlier and the temperature according to the standard temperature-time curve is lower.

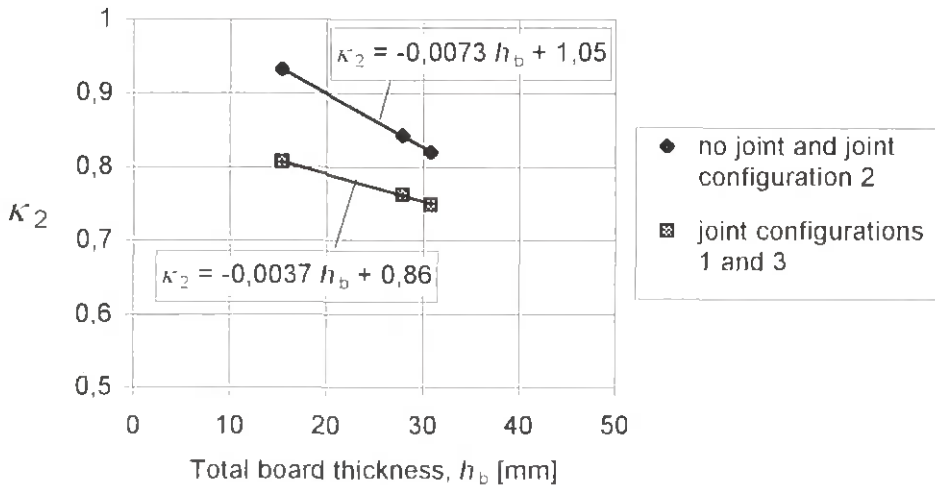


Figure 3.27: Insulation factor versus total board thickness of gypsum plasterboard

3.3.3 Post-protection phase — Charring phase 3

In the calculations of charring depth during charring phase 3, the lining was assumed to fail when the lining-wood interface temperature reached 300°C. The initial rise of the gas temperature was adjusted such that the calculated temperature gradient in the member was similar to the temperature gradient recorded in the tests when charring started. The calculations were performed for times of start of charring at intervals of approximately 10 minutes, see Figure 3.28. For comparison, also some results are shown from tests by König et al. (1997) where the lining fell off the member when charring started, or shortly after. In the tests the charring rate did not vary as much as in the calculations. For short failure times of the lining, the charring rate is underpredicted (in tests 3075 and 3092 the lining was made of two layers of 12 mm particleboard), while the calculation gives conservative results for large failure times, even if it is taken into account that the gypsum plasterboard lining did not fall off immediately after the start of charring.

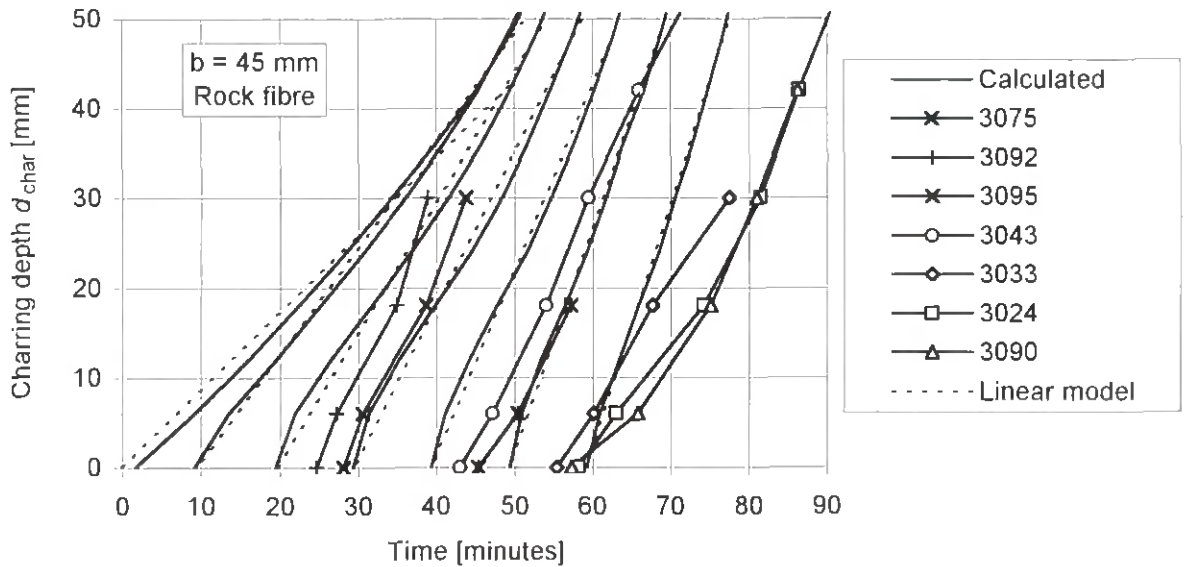


Figure 3.28: Effect of failure time of lining on charring depth versus time — Calculated values and test results for member width of 45 mm and cavity insulation of rock fibre

For simplification, the curves were fitted by a linear model. Figure 3.29 shows the variation of this constant charring rate as a function of the failure time of the lining. The post protection factor was determined by dividing these constant charring rates by the charring rate for charring phase 1 according to 3.3.1. as

$$\kappa_3 = \frac{\beta_{3,linear}}{\kappa_s \beta_0} \quad (3.7)$$

with $\beta_0 = 0,67$ mm/minute and κ_s according to equation (2.1), for members with a width of 45 mm the results are shown in Figure 3.30. The relationship between the post protection factor can be expressed as

$$\kappa_3 = 0,036 t_{bf} + 1 \quad (3.8)$$

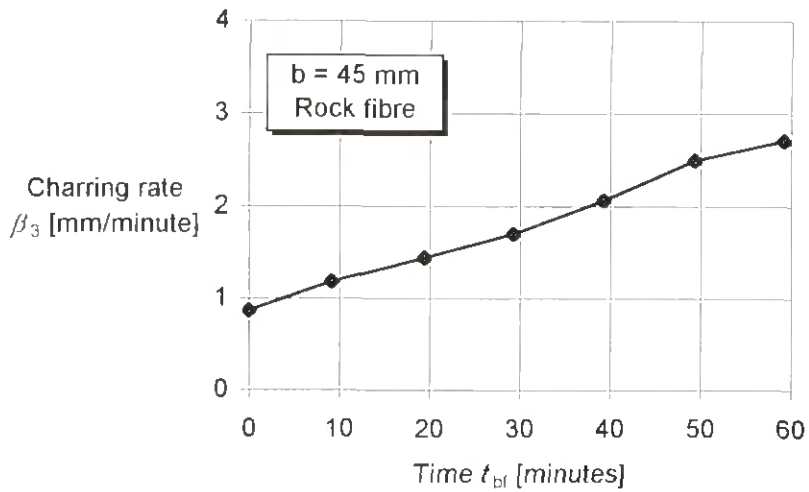


Figure 3.29: Charring rate (linear model) versus failure time of lining

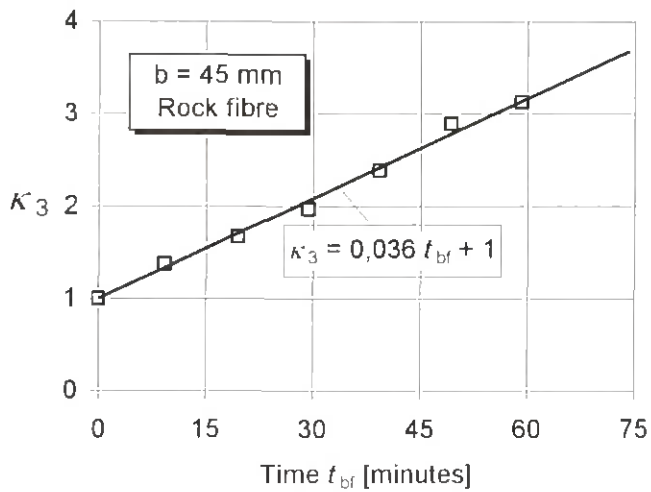


Figure 3.30: Post protection factor versus failure time of lining

Comparing Figure 3.28 with corresponding relationships (König et al. 1999) for wide members with one-dimensional heat transfer as shown in Figure 3.31, we can see that the initial slopes are about the same, since the initial heat transfer is one-dimensional in both cases. While for wide members a bilinear model was chosen in order to take into account the effect of increased insulation by the char layer, in narrow members this effect is compensated by a larger charring rate due to increased two-dimensional heat transfer.

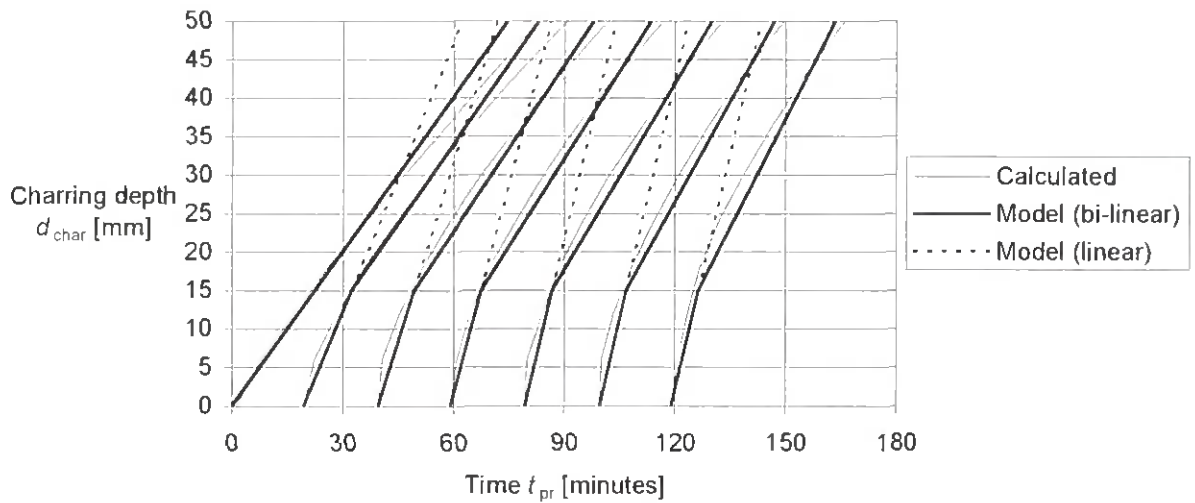


Figure 3.31: Effect of failure time of lining on charring depth versus time — Calculated values for wide members with one-dimensional heat transfer (König et al., 1999)

3.4 Residual cross section

3.4.1 Bending about stiff axis

The geometric properties of the residual cross section (see Figure 3.10) – i.e. the area, section modulus and the second moment of area – were calculated for some member dimensions and plotted against the charring depth ratio, see Figure 3.32 to 3.40. For dimensions 45 mm × 145 mm and 45 mm × 195 mm, also test results are shown as clusters of data points.

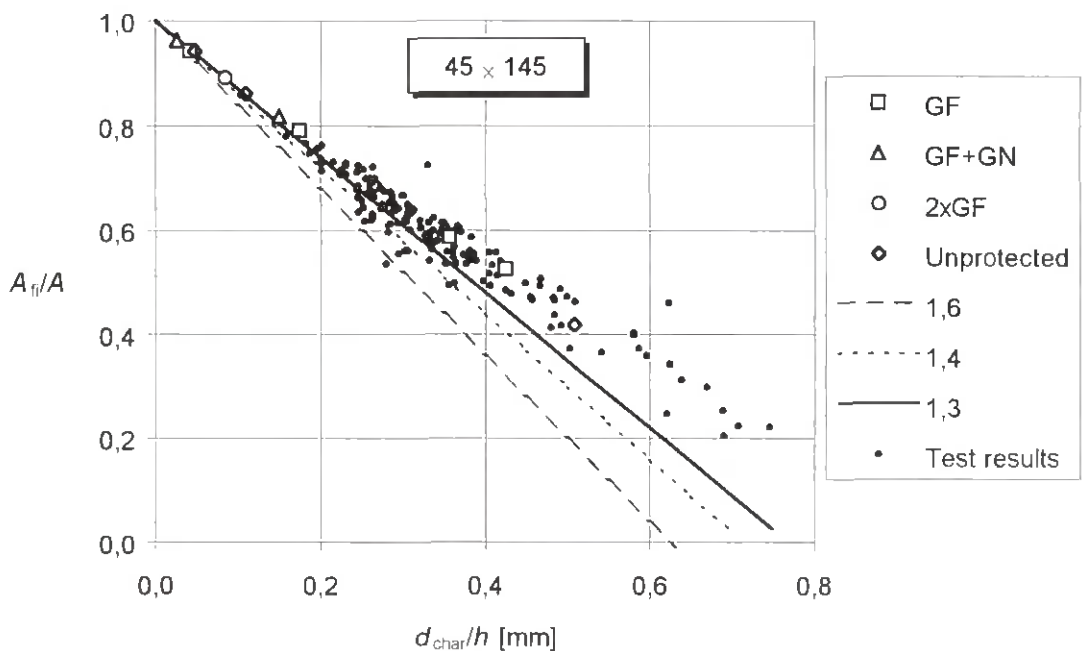


Figure 3.32: Reduction of cross section area versus charring depth ratio

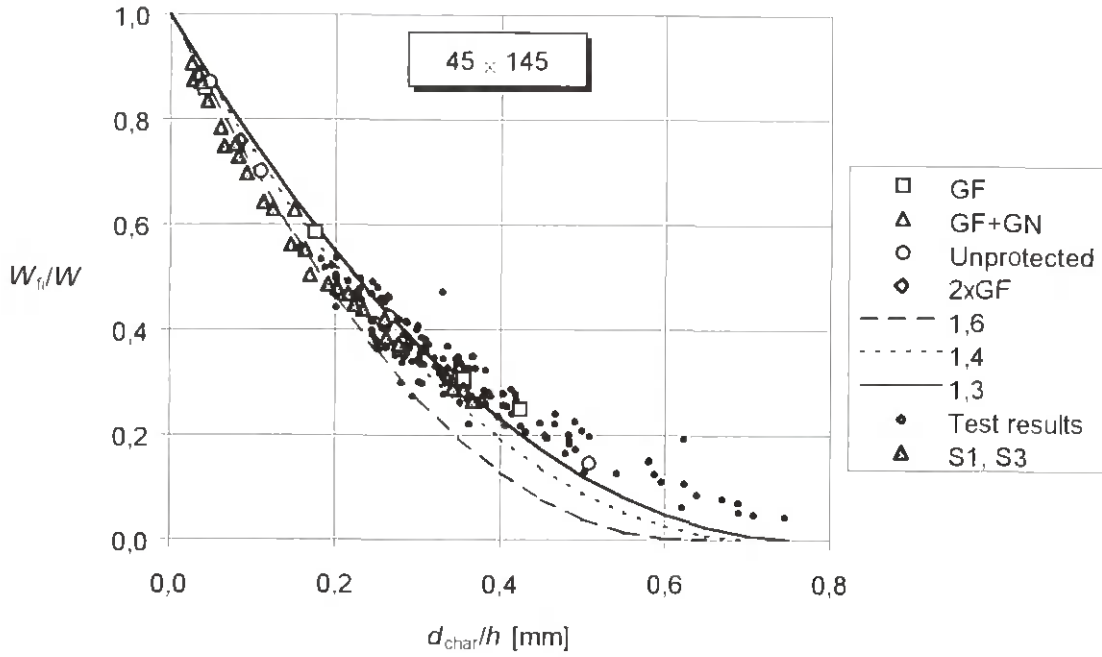


Figure 3.33: Reduction of section modulus versus charring depth ratio

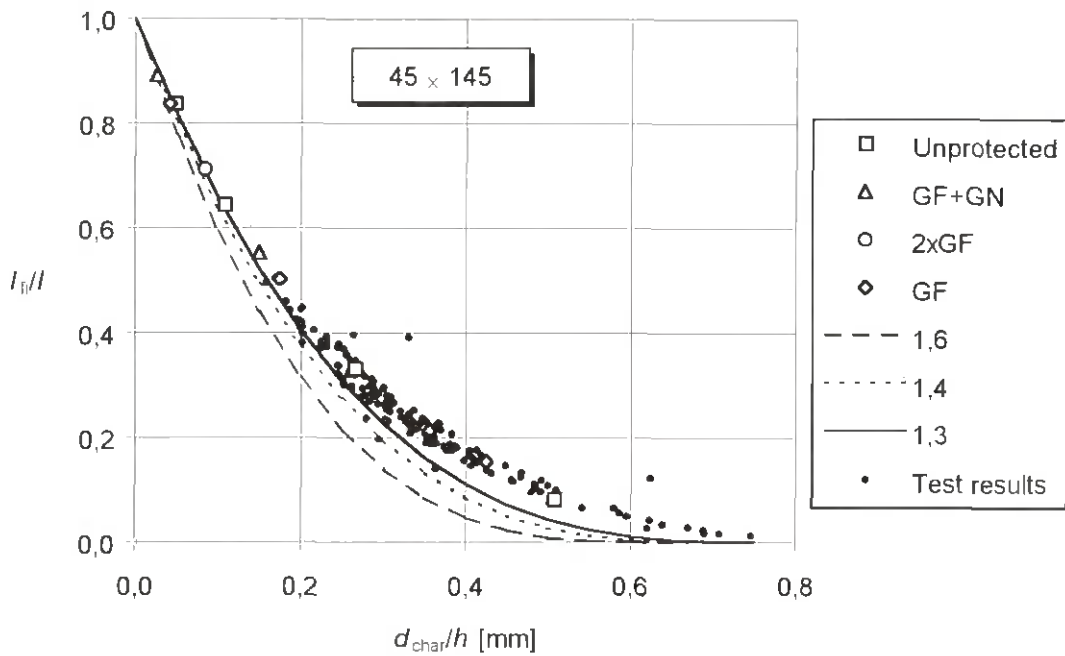


Figure 3.34: Reduction of second moment of area versus charring depth ratio

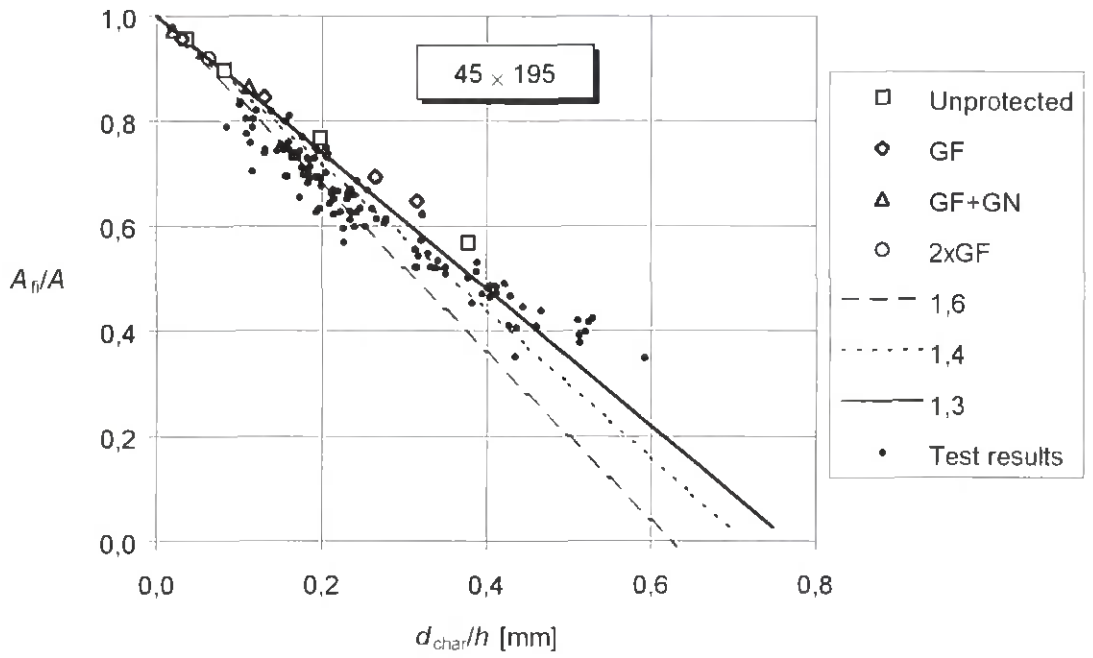


Figure 3.35: Reduction of cross section area versus charring depth ratio

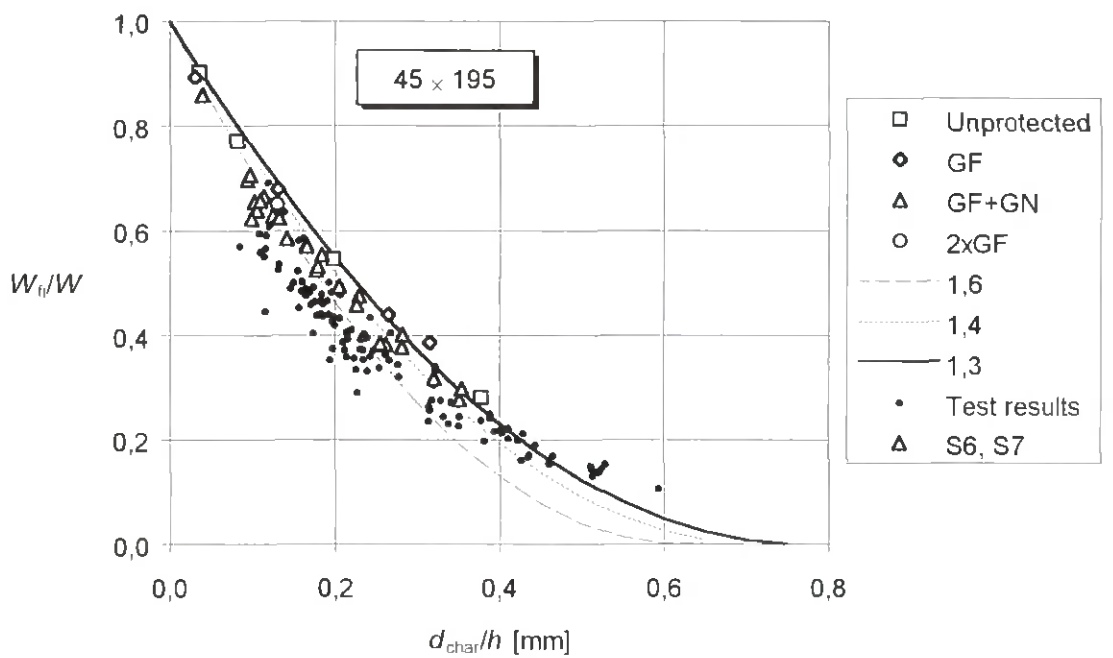


Figure 3.36: Reduction of section modulus versus charring depth ratio

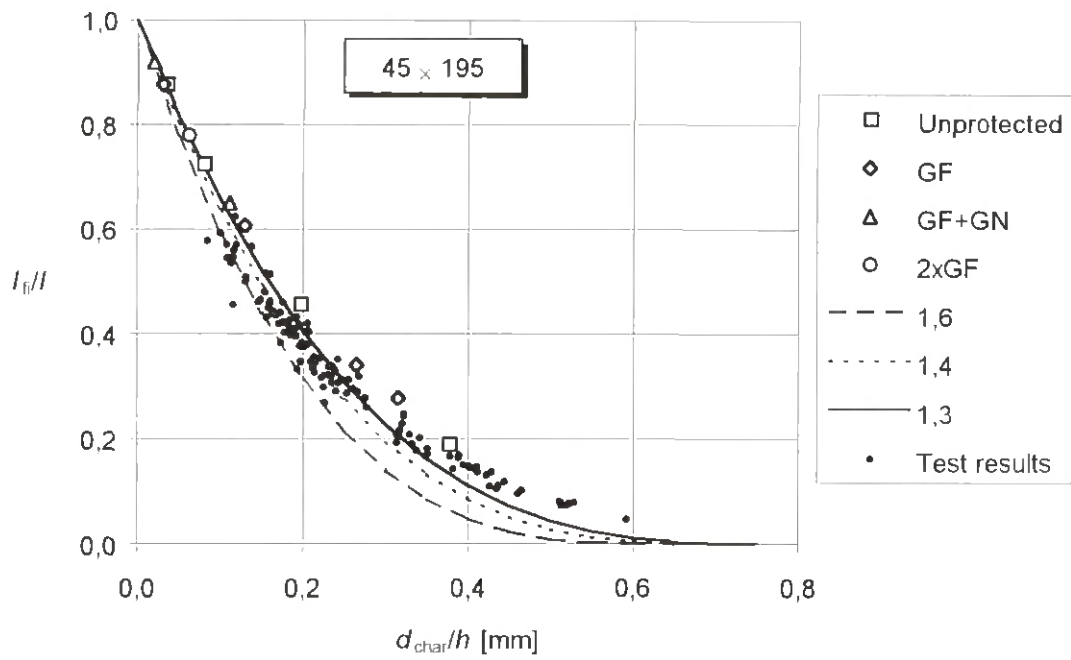


Figure 3.37: Reduction of second moment of area versus charring depth ratio

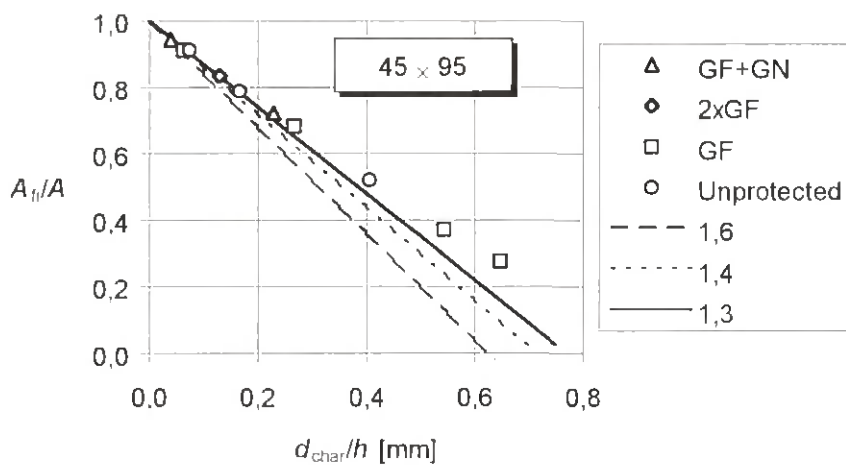


Figure 3.38: Reduction of cross section area versus charring depth ratio

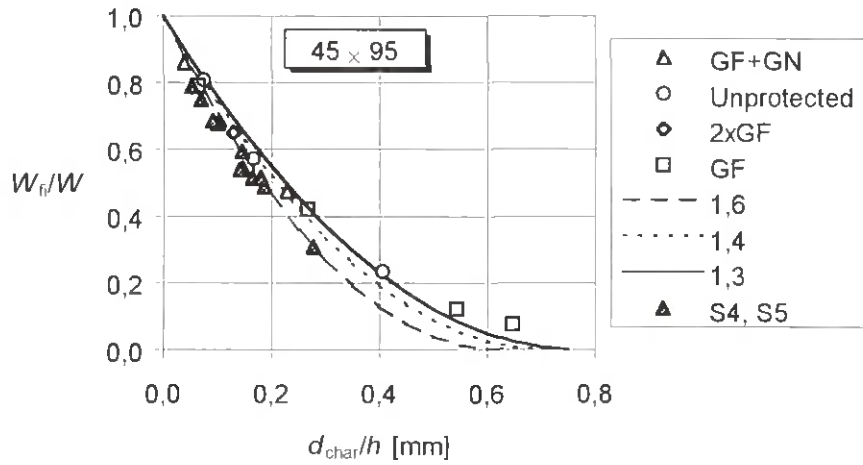


Figure 3.39: Reduction of section modulus versus charring depth ratio

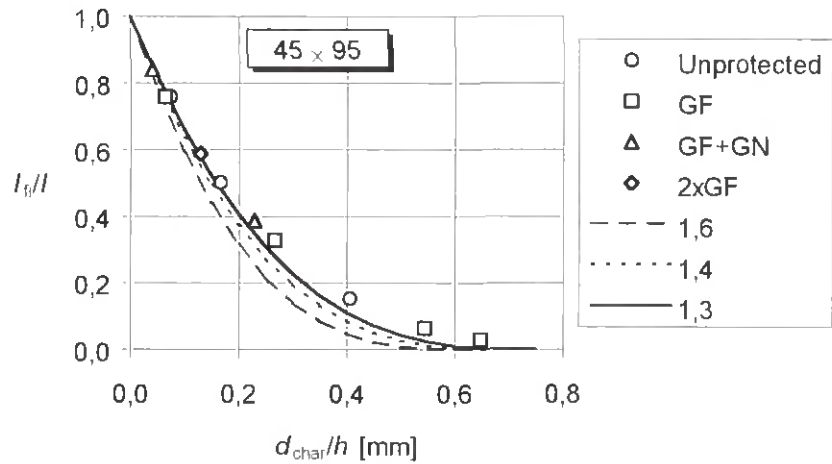


Figure 3.40: Reduction of second moment of area versus charring depth ratio

In order to simplify the calculation of cross section properties according to 2.2.2, relationships are given for notional rectangular shapes of the residual cross section, assuming that the depth of the residual cross section is given as

$$d_{char,n} = \kappa_n d_{char} \quad (3.9)$$

using different values of κ_n . Trial relationships of the cross sectional properties for $\kappa_n = 1,3$, $1,4$ and $1,5$ are included in the figures above. Unfortunately a single value does not fit all cases, however a value of $\kappa_n = 1,5$ will give conservative results in most cases.

3.4.2 Bending about weak axis

For bending about the weak axis, e.g. in the case of in-plane buckling of wall studs, $\kappa_n = 1,3$ is a reasonable approximation for the transformation of the residual cross section into a rectangular shape, see Figure 2.1. Since the same cross section should be used for bending about both axes, a value of $\kappa_n = 1,5$ should be used giving conservative results.

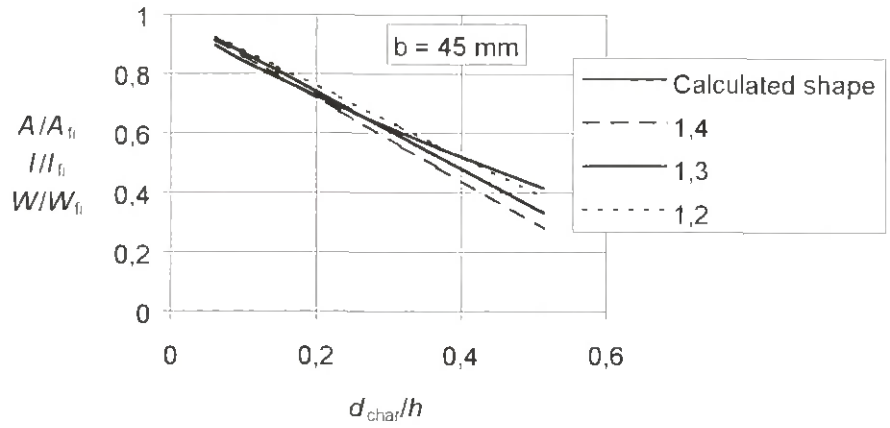


Figure 3.41: Reduction of cross section properties versus charring depth ratio — calculated cross section and simplified rectangular model for different values of κ_0

4 Mechanical model of timber cross section

4.1 General

The strength and stiffness parameters given in design codes, i.e. the strength in bending, compression and tension, and the modulus of elasticity were determined on the assumption of a linear relationship between strain and stress until failure and shall therefore only be applied for such situations. In other words, these parameters are apparent parameters, that include the effects of inhomogeneities due to knots and deviations of grain direction, and in the case of bending, also the non-linear relation between strain and stress. In the following, we have to distinguish between these apparent values and the localized values that are used in order to derive apparent strength and stiffness parameters of timber exposed to fire. The localized values correspond normally to the properties of small pieces of clear wood without, or almost without, defects. The objective of this section is the determination of apparent strength and stiffness parameters of cross sections, using localized material strength and stiffness properties under the influence of localized temperature and moisture conditions in the member.

Since deformation verification is not required in structural fire design, the flexural stiffness of members is not used other than in buckling analyses e.g. of wall studs. In the following, for simplification, the flexural stiffness was determined for pure bending, having in mind, that these conditions correspond to the ultimate stage of buckling of slender compression members where the bending moment is prevailing rather than the compressive force.

Efforts have been made to determine the mechanical properties of timber cross sections at elevated temperatures, taking into account the localized temperature and moisture conditions in the member and the temperature and localized moisture-dependent strength and stiffness parameters of wood. For glued-laminated beams, the load-carrying capacity was determined by Schaffer et al. (1986), using localized strength and stiffness properties as reported by Schaffer (1984). A fictitious zero-strength layer of thickness 7,6 mm was determined that should be subtracted from the residual cross section, such that the remaining cross section with unreduced strength and stiffness values would have the same bending moment capacity as the residual cross section with reduced values. This method was adopted in ENV 1995-1-2 (1994) with a fictitious zero-strength layer of 7 mm. For large cross sections, these calculations give reasonable results, since only limited parts of the cross section are affected by elevated temperature. For small cross sections as they are used in light timber frame construction, however, the calculations lead to unsafe results.

In a previous investigation, König (1995) studied the performance of timber frame members in bending at standard fire exposure. The test results showed that extensive plastic flow occurred in the timber members, giving rise to the neutral axis being moved towards the unexposed side of the member. This effect was more pronounced when the exposed side of the timber member was in compression. It was argued that the conditions in the wood were to some extent similar to those when applying the technique of steaming for bending of wood, e.g. when manufacturing furniture. Evaluating the test results by König (1995), Thomas (1997) simulated these conditions by assuming a pronounced decrease of the localized compressive strength in the region of 100°C, while the reduction of tension strength was less, see Figure 4.1. Corresponding reductions of the modulus of elasticity as used by Thomas are shown in Figure 4.2. Since more test results (König et al., 1997) are now available, in the following further calibration of wood properties to test results is performed.

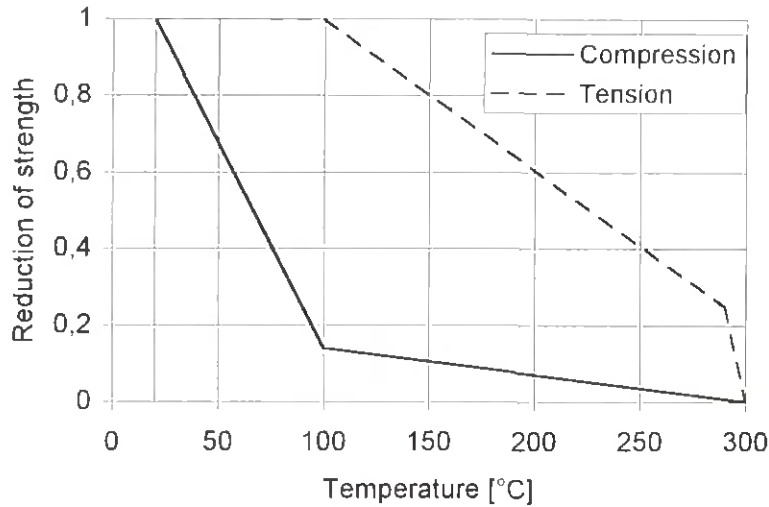


Figure 4.1: Effect of temperature on strength (Thomas, 1997)

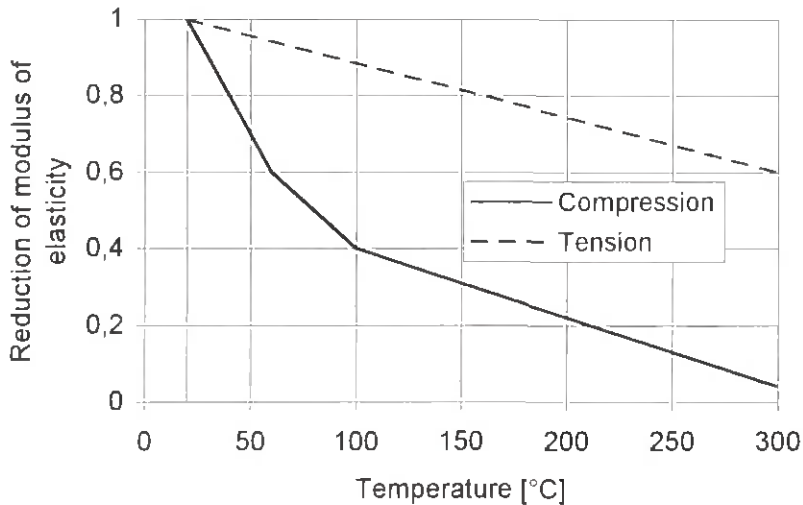


Figure 4.2: Effect of temperature on modulus of elasticity (Thomas, 1997)

4.2 Computer program for cross section of timber member

For the calculation of the moment capacity and the flexural stiffness of timber members, a computer program was developed applying spreadsheet modelling. The cross section was defined by a grid dividing half of the width into ten and the depth into forty elements, i.e. the same grid was used as in the calculations of the temperature field in the cross section. Where charring occurred, only elements with a maximum mean temperature of 300°C were included in the residual cross section. For each element the stress was determined assuming linear strain variation across the depth of the cross section adopting a relevant stress-strain relationship, see below (Figure 4.16). The stress distribution across the depth was determined by iteration, with the extreme fibre strain at one side and the curvature of the member as input parameters until equilibrium of forces in axial direction was satisfied. The resulting bending moment was then determined by taking the sum of moments of internal forces of each element about the neutral

axis. This procedure was repeated with a new higher edge strain, until the moment capacity reached a maximum, or a specified bending moment.

4.3 Determination of apparent bending strength

4.3.1 Expressions

The bending moment capacity of a member exposed to fire is

$$M_{fi} = M_{ult} \frac{W_{fi}}{W} \frac{f_{m,fi}}{f_m} \quad (4.1)$$

where

- M_{ult} is the bending moment of the member at normal temperature
- W is the section modulus of the original cross section
- W_{fi} is the section modulus of the residual cross section
- f_m is the bending strength at normal temperature
- $f_{m,fi}$ is the bending strength of the residual cross section.

Inserting

$$k_{mod,fi,lim} = \frac{f_{m,fi}}{f_m} \quad (4.2)$$

and rearranging expression (4.1) gives the following expression for the calculation of the modification factor for fire:

$$k_{mod,fi,lim} = \frac{M_{fi}}{M_{ult}} \frac{W}{W_{fi}} \quad (4.3)$$

4.3.2 Mechanical properties of timber

4.3.2.1 Normal temperature

In the tests conducted by König (1995) and König et al. (1997) timber was used that was fairly free from knots and other defects. Thus the bending strength of the members was high as can be seen from the results of reference tests conducted at normal temperature. Further, the bending strength of members used in the fire tests could be predicted fairly well by taking into account only dry density as relevant parameter. In Part 1 of this investigation (König et al., 1997), the following expressions for the regression between dry density ρ_{0w} and bending strength f_m were found:

For cross sections of size 45 mm × 145 mm

$$f_m = 0,1484 \rho_{0w} \quad (4.4)$$

and for size 45 mm × 195 mm

$$f_m = 0,1215 \rho_{0w} \quad (4.5)$$

Since the compression strength of the material used in the reference tests was not determined, we have to make assumptions when describing the stress distribution across the depth of the members. A typical stress-strain relationship for wood is shown in Figure 4.3 a

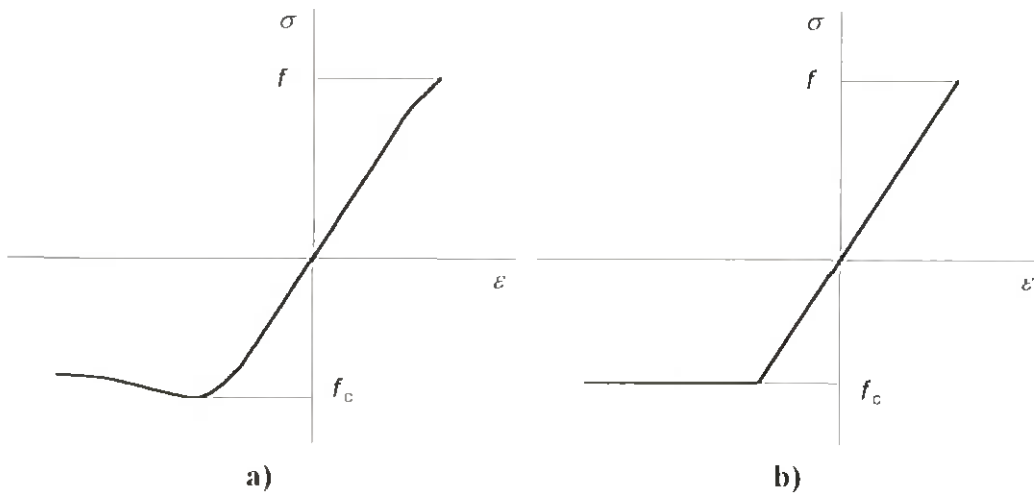


Figure 4.3: Stress-strain relationship for wood
a) nonlinear, b) simplified

For simplicity, the nonlinear behaviour is often replaced by linear elastic behaviour for tension and bilinear elastic-plastic behaviour for compression according to Figure 4.3b. Using this simplified relationship, the maximum value of the compression strength f_c is somewhat smaller than the exact value due to the decrease of compression strength when the strain increases.

Bazan (1980), as referenced by Buchanan (1990), proposed a bilinear stress-strain relationship that takes into account the falling branch beyond maximum compression strength. Buchanan (1990) used this approach for explaining the bending behaviour of timber beams.

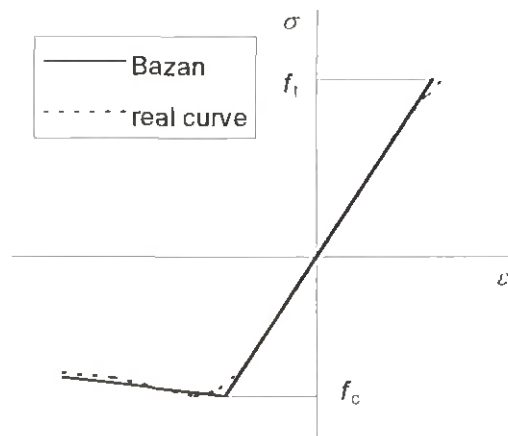


Figure 4.4: Simplified stress-strain relationship proposed by Bazan (1980)

Considering a cross section of size $45 \text{ mm} \times 145 \text{ mm}$, from expression (5.1) we obtain for a dry density of 438 kg/m^3 a bending strength of 65 N/mm^2 and a moment capacity of $10,25 \text{ kNm}$. For a cross section of size $45 \text{ mm} \times 195 \text{ mm}$ with the same dry density, from expression (5.2) we obtain a bending strength of 53 N/mm^2 and a moment capacity of $15,18 \text{ kNm}$.

For clear wood of pine and spruce, typical values of compression strength are between 40 and 50 N/mm². Assuming a density of 438 kg/m³ (see above) and a moisture content of about 13 %, according to Thunell (1941), the compression strength of clear wood of Swedish pine is about 47 N/mm². Considering that the compression strength of spruce is slightly lower than the compression strength of pine (Kollmann, 1951a), it is assumed that the compression strength is 44 N/mm². Using the stress-strain relationship according to Figure 4.3b, for a cross section of 45 mm × 145 mm and a moment capacity of 10,25 kNm, the tensile stress is determined as 72 N/mm². The resultant simplified stress distribution at ultimate limit state is shown in Figure 4.5a.

For member size 45 mm × 195 mm the corresponding stress distribution at ultimate limit state at normal temperature is shown in Figure 4.5b with 54,6 N/mm² as the maximum tensile stress.

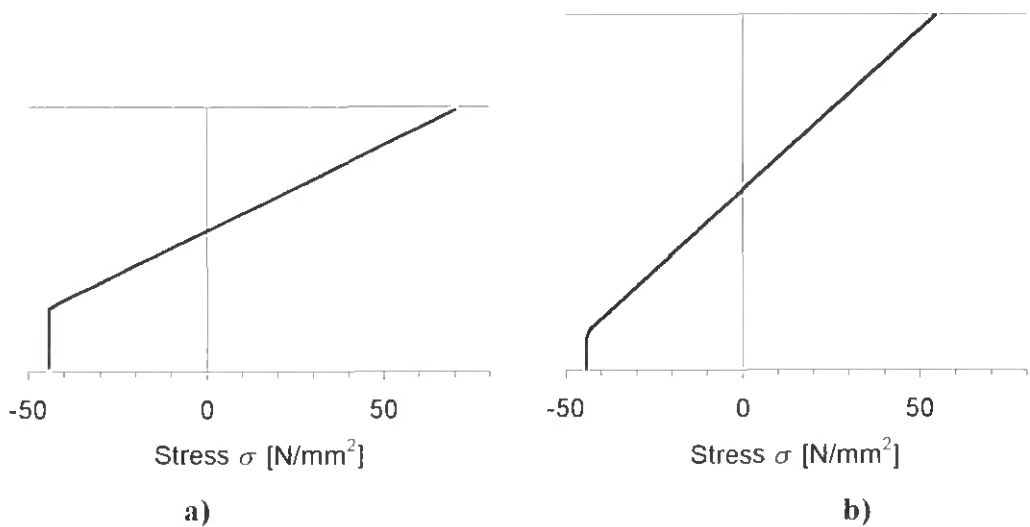


Figure 4.5: Stress distribution at normal temperature for a cross section of
a) 45 mm × 145 mm
b) 45 mm × 195 mm

Both stress distributions of Figure 4.5 show that the degree of compression yielding is moderate. This justifies the use of the simplified stress-strain relationship of Figure 4.3b.

Moment-curvature relationships were determined for both cross sections, see Figure 4.6. The curves bear a close resemblance with test results where crushing of the wood is observed on the compression side of the member.

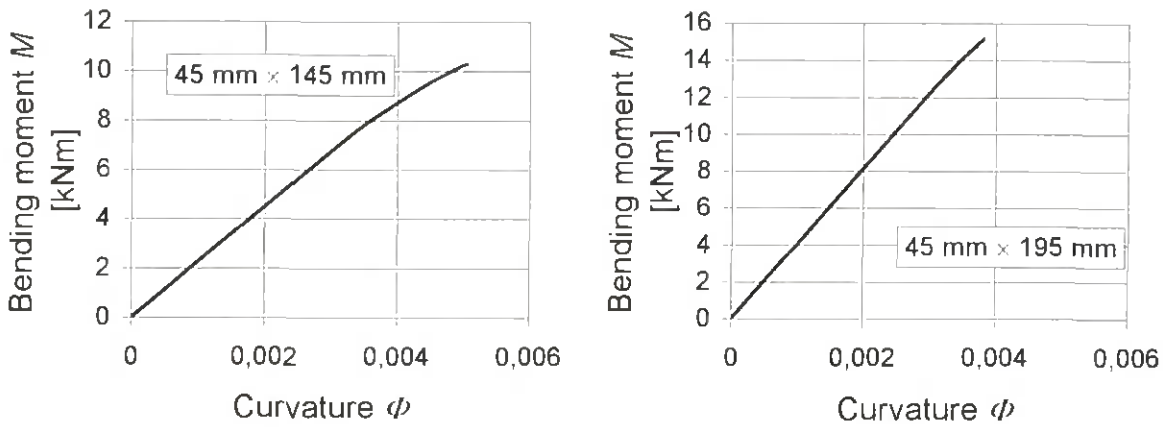


Figure 4.6: Calculated moment-curvature relationships

4.3.2.2 Mechanical properties of timber at elevated temperature

4.3.2.2.1 General

Using the approach by Thomas (1997) as a starting point, see 4.1, in the following the effect of temperature on strength and stiffness both in compression and tension is determined. During this process data found in other sources were used and calibrated to fit the test results given by König (1995) and König et al. (1997). Since the members were exposed to fire on one side only, it was possible to study each of the four parameters separately. Where, for example, the fire-exposed side was in compression, the parts of the cross section that were in tension were not, or only to a small degree, affected by elevated temperature.

The first step was to determine the effect of temperature on the modulus of elasticity. The calibration was done using test results regarding the relationship between flexural stiffness and time, see 4.3.2.2.2.

Having determined the effect of temperature on the modulus of elasticity, in the next step the effect of temperature on material strength was determined, using the test results at failure, see 4.3.2.2.3.

4.3.2.2.2 Modulus of elasticity

The effect of temperature on the modulus of elasticity is given in some sources. Kollmann (1951b) measured the effect of temperature on the modulus of elasticity of heated specimens in bending. The tests were performed using specimens that were at room temperature or heated to a constant temperature of 40, 60, 80 and 100°C respectively, each of them repeatedly being loaded and unloaded at time intervals of 1,5 minutes or more during a total test duration of 60 minutes. The lowest moduli of elasticity were recorded at the second or third loading cycle when the target temperature was almost uniform in the specimen. During the following loading cycles, due to the drying of the material beginning on the surface and then continuing to the middle of the specimens, the modulus of elasticity increased again. For specimens with an initial moisture content of 11,4 percent, the minimum modulus of elasticity decreased linearly

to about 40 percent of its initial value between room temperature and 80°C, see Figure 4.7. For a temperature of 100°C the modulus of elasticity increased again to 55 percent due to the drying of the material. Since the obtained relationship is for bending, it can be assumed that corresponding relationships for tension and compression should be in the same order of magnitude.

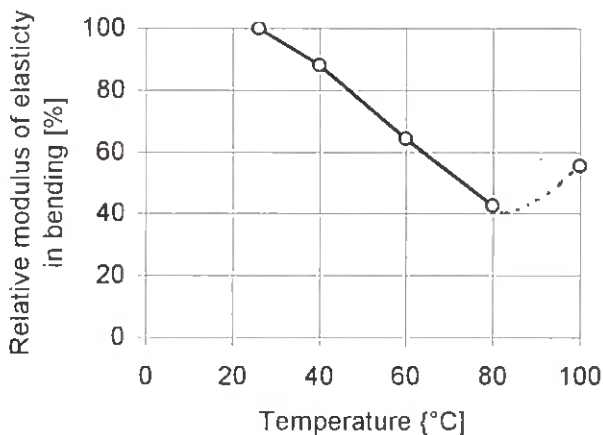


Figure 4.7: Effect of temperature on relative modulus of elasticity in bending (Kollmann, 1951b)

The data given in most other sources deviate considerably from these values. Some of them are given in the following.

As referenced by Kollmann (1951a), Kollmann et al. (1944) found that the modulus of elasticity of pine in compression decreased between 20 and 100°C by approximately 33 percent.

Schaffer (1984) gives data for the modulus of elasticity parallel to grain without distinguishing between compression, tension or bending. In the range between 20 and 180°C for a moisture content of 12 percent, the effect of temperature is very small (approximately 12 percent). From 180°C the modulus of elasticity linearly to zero at 300°C.

Glos et al. (1991) conducted tests on structural timber of sizes used in practice in bending, compression and tension. For tension and bending, for timber with an initial moisture content between 7 and 10 percent, at 100°C the modulus of elasticity has decreased to 88 percent of its initial value in tension, and to 75 percent in bending. The loading rate was constant, leading to failure after approximately 80 seconds in the tension tests and 130 seconds in the bending tests.

Other sources are Gerhards (1982) and Östman (1985) with similar values for modulus of elasticity in tension. The tests by Östman (1985) were conducted with a strain rate of 8 percent per minute and times to failure of as short as approximately 10 to 12 seconds.

All these values deviate considerably from those given by Kollmann (1951b) for the temperature range between 20 and 100°C. There are several reasons for this. One is that it is difficult to maintain a controlled level of moisture content during the tests, except the tests conducted by Östman (1985) where wood specimens were submerged in silicone oil in order to obtain stable moisture conditions. Another reason is the effect of loading rate; already

considerable at normal temperature, it is much greater at elevated temperatures and sensitive to moisture. At elevated temperatures and high moisture content creep deformations increase dramatically (Arima, 1979 and Bach, 1965, as referenced by Schaffer, 1984). This effect is important since moisture accumulation up to 20 percent and more occurs in the parts of the cross section with temperatures near 100°C (White et al., 1981, Fredlund, 1988). Since most researchers referenced above used high loading rates, the effect of time dependent creep prior to the wood drying out (starting at temperatures above 100°C) is not, or only to a minor degree, included.

When temperature exceeds above 100°C, the wood starts to dry out. As long as moisture is left in the wood, creep will occur as described above. Additionally, mechano-sorptive creep can be assumed to play an important role during the drying of the wood. The existence of steam as such, however, has no influence on creep (Kollmann, 1939). In industrial processes as steaming for bending of wood, the steam is rather a tool for heating than making the wood soft. Any treatments that heats the wood to about the boiling point of water without causing it to dry would serve (Stevens et al., 1970).

In the fire tests by König et al. (1997), during the pre-charring phase the flexural stiffness decreased at an approximately constant rate, see Figure 4.8. From the temperature histories can be seen that this rate changes immediately when the temperature of the timber member leaves the one-hundred degree level, and finally at the time of onset of charring behind the protection of gypsum plasterboard. At normal load levels, at this stage the state of stress is still elastic, see below. Therefore, it is possible to calibrate the effect of temperature without the results being influenced by the effect of temperature on the compression and tension strength.

The tests mentioned above were conducted such that the fire-exposed side was in compression or tension. Thus, during the calibration using the model described in 4.2, it was possible separate the effect of temperature on the modulus of elasticity in compression and tension. The test results of König et al. (1997) show that the flexural stiffness decreases somewhat more when the fire-exposed side is in compression, see Figure 4.8. The curves were taken from Figure 6.8, 6.9, 6.24 and 6.25 of Part I of this investigation (König et al., 1997) and refer to assemblies with double layers of gypsum plasterboard and cavity insulation made of rock or glass fibre.

The same can be seen from test results reported by König (1995), see the relationships between flexural stiffness ratio and time, some of which are shown in Figure 4.9 for tests with load ratios of about between 0,1 and 0,3 of test series S1 and S3. During the first ten minutes of fire exposure, the difference of flexural stiffnesses between the two series is small since the stresses are small and still in the elastic range. Later on, the difference increases due to plastic flow on the compression side when exposed to fire (see 4.3.2.2.3).

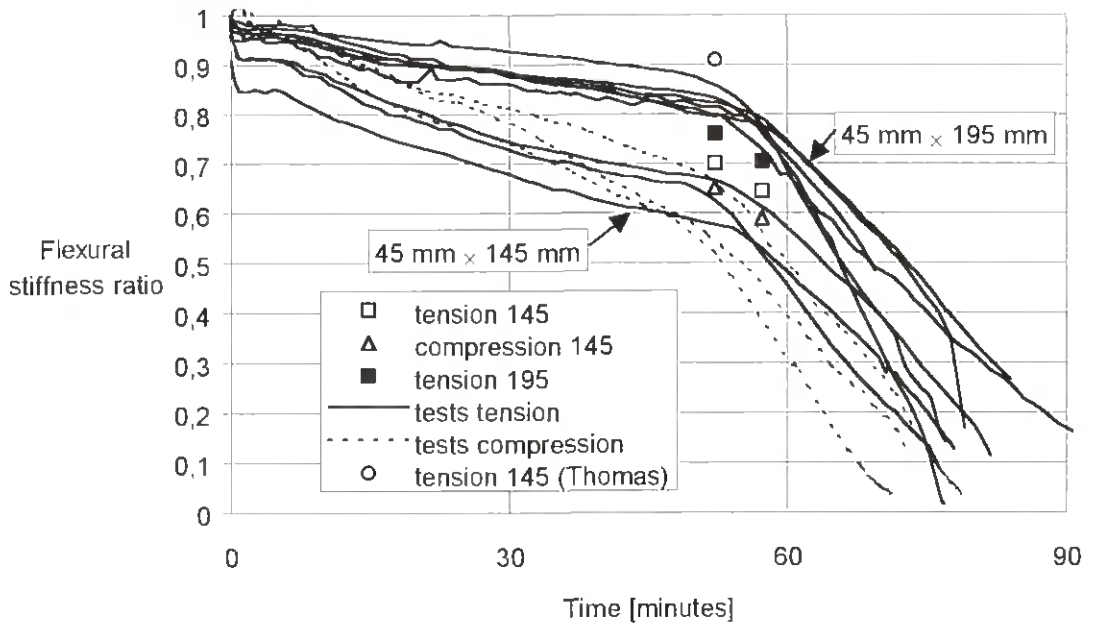


Figure 4.8: Flexural stiffness ratio versus time for assemblies exposed to standard fire with two layers of gypsum plasterboard (GN+GF, values from König et al., 1997) – Test results and calculated values at start of charring at arrises and middle of member

The reduction model chosen here was bilinear with a breakpoint at 100°C, see Figure 4.10, with coordinates of the breakpoints determined by calibration. We can see that the effect of temperature on the modulus of elasticity in tension is of the same order of magnitude as in compression, contrary to the values reported by most sources.

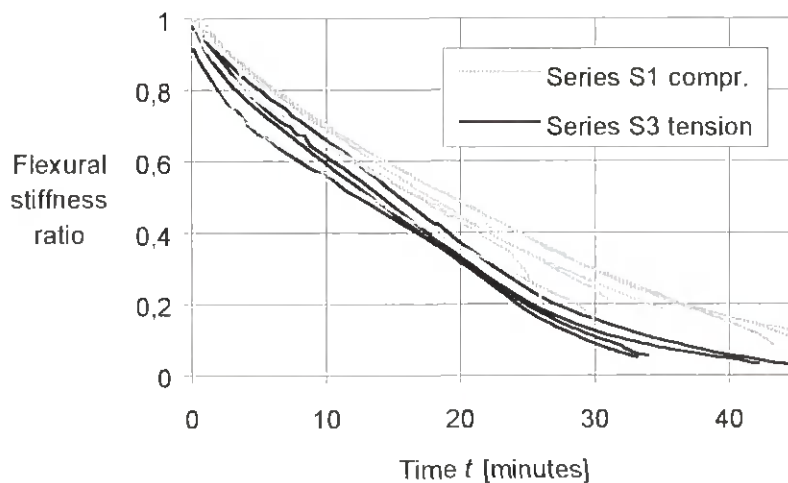


Figure 4.9: Flexural stiffness ratio versus time for members without lining and load ratios between about 0,1 and 0,3 (König, 1995)

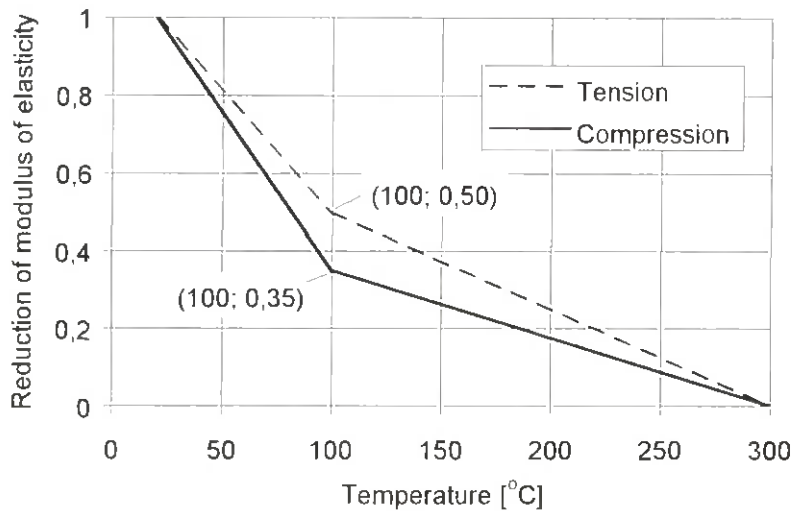


Figure 4.10: Effect of temperature on modulus of elasticity as used in this study

The reduction of the flexural stiffness was calculated for two stages: When

1. charring started at the arrises and
2. charring started in the middle of the width of the member.

At these stages the cross section is not, or only to a small degree, reduced by charring. Since the timber member is preheated when charring starts, with a stable temperature profile, the effect of the reduction of the modulus of elasticity on flexural stiffness can be separated from the effect of charring. Figure 4.11 shows the temperature profile along the centre line of the cross section when charring starts (stage 2 above).

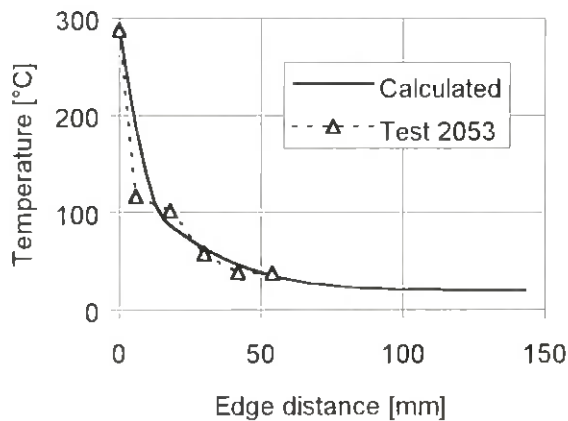


Figure 4.11: Calculated temperature profile along centre line of cross section at start of charring compared with an example of test result (König et al., 1997)

In the first case, the residual cross section was still equal to the original cross section, while there was some reduction of the cross section in the second case. In Figure 4.8 the results are compared with test results. For case 2, the calculated flexural stiffness ratios were plotted at 57,3 minutes, that is the mean value of start of charring recorded in the tests. At this stage the second moment of area of the original cross section is reduced by 3,3 percent, i.e. the major part of the reduction of flexural stiffness is due to the reduction of modulus of elasticity. From

Figure 4.12, showing the stress distribution along the centre line of the member, it can be seen that failure stresses are not reached in the cross section. Since the time of start of charring at the arrises of the member could not be determined during the tests, it was determined by calculation as 5 minutes prior to case 2.

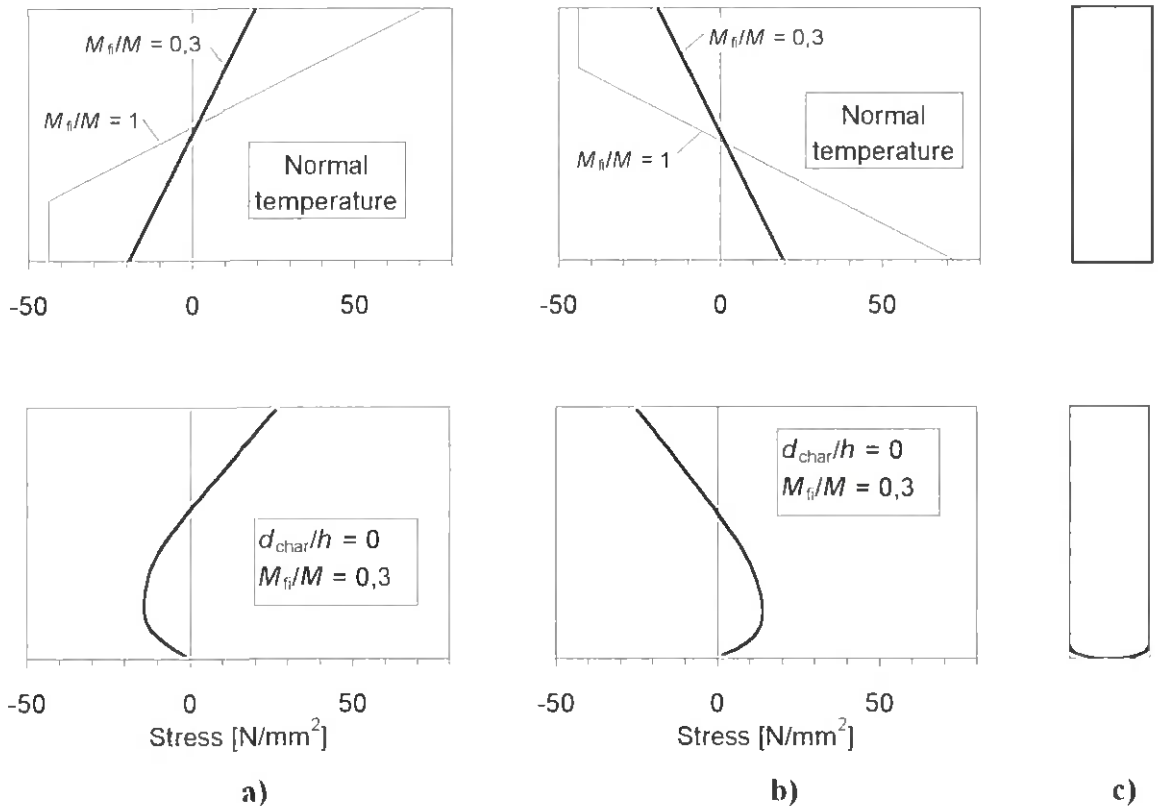


Figure 4.12: Stress distribution along centre line of member at normal temperature and at start of charring in the middle of the member for the exposed side in compression (a) and tension (b), and residual cross section (c)

Compared to the experimental results, the values for 145 mm deep members are a little too high, while the value for 195 mm deep members is a little too low, see Figure 4.8. For 195 mm deep sections with the fire exposed side in compression no tests were performed.

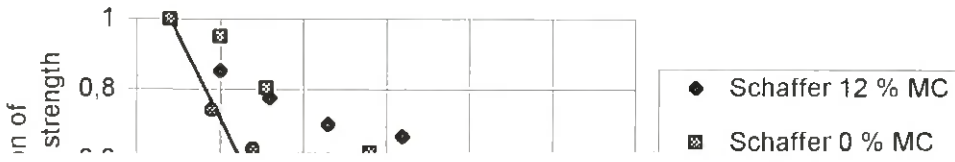
For comparison, for a cross section of size 45 mm × 145 mm, using the effect of temperature on the modulus of elasticity in tension as assumed by Thomas (1997) (see Figure 4.2, and similar to most other sources), a value of $k_{\text{mod,fi,E}} = 0,91$ was calculated, see Figure 4.8. This value is considerably greater than 0,70, calculated using the relationship for tension of Figure 4.10, and the test results.

A conclusion is that the assumption of this study regarding the effect of temperature on the modulus of elasticity is more reasonable than values given in other sources. The assumed relationships are justified by

1. the effect of elevated temperature and moisture content in the wood for temperatures including creep
2. the effect of elevated temperature and mechano-sorptive creep at temperatures above 100°C
3. the effect of increasing degradation of wood at temperature above 200°C.

4.3.2.2.3 Strength

Strength versus temperature values reported in different sources exhibit a large scatter and are partially in contradiction to each other. Data from some sources (Schaffer, 1984, Glos et al., 1991, Kollmann, 1951a) are shown in Figure 4.13 and 4.14 together with relationships used in this study, see below. Both relationships are also shown in Figure 4.15. Schaffer's (1984) values had to be transformed by decreasing them by approximately two percent, since they were related to an ambient temperature of 25°C instead of 20°C. The discrepancies between the values from different sources can be explained by difficulties in achieving well-defined test conditions of equal temperature and moisture content in the test pieces, especially when timber of structural sizes were tested (Glos et al., 1991).



Jürgen König, Lars Walleij

Timber frame assemblies exposed to standard and parametric fires Part 2: A design model for standard fire exposure

TräteK, Rapport I 0001001

ISSN 1102 – 1071

ISRN TRÄTEK – R – 00/001 – SE

Nyckelord

assemblies
design
fire
floors
model
timber
walls
wood

Unlike the values given above, there is a considerable effect of moisture content on the tensile strength, see Figure 4.14. For temperatures greater than 150°C, due to the drying of the wood, the values are similar independently of the initial moisture content. This is contradictory to the test results by Kollmann (1951b) where increased values of modulus of elasticity were measured for temperatures greater than 100°C, see Figure 4.7.

The values for strength reduction used in this study are throughout smaller than those from other sources. A simple bilinear relationship was chosen with a breakpoint at 100°C. For temperatures between 100 and 300°C this is certainly a crude approximation, since the relationship takes not into account that the drying of the wood causes a smaller reduction than assumed. The relationship chosen is justified since only a small portion of the heat affected zone is in the temperature range between 100 and 300°C while the greater portion is in the range up to 100°C.

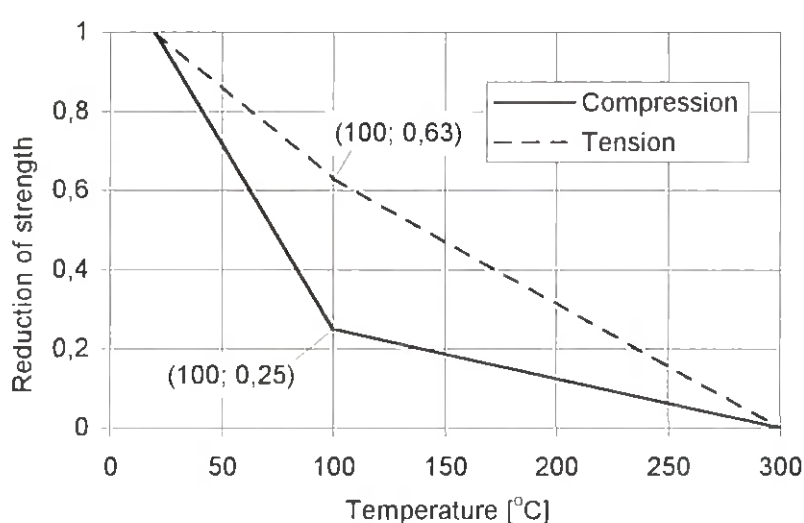


Figure 4.15: Reduction of strength versus temperature as used in this study

Assuming the strain-stress relationship at normal temperature according to Figure 4.3b and applying the reduction curves of Figure 4.10 and 4.15, resultant relationships for different temperatures are shown in Figure 4.16.

Figure 4.18 shows strain-stress relationships along the centre line of the cross section of size 45 mm × 145 mm, determined for ultimate bending moments at different stages of charring for the fire exposed side in compression (left) or tension (right). It is assumed that the member is protected by a lining consisting of two layers of gypsum plasterboard. When charring starts, the zone in the member near the interface between the member and the lining is preheated, causing a reduction of moment capacity even though there is no charring except near the arrises of the member. As a completion to one of the stress distributions shown in the figure, the entire stress distribution is shown in Figure 4.19.

Citat tillåtes om källan anges.

Reports issued by the Swedish Institute for Wood Technology Research comprise complete accounts for research results, or summaries, surveys and studies. Published reports bear the designation I or P and are numbered in consecutive order together with all the other publications from the Institute.

Extracts from the text may be reproduced provided the source is acknowledged.

som utörs med egna, samverkande och externa resurser. Träteknik har forskningsenheter i Stockholm, Jönköping och Skellefteå.

The Swedish Institute for Wood Technology Research serves the five branches of the industry: sawmills, manufacturing (joinery, wooden houses, furniture and other woodworking plants), fibre board, particle board and plywood. A research and development agreement between the industry and the Swedish National Board for Industrial and Technical Development forms the basis for the Institute's activities. The Institute utilises its own resources as well as those of its collaborators and other outside bodies. Our research units are located in Stockholm, Jönköping and Skellefteå.

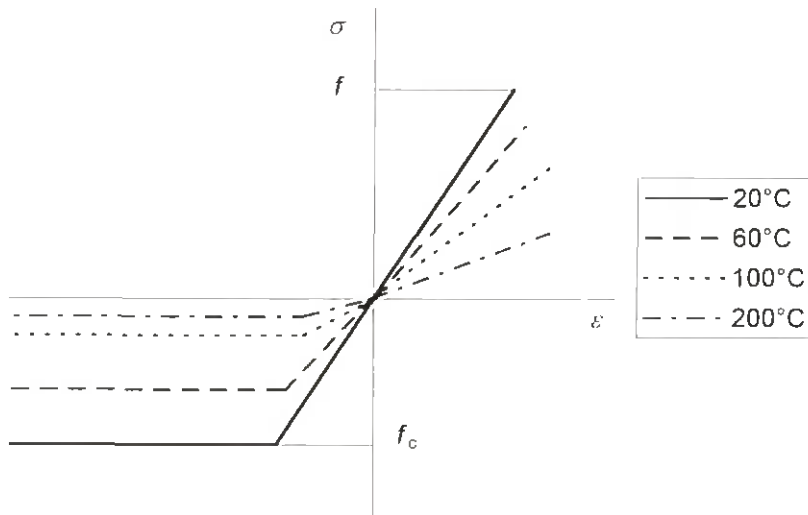


Figure 4.16: Temperature dependent strain-stress relationships

The variation of load bearing capacity dependent on the degree of charring is shown in Figure 4.17 in comparison with test results from König (1995) of members without a lining. Since the original test results were given as a relationship between load ratio and time, the time axis was transformed into a charring ratio axis using the polynomial fitting the test results shown in Figure 3.21. Both calculations and tests reflect the effect of the state of stress of the exposed side on the load bearing capacity. Since the members used in the tests were unprotected on the exposed side, the bending moment capacity is greater in the beginning since it takes some time before a stable temperature profile has developed.

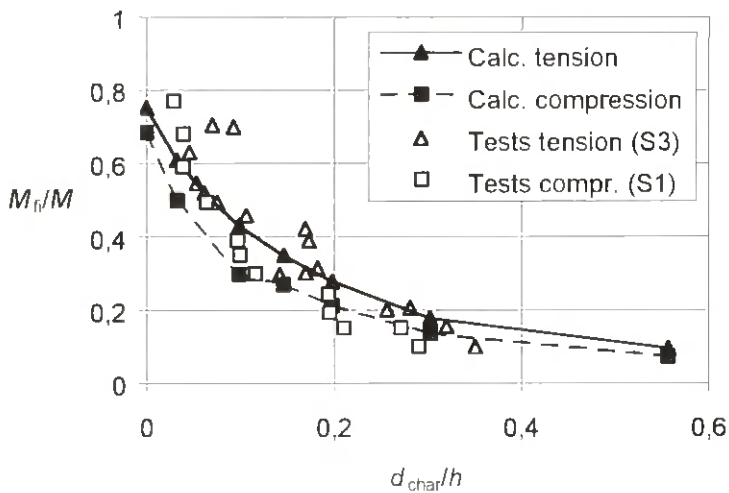


Figure 4.17: Bending moment ratio versus charring ratio – Calculated values and test results from König (1995)

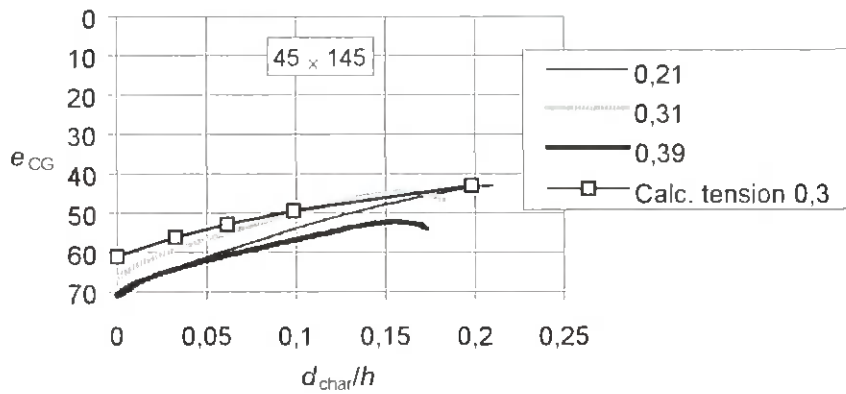


Figure 4.21: Position of neutral axis (centre of gravity) versus charring depth ratio for members with the fire exposed side in tension

In the following, using the model described in 4.2 and equation (4.3), the calculated values of the modification factor for fire $k_{mod,fi,fm}$ are compared with test results of test series J from König et al. (1997) and of test series S1 and S3 to S7 from König (1995). Since the members of test series S1 and S3 to S7 were initially unprotected, i.e. no boards were attached to the members on the fire-exposed side, values for failure times less than twenty minutes were omitted, assuming that it would take twenty minutes to allow quasi-steady state moisture and temperature gradient to develop (Schaffer). This assumption is confirmed by the test results reported by König et al. (1997, 1999).

Figure 4.22 shows data for members of size 45 mm × 195 mm in pure bending and the fire-exposed side in tension. From test results of series J only tests with standard fire exposure were taken into account. There is a considerable scatter of the test data, mainly due to errors

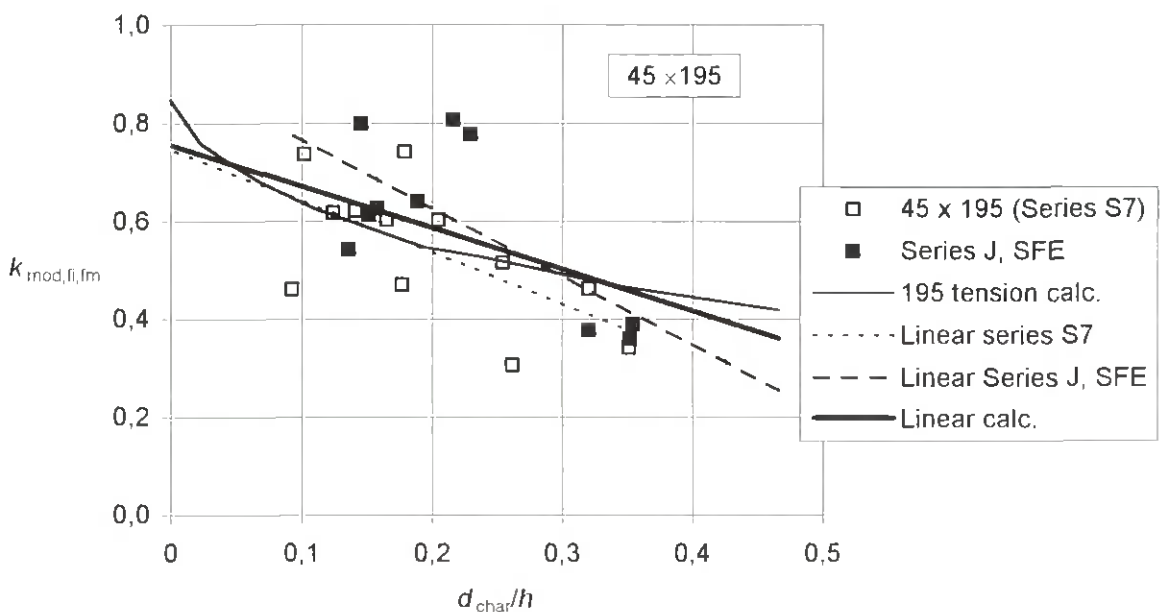


Figure 4.22: Modification factor for fire versus relative charring depth – Comparison of calculated values with test results for members in bending with the fire-exposed side in tension

predicting the load-bearing capacity at normal temperature, and recording the residual cross sections, see König et al. (1997). For simplification, the non-linear relationship obtained by calculation was fitted by a linear relationship. Such linear relationships given as

$$k_{\text{mod,fi,fin}} = \alpha_0 - \alpha_1 \frac{d_{\text{char}}}{h} \quad (4.6)$$

are proposed for design practice. Values of α_0 and α_1 are given in Appendix A

Similarly, in Figure 4.23-4.25 for different depths the effect of the state of stress, i.e. whether the fire-exposed side is in tension or compression, is shown for calculated values in comparison with test results.

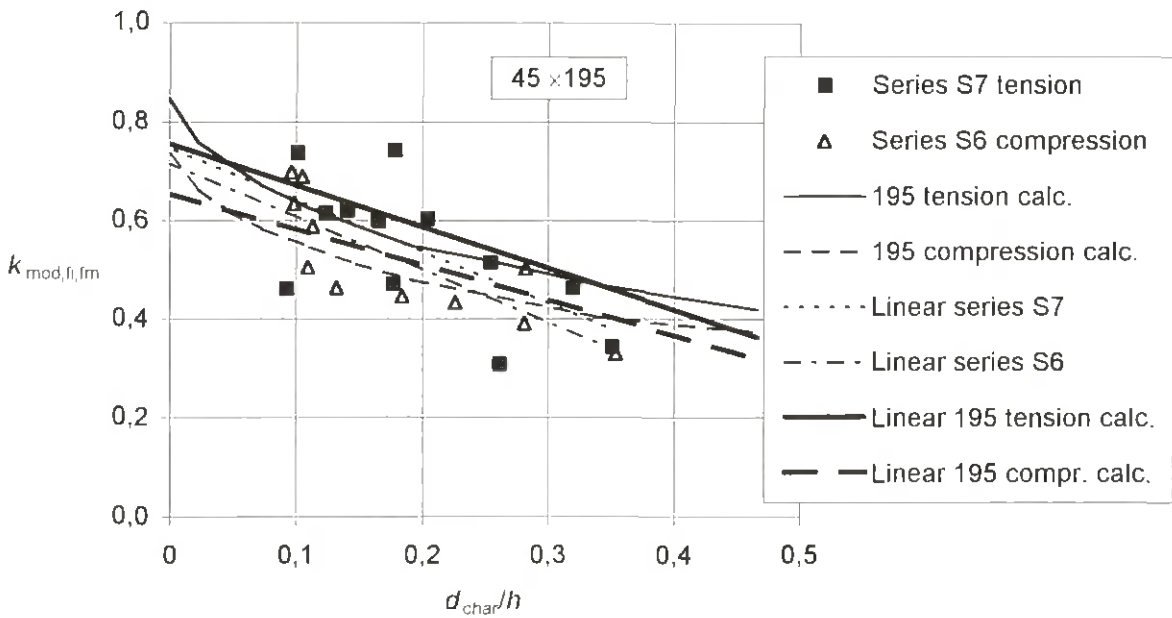


Figure 4.23: Modification factor for fire versus relative charring depth – Comparison of calculated values with test results: Effect of state of stress (tension or compression) on fire-exposed side

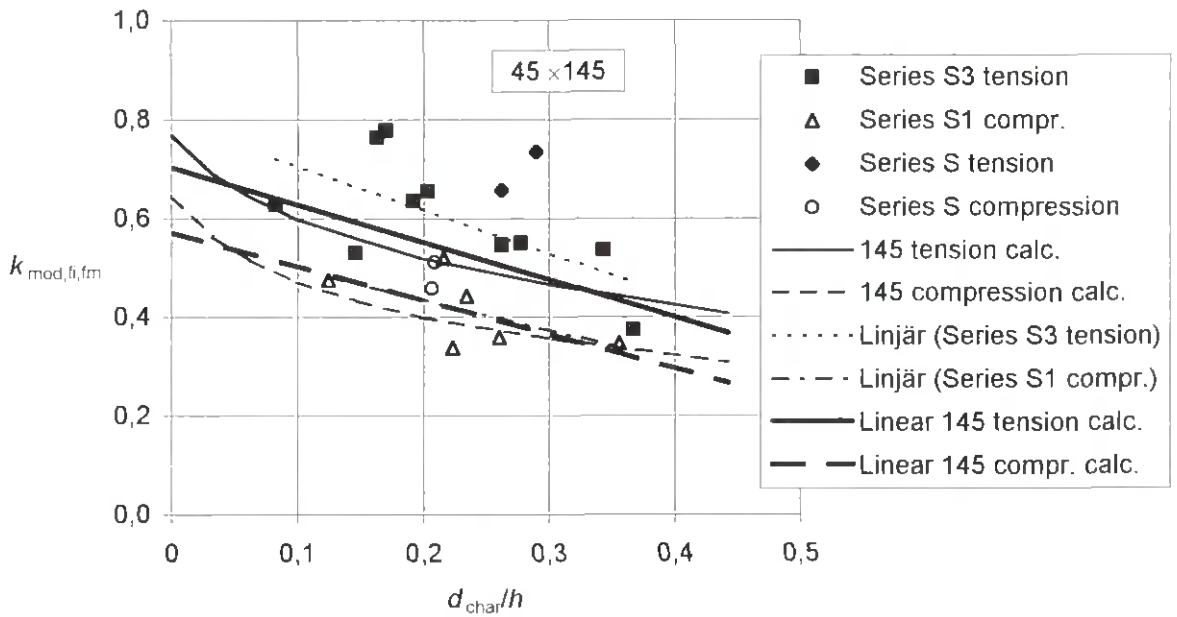


Figure 4.24: Modification factor for fire versus relative charring depth – Comparison of calculated values with test results: Effect of state of stress (tension or compression) on fire-exposed side

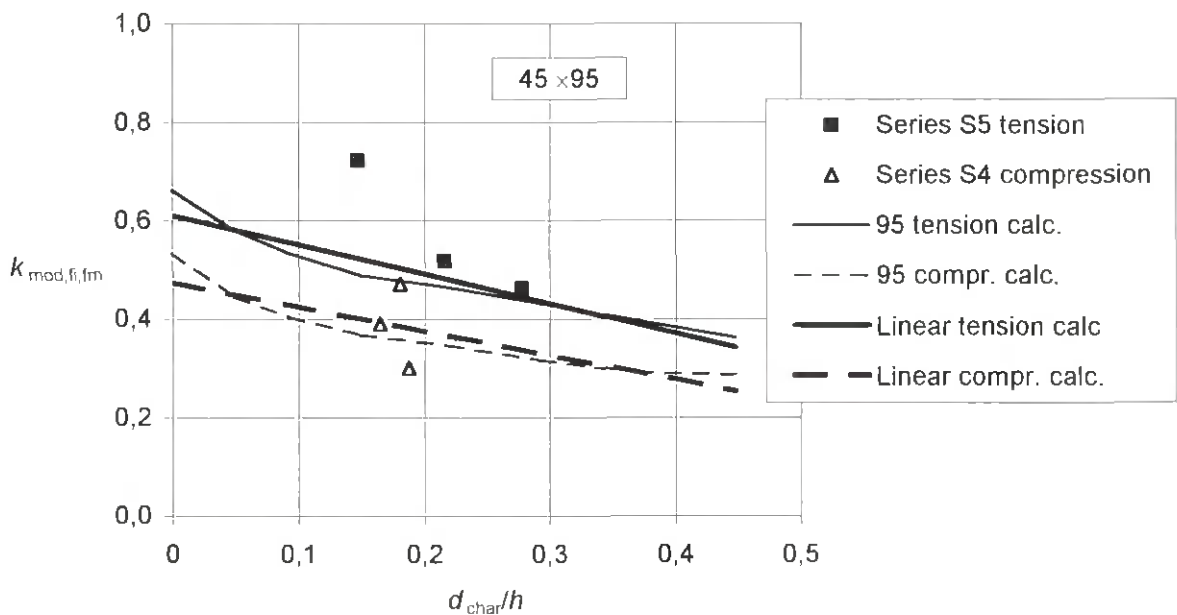


Figure 4.25: Modification factor for fire versus relative charring depth – Comparison of calculated values with test results: Effect of state of stress (tension or compression) on the fire-exposed side

The effect of the depth of the members is shown in Figure 4.26 and 4.27 for the fire-exposed side in tension and compression respectively. Due to the large scatter of results, in the tension case, the effect of depth of the member cannot be observed from the test data. The calculations however, indicate that such influence exists, although it is not very large, see Figure 4.26. For the case of the fire-exposed side in compression, due to a more ductile behaviour, the effect of the depth of the member can also be seen from the test results, as can be seen from the

calculated values, see Figure 4.26. In this case the effect is somewhat greater than in the previous case.

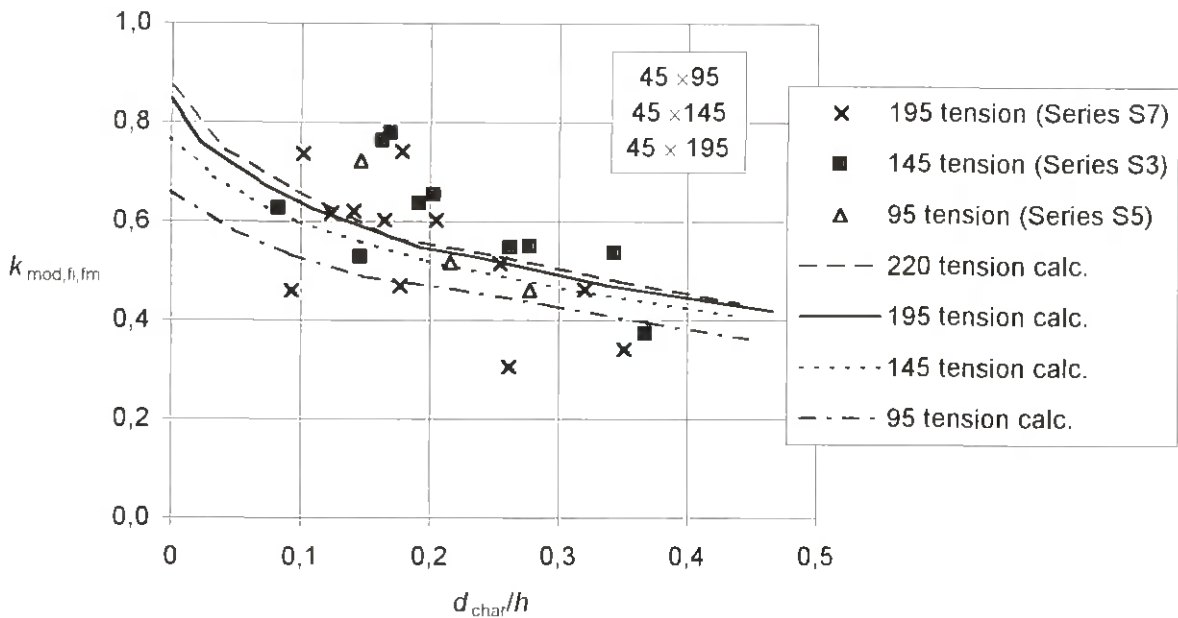


Figure 4.26: Modification factor for fire versus relative charring depth – Comparison of calculated values with test results for members with the fire-exposed side in tension: Effect of depth of member

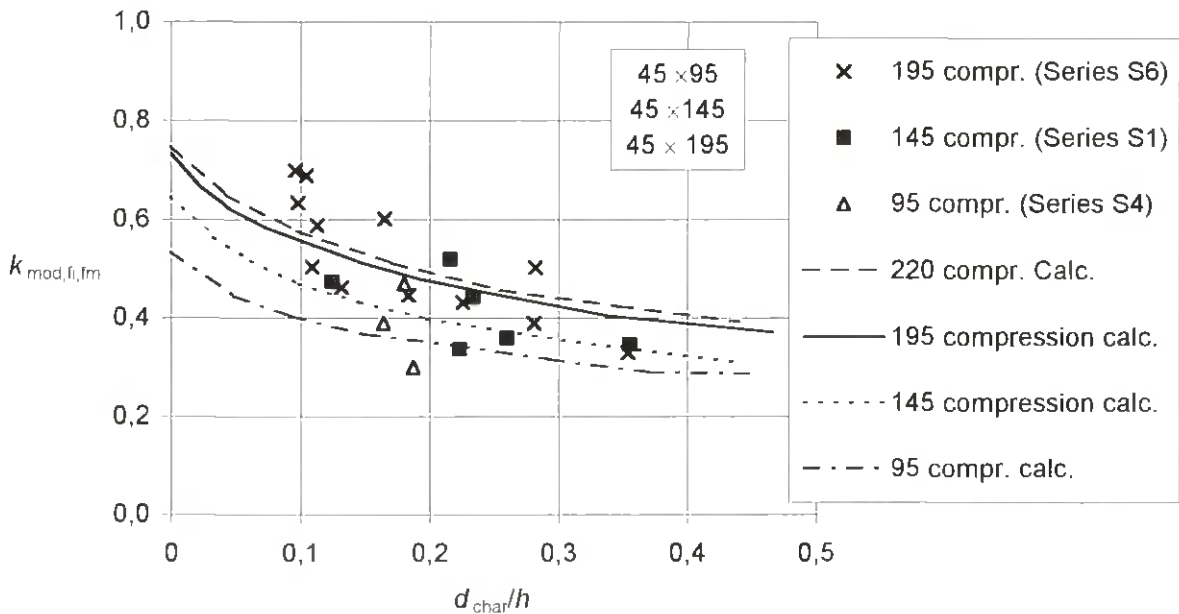


Figure 4.27: Modification factor for fire versus relative charring depth – Comparison of calculated values with test results for members with the fire-exposed side in compression: Effect of depth of member

4.3.2.3 Effect of timber quality

In the calculations of the previous clauses, the assumed bending strength of members of size 45 mm × 145 mm was 65 N/mm² with localized compressive and tensile strength values of 44 and 72 N/mm² respectively, see 4.3.2.1. In order to see the effect of timber quality, calculations were performed for timber with lower localized tensile strength values of 53,5 and 35 N/mm² due to the existence of knots, while the localized compressive strength was kept unchanged. The corresponding bending strengths are 52,5 and 35 N/mm² respectively. In the latter case, since the tensile strength was lower than 44 N/mm², no plastic flow occurs on the compression side. See Figure 4.28 showing the ultimate stress distributions at normal temperature.

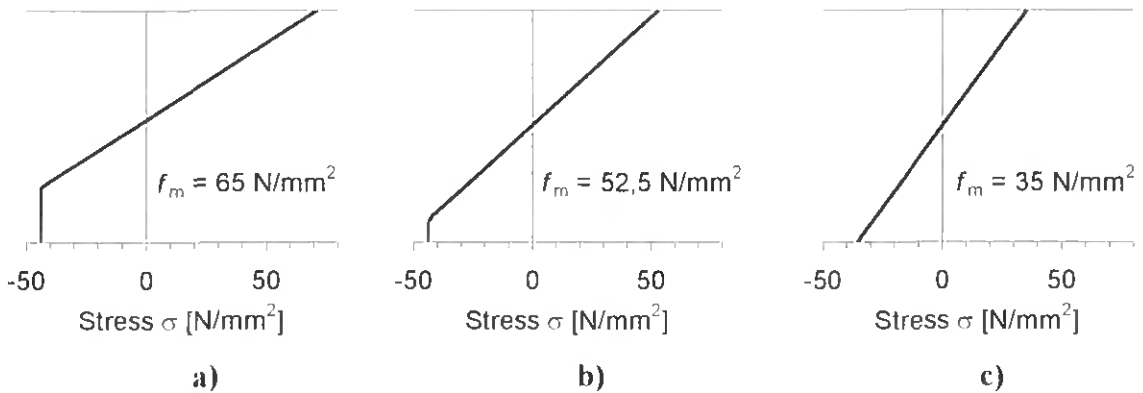


Figure 4.28: Ultimate stress distributions at normal temperature for depth 145 mm and different bending strengths

The results presented in Figure 4.29 and 4.30 show that there is a small influence of bending strength of the cross section when the fire-exposed side is in tension and a somewhat greater influence when the fire-exposed side is in compression. For all bending strength values not greater than 44 N/mm², i.e. for purely elastic conditions at normal temperature, the results would be the same as for the 35 N/mm² curves. Considering the scatter of test results shown e.g. in Figure 4.24, it should be reasonable to neglect this influence in practice. These results agree with the test results reported by Norén (1988) studying the effect of timber quality on time to failure of timber members in bending exposed to fire on four sides.

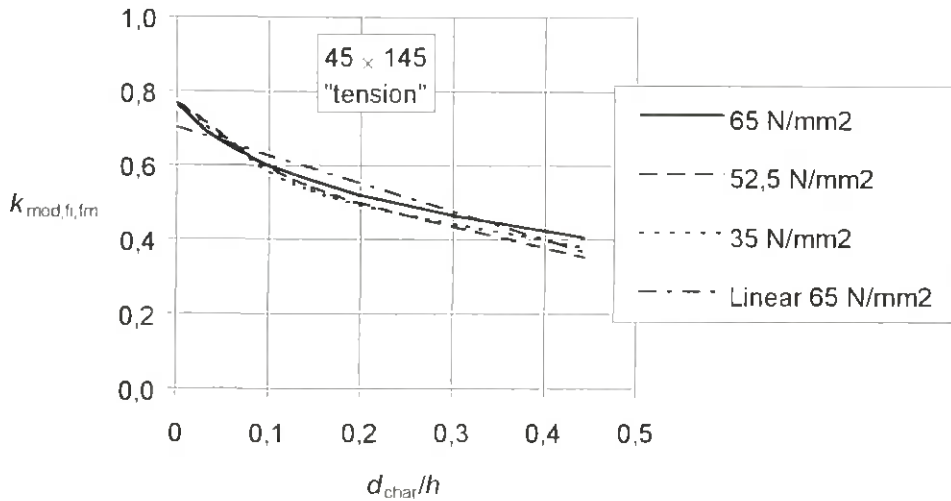


Figure 4.29: Effect of bending strength on modification factor for fire for bending strength — fire exposed side in tension

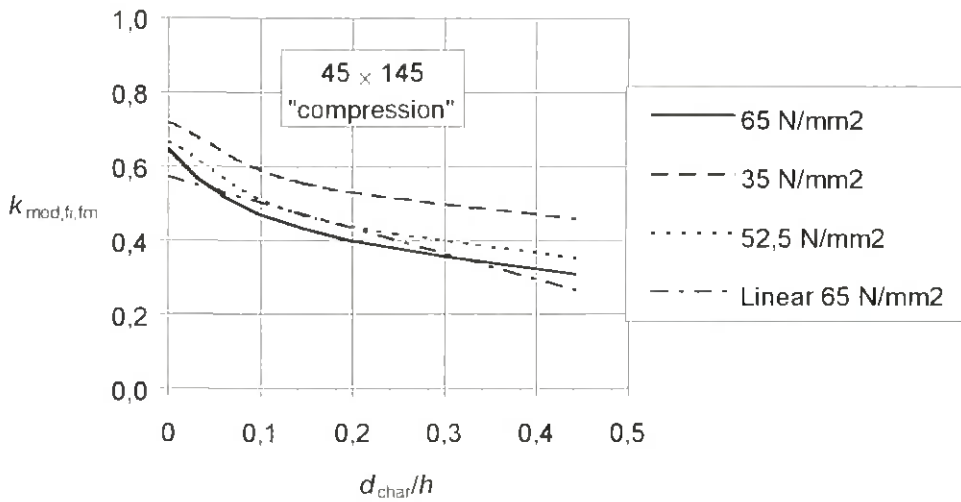


Figure 4.30: Effect of bending strength on modification factor for fire for bending strength — fire exposed side in compression

4.4 Determination of apparent modulus of elasticity in bending

In general, at elevated temperature the modulus of elasticity decreases more for wood in compression than for wood in tension. Especially when plastic flow occurs on the compression side, curvature of the member increases considerably. The reduction of the flexural stiffness consists first of the reduction of second moment of area and second of an apparent reduction of the modulus of elasticity.

When the member is exposed to fire, the deflection is

$$w_{fi} = w \frac{E}{E_{fi}} \frac{I}{I_{fi}} \quad (4.7)$$

where

w is the deflection at normal temperature
 E is the modulus of elasticity at normal temperature
 I is the second moment of area of the original cross section
 I_{fi} is the second moment of area of the residual cross section.

Substituting

$$k_{\text{mod,fi,E}} = \frac{E_{fi}}{E} \quad (4.8)$$

gives

$$k_{\text{mod,fi,E}} = \frac{w}{w_{fi}} \frac{I}{I_{fi}} \quad (4.9)$$

At normal temperature, for a constant bending moment M , the mid-deflection is given as

$$w = \frac{M L^2}{8 E I} \quad (4.10)$$

The mid-deflection of the member exposed to fire acted upon by the same bending moment can be determined knowing the curvature of the member and the position of the centre of gravity, obtained according to 4.2, stopping the calculation when the bending moment M is reached. The curvature of the member is determined as

$$\frac{1}{r} = \Theta = \frac{\varepsilon}{z_{cg}} \quad (4.11)$$

where

r is the radius of curvature
 ε is the edge strain
 z_{cg} is the distance between the edge and the centre of gravity.

Therefore

$$r = \frac{z_{cg}}{\varepsilon} \quad (4.12)$$

Within the length L with a constant curvature, the mid-deflection of the fire-exposed member is

$$w_{fi} = r - \sqrt{r^2 - \frac{L^2}{4}} \quad (4.13)$$

Inserting expressions (4.10) and (4.13) into (4.9) we can determine the reduction coefficient for the modulus of elasticity.

For a member of size 45 mm × 145 mm, the results of the calculations are shown in Figure 4.31. When the fire-exposed side is in compression, there is a considerable effect of load ratio. The member can take the load before reaching the breakpoints A, B, C or D of the curves. Beyond these breakpoints the load decreases in order to satisfy the conditions of equilibrium. In practice, the member would fail when the charring depth ratios of the breakpoints are reached. This applies also to members with the fire-exposed side in tension however much less pronounced, c.f. breakpoint E of the curve for load ratio of 30 %.

This influence of load ratio on flexural stiffness can also be seen from the test results obtained by König (1995).

In Figure 4.32 the calculated values are compared with derived values from test results by König et al. (1997). These were determined using the deflection and charring depth propagation versus time recorded during the tests. The variation of second moment of area was determined using the values for the residual cross section at failure and exponential expressions of their variation with time, similarly as presented for section moduli shown in 6.5.5.3 of König et al. (1997). The tests were conducted with a load ratio of 0,2. As shown previously in Figure 4.8, at start of charring, the calculated values overpredict the test values for a member depth of 145 mm.

Correspondingly, in Figure 4.33, for fire exposed side in tension, the calculated values are compared with test results. As mentioned before (Figure 4.8), the model underpredicts the test results at the start of charring. In both graphs, apart from the large scatter of the derived test values, there is a fairly good agreement between the calculation and the tests.

For buckling verification of members in compression, in Figure 4.31 a simple linear model is also shown, using the starting point and breakpoint of the relationship for a load ratio of 20 %. Such linear relationship given as

$$k_{\text{mod,fi,E}} = b_0 - b_1 \frac{d_{\text{char}}}{h} \quad (4.14)$$

is proposed for design practice. Values of b_0 and b_1 are given in Appendix B.

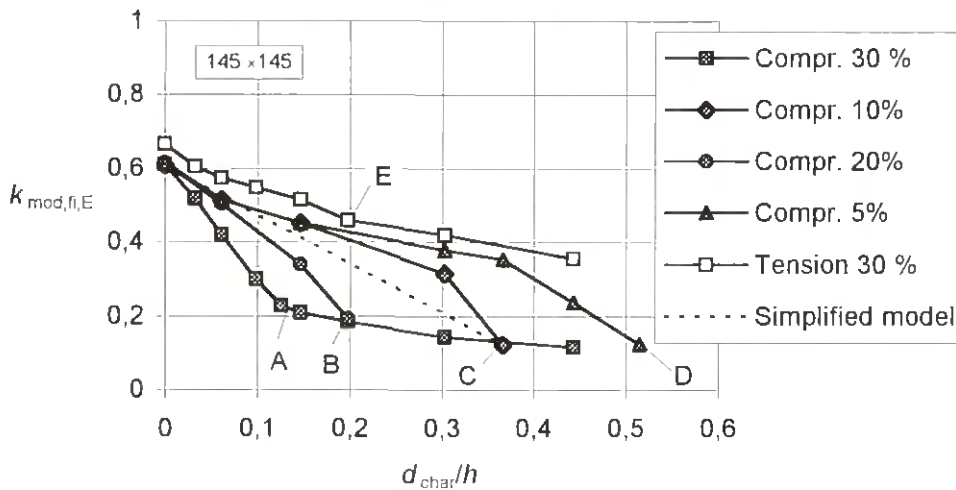


Figure 4.31: Reduction of apparent modulus of elasticity of residual cross section versus charring depth ratio — Effect of load ratio and state of stress on the fire-exposed side

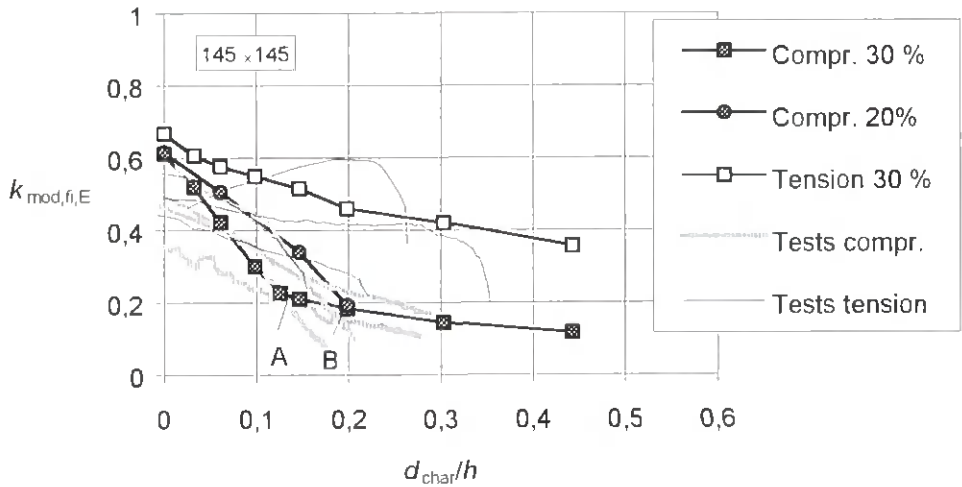


Figure 4.32: Reduction of apparent modulus of elasticity of residual cross section versus charring depth ratio — Comparison with test results (König et al., 1997)

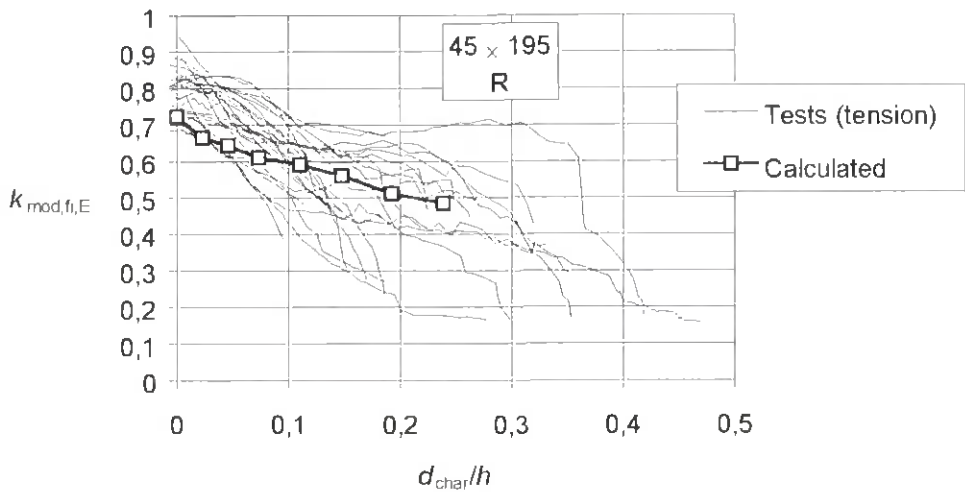


Figure 4.33: Reduction of apparent modulus of elasticity of residual cross section versus charring depth ratio — Comparison with test results (König et al., 1997)

4.5 Mechanical properties for bending about weak axis

Normally, timber frame members are loaded such that bending occurs about the stiff axis of the cross section, i.e. edgewise bending. Only where wall studs are unbraced with respect to in-plane column buckling, are flexural stiffness values with respect to bending about the weak axis, i.e. flatwise bending, needed. Modification factors for fire were calculated using the same reductions for strength and stiffness parameters as for edgewise bending, see Appendix B.

5 Performance of linings

5.1 General

The fire protection provided by linings is crucial to the fire resistance of wall and floor assemblies. The contribution to fire resistance with respect to the load-bearing function may be due to the ability to

- delay the start of charring in the timber frame members
- reduce the charring rate where the lining remains in place during the stage following start of charring

i.e. when charring phase 2 starts and its duration, see 2.1.1. Values are derived in 3.3.2.

The duration of the protection phase, see 2.1.1, depends on when the lining fails, see next subclause 5.2.

5.2 Failure of lining

While regular gypsum plasterboard of type A according to prEN 520 (1999) normally would fall off shortly after that the timber member has started to char behind the lining, i.e. $t_{br} = t_{pr}$, gypsum plasterboard with improved core cohesion (type F) remains in place during a period of time beyond the start of charring dependent on material resistance of the boards and/or the length of fasteners.

In the tests reported by König et al. (1997), horizontal linings with an outer layer of gypsum plasterboard type F fell off earlier than corresponding vertical ones. As a design criterion for failure, a temperature of 600°C can be assumed for ceiling linings, and 800°C for wall linings, in both cases referring to the temperature reached on the non-exposed side of the board. These assumptions agree with data reported by Haraldsson (1996) who analysed results of full-scale tests of walls, floors and columns. Failure times of linings versus temperature exhibited, however, a considerable scatter that was further increased since the temperature was not measured at locations where lining failure occurred first.

In Figure 5.1 time-temperature curves are shown for the unexposed side of the gypsum plasterboard GF forming the lining (curves A), or the outer layer where the lining consisted of two layers GN + GF (curves B). Times of board failure observed during the tests are marked by squares. The values for vertical position refer to wall tests in medium scale, while the values for horizontal position refer to small-scale tests. Using the calculated relationships and the failure criteria of 600 and 800°C, the failure times of the (outer) layer of gypsum plasterboard GF are obtained as shown in Table 5.1

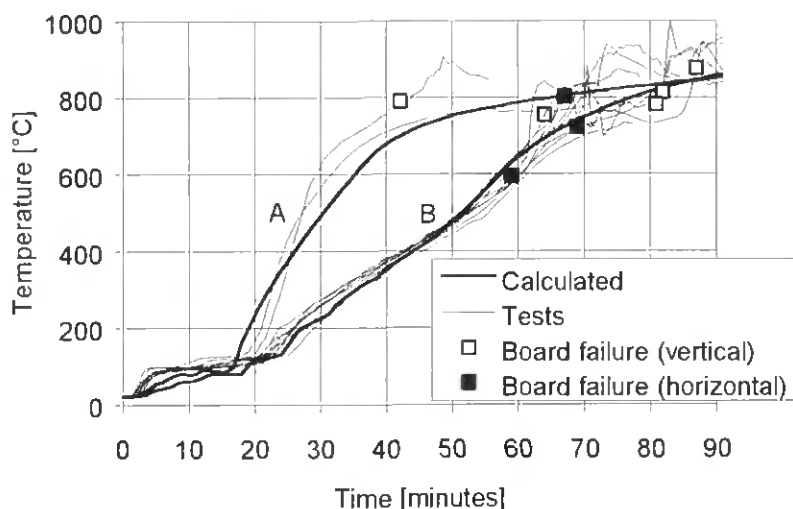


Figure 5.1: Temperature on unexposed side of gypsum plasterboard GF.
A: Lining consisting of one layer GF
B: Lining consisting of two layers GN + GF

Table 5.1: Failure times of linings made of gypsum plasterboard according to temperature criteria

Lining	Vertical position (walls)	Horizontal position (ceilings)
1 layer 15,4 mm GF	65	35
1 inner layer 12,5 mm GN 1 outer layer 15,4 mm GF	77	57

Resilient channels made of cold-formed steel sheeting are sensitive to elevated temperature. At standard fire exposure, the maximum gas temperature after one hour is about 950°C. Assuming that the resilient channels are reaching that temperature, according to ENV 1993-1-2, the yield strength of steel is reduced to 5 %. They certainly loose most of their strength, however, after failure of the boards they are still capable of carrying their own weight and the cavity insulation where a fire resistance of 60 minutes is required.

When the board material is not seriously affected by temperature, e.g. in the case of calcium silicate board, or when fasteners of small length are used for fixing the lining, failure may occur due to insufficient penetration length of the fasteners into the unburned residual cross section, see Figure 5.2.

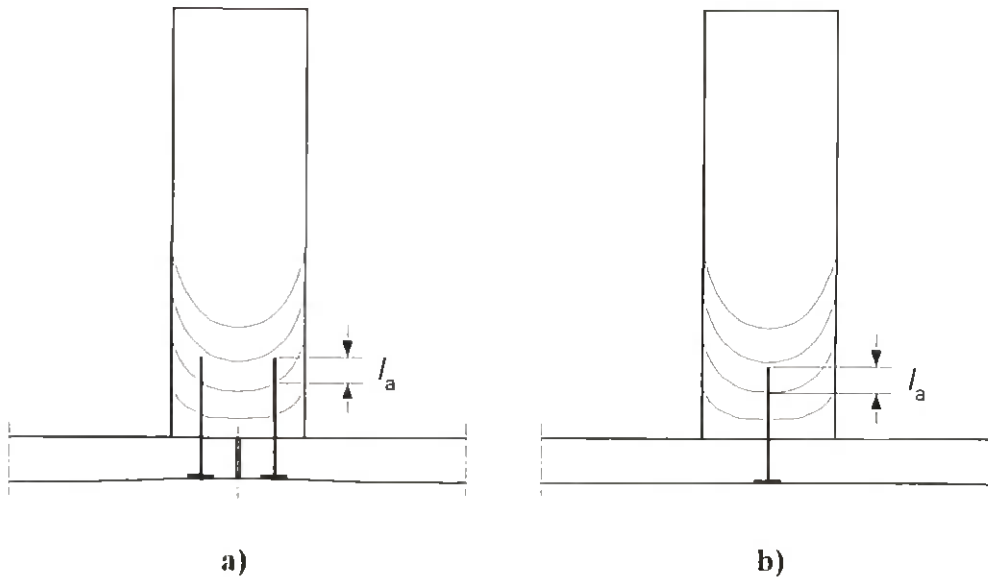


Figure 5.2: Fixing of lining — penetration of fastener into unburned wood

Where boards are jointed at timber frame member, the distance of screws from the board edge is normally about 10 mm. At this location, the charring depth is approximately 15 % greater than in the middle. Assuming that the screw will be pulled out when the penetration length into the unburned wood is below 10 mm, the time of pull-out failure is – for linings without a joint in the outer layer –

$$t_{bl} = t_{pr} + \frac{l_f - l_{a,min} - h_{b,tot}}{\beta_0 \kappa_s \kappa_2} \quad (5.1)$$

and for linings with a joint in the outer layer

$$t_{bl} = t_{pr} + \frac{l_f - l_{a,min} - h_{b,tot}}{1,15 \beta_0 \kappa_s \kappa_2} \quad (5.2)$$

where

- t_{pr} is the time of protection against charring
- l_f is the total length of the fastener
- $l_{a,min}$ is the minimum penetration length into unburned wood (= 10 mm)
- $h_{b,tot}$ is the total thickness of lining
- β_0 is the basic charring rate (= 0,67 mm/minute)
- κ_s is the cross section factor
- κ_2 is the insulation factor of the lining.

For fixing of resilient channels, the failure time of the connection is according to equation (5.1) with $h_{b,tot}$ replaced by the thickness of the steel sheeting.

Resilient channels are capable of keeping rock fibre bats in place after failure of the boards. The time of failure of the fixing of the resilient channels is determined by

$$t_{pr} = t_{bf} + \frac{I_f - I_{a,\min} - \beta_0 \kappa_s \kappa_2 (t_{bf} - t_{pr})}{\beta_0 \kappa_s \kappa_3} \quad (5.3)$$

where

t_{bf} is the failure time of the boards

κ_3 is the post protection factor.

6 Structural model for wall studs

The load-bearing capacity of wall studs is normally determined assuming pinned end supports. In timber frame construction where each floor acts as a platform for the next storey (platform timber frame construction), for out-of wall plane buckling, it is possible to take advantage of a more favourable buckling performance, since the rotation of the stud ends and the subsequent movement of the reaction force towards the unexposed edge of the stud gives rise to a stabilising reaction moment. These conditions were modelled by assuming cylindrically shaped end surfaces of the studs, see König (1988) and König et al. (1988). In the second source, the end conditions were also modelled by assuming a compressible bedding at the supports.

Applying the cylindrical end surface model, for two stud lengths 2500 and 3500 mm including head and top plates and a stud depth of 60 mm, critical buckling lengths were determined in relation to the mid-deflection of the stud, see Figure 6.1. Typical deflection ratios at failure in fire tests of walls are 0,02 (König et al., 1997). For wall heights up to approximately 3,5 m, for design practice, a buckling length ratio of $l_{cr}/l = 0,7$ would give conservative results.

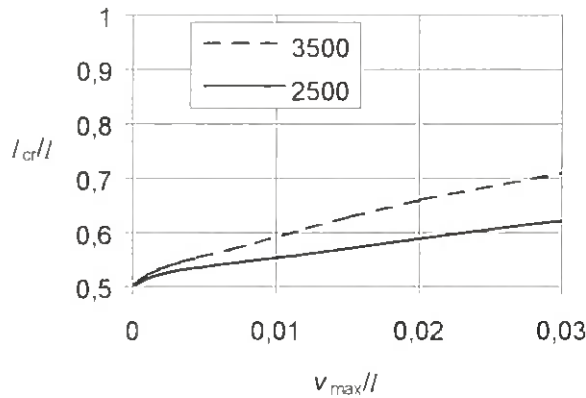


Figure 6.1: Buckling length ratio versus deflection ratio

7 References

- Andersson, L. and Jansson, B., 1986, En undersökning av gipsskivans termiska egenskaper – teori och försök. Department of Fire Safety Engineering, Lund University, Lund
- Arima, T., 1979, Creep in process of temperature change. III Prediction of creep at elevated temperature. J. Jap. Wood Research Soc. 19(2), pp 75-79
- ASCE Committee on Fire Protection, Structural Division, 1992, Structural fire protection. New York
- Bach, L., 1965, Non-linear mechanical behavior of wood in longitudinal tension. Ph.D. Thesis, Syracuse Univ., Syracuse, N.Y.
- Bazan, I. M. M., 1980, "Ultimate bending strength of timber beams". Thesis presented to Nova Scotia Technical College, Halifax, Nova Scotia, in partial fulfillment of the requirements for the degree of Doctor of Philosophy
- Buchanan, A. H., 1990, "Bending strength of lumber". Journal of Structural Engineering, Vol. 116, No. 5
- ENV 1991-2-2: 1994, Eurocode 1 – Basis of design and actions on structures, Part 2-2 – Actions on structures exposed to fire
- ENV 1995-1-1: 1993, Eurocode 5 – Design of timber structures, Part 1-1 – General rules and rules for buildings
- ENV 1995-1-2: 1994, Eurocode 5 – Design of timber structures, Part 1-2 – Structural fire design
- Fredlund, B., 1988, A model for heat and mass transfer in timber structures during fire. Lund University, Lund
- Gerhards, C.C., 1982, Effect of moisture content and temperature on mechanical properties of wood: an analysis of immediate effects. Wood and Fiber. 14(1), pp 4-36
- Glos, P. and Henrici, D., 1991, Festigkeit von Bauholz bei hohen Temperaturen. Institut für Holzforschung der Universität München, Munich
- Haraldsson, I., 1966, Nedfallstemperaturer för Gyproc Protect F. Gyproc Group AB, Sweden, not published internal report, Malmö, Reference with permit by Gyproc Group AB
- Harmathy, T. Z., 1995, Properties of building materials. The SFPE Handbook of Fire Protection Engineering, 2nd edition
- Janssens, M., 1994, Thermo-physical properties for wood pyrolysis models. Pacific Timber Engineering Conference Gold Coast, Australia
- Kollmann, F. und Schulz, F., 1944, Versuche über den Einfluss der Temperatur auf die Festigkeitswerte von Flugzeugbaustoffen, 1. und 2. Teilbericht, Reichsanstalt für Holzforschung, Eberswalde, (published as typescript)

- Kollmann, F., 1939, Vorgänge und Änderungen von Holzeigenschaften beim Dämpfen. Holz als Roh- und Werkstoff. 2(1), pp 1-11
- Kollmann, F., 1951a, Technologie des Holzes und der Holzwerkstoffe. Zweite Auflage, erster Band, pp. 737, 742
- Kollmann, F., 1951b, Über das mechanische Verhalten von Kiefernholz bei Biegung und Temperaturen zwischen 20° und 100°. Svenska Träforskningsintitutet, Trätekniska Avdelningen, Meddelande 22, Stockholm
- König, J. 1988. The structural behaviour of axially loaded wood studs exposed to fire on one side. Swedish Inst. for Wood Technology Research. Report I 8808057
- König, J and Källsner, B., 1988, The influence of the support conditions on the loadbearing capacity of axially loaded wood studs under simulated fire exposure. Proceedings of the International Conference on Timber Engineering, Seattle. Vol. 2, p 423-440
- König J., Norén J., Bolonius Olesen F. & Toft Hansen F., 1997, Timber frame assemblies exposed to standard and parametric fires - Part 1: Fire tests. Swedish Institute for Wood Technology Research, Report No. I 9702015
- König, J. And Walleij, L., 1999, One-dimensional charring of timber exposed to standard and parametric fires in initially unprotected and post-protection fire situations. Swedish Institute for Wood Technology Research, Report No. I 9908029
- König, J., 1995, Fire resistance of timber joists and load bearing wall frames. Swedish Institute for Wood Technology Research, Report No: I 9412071
- Mehaffey, J., R., Cuerrier, P., Carisse, G., 1994, A model for predicting heat transfer through gypsum board/wood stud walls exposed to fire. Fire and materials, Vol. 18.
- Norén, J., 1988, Failure of structural timber when exposed to fire. Proceedings of 1988 Int. Conf. on Timber Engineering, Seattle
- Östman, B., 1985, Wood tensile strength at temperatures and moisture contents simulating fire conditions. Wood and Science technology, 19, pp 103-106
- Östman, B., König, J., Mikkola, E., Stenstad, V., Karlsson, B., and Walleij, L., 1999, Brandsäkra trähus – Kunskapsöversikt och vägledning för lättbyggsystem i Norden. Swedish Inst. for Wood Technology Research. Publ. nr 9908034
- prEN 520, 1999, Draft European Standard, Gypsum plasterboards – Definitions, requirements, test methods
- Roberts, A., F., 1971, The heat reaction during the pyrolysis of wood. Combustion and flame, Vol. 17
- Schaffer, E. L., 1984, Structural fire design: Wood. Forest Products Laboratory, Research Paper FFL 450, Madison

- Schaffer, E. L., Marx, C. M., Bender, D. A., and Woeste, F. E., 1984, Strength validation and fire endurance of glued-laminated timber beams. Forest Products Laboratory, Research Paper FFL 467, Madison
- Sterner, E. And Wickström, U., 1990, TASEF – Temperature analysis of structures exposed to fire – User’s manual. Fire Technology, SP Report 1990:05, Borås, Sweden
- Stevens, W.C. and Turner, N., 1970, Wood Bending Handbook, London
- TCD 3.0, 1990. User’s Manual for TCD 3.0 with Tempcalc. Fire Safety Design, Lund
- TCD 5.0, 1999, User’s Manual for TCD 5.0 with *Tempcalc*. Fire Safety Design, Lund
- Thomas, G. C., 1997, Fire resistance of light timber framed walls and floors. University of Canterbury, Canterbury, New Zealand
- Thunell, B., 1941, Hållfasthetsegenskaper hos svenskt furuvirke utan kvistar och defekter. Ingenjörsvetenskapsakademien, Handlingar Nr. 161, Stockholm
- Tsantaridis, L. D., Östman, B. and König, J., 1999, Fire protection of wood by different gypsum plasterboards. Fire and Materials, Vol. 23, pp 45-48
- White, R. and Schaffer, E.L., 1981, Transient moisture gradient in fire-exposed wood slab. Wood and Fiber, 13(1) pp17-38

Appendix A – Effect of grid configuration

The computations of model parameters were performed using TCD (1990). The structure was modelled using a coarse grid as shown in Figure A.1a. Considering a structure consisting only of the timber member and the cavity insulation (see 3.2.2), temperatures were determined, see Figure A.2, showing isotherms at 15 minutes of fire exposure. For comparison, performing a calculation using TCD (1999) with the same thermal properties of materials, however with the improved grid according to Figure A.1b (without boards), the resultant corresponding isotherms are shown in Figure A.3.

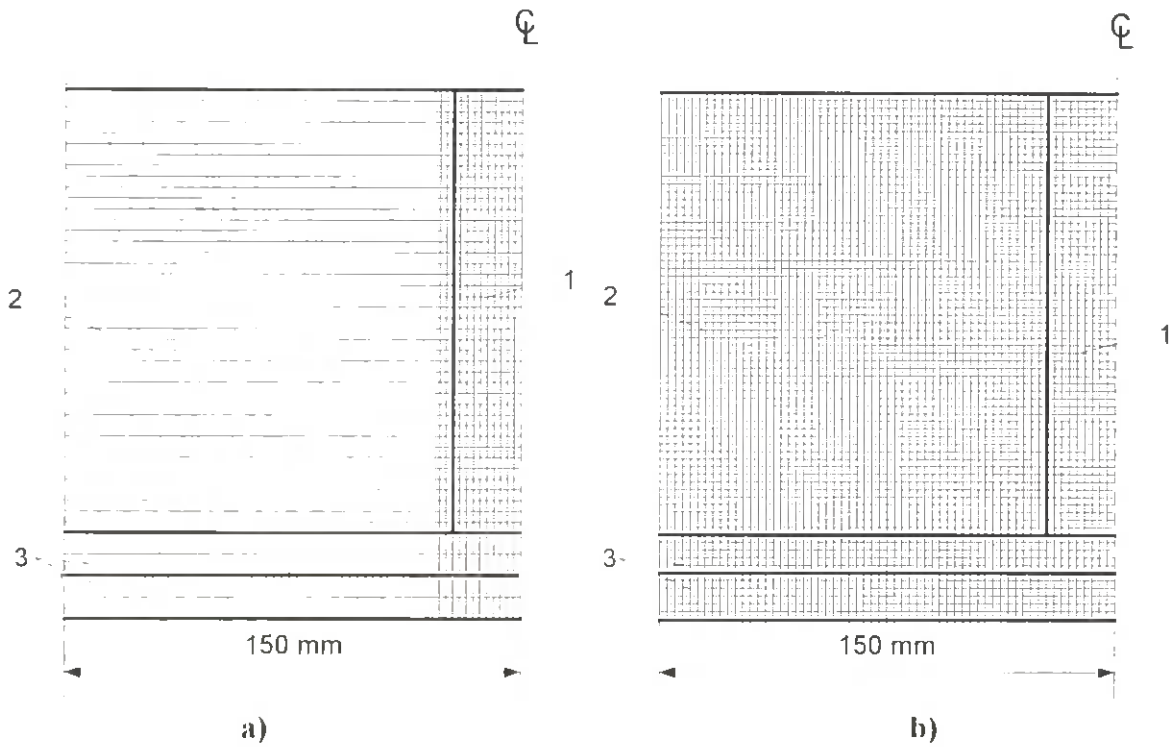


Figure A.1: Grid modelling the timber member, cavity insulation and lining consisting of two board layers: a) Coarse grid, b) Improved grid

As expected, there is a considerable effect of the grid configuration on the temperature in the region of coarse elements, however, the difference of temperatures in the timber member is small. Considering the 300-degree isotherm in the timber member used as the char line, the coarse grid gives better agreement with the typical shapes of residual cross sections shown in König et al (1997). A conclusion is that the material properties of mineral wool used in the calculations are partially calibrated to compensate for the shortage of the coarse grid modelling.

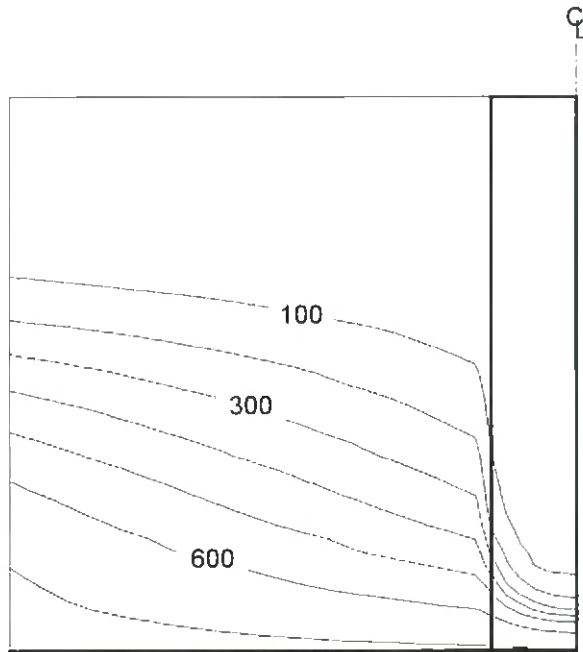


Figure A.2: Isotherms in structure modelled by the coarse grid at 15 minutes of fire exposure

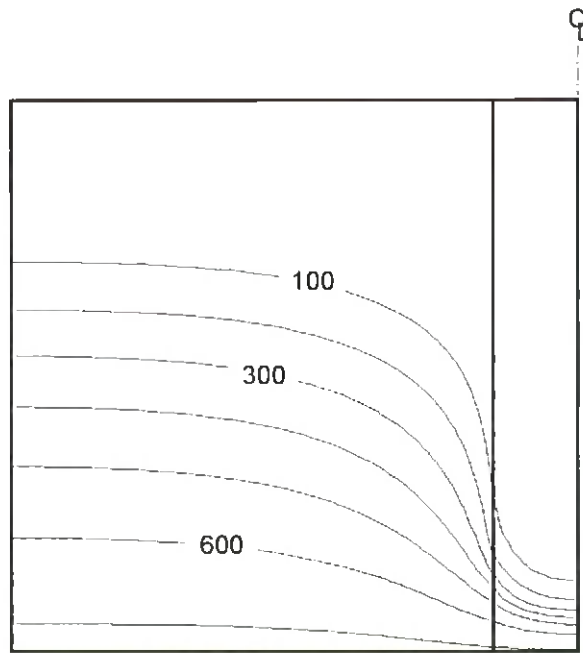


Figure A.2: Isotherms in structure modelled by the improved grid at 15 minutes of fire exposure

Appendix B – Modification factors for fire

Simplified linear expressions of modification factors of fire are given as (see 2.2.4):

– for bending strength

$$k_{\text{mod,fi,fm}} = a_0 - a_1 \frac{d_{\text{char}}}{h} \quad (\text{B.1})$$

– for modulus of elasticity

$$k_{\text{mod,fi,E}} = b_0 - b_1 \frac{d_{\text{char}}}{h} \quad (\text{B.2})$$

where

d_{char} is the charring depth in the middle of the cross section, see Figure 2.7

h is the depth of the beam.

The parameters a_0 , a_1 , b_0 and b_1 , previously published in Östman et al. (1999), are given in Tables B.1-B.7 for specified sizes of cross sections and state of stress.

Table B.1: Fire exposure on one side: Parameters for bending strength with exposed side in tension

	$h = 95 \text{ mm}$		$h = 145 \text{ mm}$		$h = 195 \text{ mm}$		$h = 220 \text{ mm}$	
	a_0	a_1	a_0	a_1	a_0	a_1	a_0	a_1
$b = 38 \text{ mm}$	0,60	0,69	0,68	0,73	0,73	0,77	0,76	0,77
$b = 45 \text{ mm}$	0,61	0,60	0,70	0,76	0,75	0,84	0,79	0,90
$b = 60 \text{ mm}$	0,66	0,63	0,73	0,78	0,80	0,98	0,81	0,93

Table B.2: Fire exposure on one side: Parameters for bending strength with exposed side in compression (approximately also for compressive strength of wall studs)

	$h = 95 \text{ mm}$		$h = 145 \text{ mm}$		$h = 195 \text{ mm}$		$h = 220 \text{ mm}$	
	a_0	a_1	a_0	a_1	a_0	a_1	a_0	a_1
$b = 38 \text{ mm}$	0,46	0,55	0,55	0,59	0,65	0,71	0,67	0,70
$b = 45 \text{ mm}$	0,47	0,50	0,57	0,69	0,66	0,72	0,68	0,75
$b = 60 \text{ mm}$	0,53	0,53	0,61	0,69	0,70	0,83	0,72	0,81

Table B.3: Fire exposure on one side: Parameters for modulus of elasticity with exposed side in compression – buckling about stiff axis (perpendicular to wall plane)

	$h = 95 \text{ mm}$		$h = 145 \text{ mm}$		$h = 195 \text{ mm}$	
	b_0	b_1	b_0	b_1	b_0	b_1
$b = 38 \text{ mm}$	0,50	1,18	0,60	1,25	0,68	1,15
$b = 45 \text{ mm}$	0,52	1,21	0,61	1,32	0,70	1,24
$b = 60 \text{ mm}$	0,55	1,25	0,65	1,34	0,70	1,20

Table B.4: Fire exposure on one side: Parameters for modulus of elasticity – buckling about weak axis (in wall plane)

	$h = 95 \text{ mm}$		$h = 145 \text{ mm}$		$h = 195 \text{ mm}$	
	b_0	b_1	b_0	b_1	b_0	b_1
$b = 38 \text{ mm}$	0,54	0,74	0,66	0,82	0,73	0,94
$b = 45 \text{ mm}$	0,57	0,80	0,63	0,79	0,72	0,93
$b = 60 \text{ mm}$	0,58	0,91	0,67	1,03	0,73	1,08

Table B.5: Fire exposure on one side: Parameters for bending strength about weak axis (approximately also for compressive strength)

	$h = 95 \text{ mm}$		$h = 145 \text{ mm}$		$h = 195 \text{ mm}$	
	α_0	α_1	α_0	α_1	α_0	α_1
$b = 38 \text{ mm}$	0,53	0,65	0,64	0,65	0,75	0,95
$b = 45 \text{ mm}$	0,55	0,60	0,62	0,63	0,74	0,90
$b = 60 \text{ mm}$	0,59	0,75	0,68	0,92	0,74	1,05

Table B.6: Fire exposure of walls on two sides: Parameters for bending strength (approximately also for compressive strength) and modulus of elasticity for buckling about stiff axis (perpendicular to wall plane)

	$h = 145 \text{ mm}$			
	α_0	α_1	b_0	b_1
$b = 38 \text{ mm}$	0,39	2,43	0,37	2,80
$b = 45 \text{ mm}$	0,41	2,67	0,37	2,80
$b = 60 \text{ mm}$	0,46	3,00	0,44	3,26

Table B.7: Fire exposure of walls on two sides: Parameters for bending strength (approximately also for compressive strength) and modulus of elasticity for buckling about weak axis (in wall plane)

	$h = 145 \text{ mm}$			
	α_0	α_1	b_0	b_1
$b = 38 \text{ mm}$	0,46	3,15	0,44	3,27
$b = 45 \text{ mm}$	0,48	3,55	0,46	3,62
$b = 60 \text{ mm}$	0,55	5,06	0,55	7,76

Detta digitala dokument
skapades med anslag från
**Stiftelsen Nils och Dorthi
Troëdssons forskningsfond**

Träte

INSTITUTET FÖR TRÄTEKNISK FORSKNING

Box 5609, 114 86 STOCKHOLM
Besöksadress: Drottning Kristinas väg 67
Telefon: 08-762 18 00
Telefax: 08-762 18 01

Åsensvägen 9, 553 31 JÖNKÖPING
Telefon: 036-30 65 50
Telefax: 036-30 65 60

Skeria 2, 931 77 SKELLEFTÅ
Besöksadress: Laboratorgränd
Telefon: 0910-58 52 00
Telefax: 0910-58 52 65

Hemsida: www.tratek.se · E-post: tratek@tratek.se